



Defense Threat Reduction Agency
8725 John J. Kingman Road, MS
6201 Fort Belvoir, VA 22060-6201



DTRA-TR-16-52

TECHNICAL REPORT

Effects of Mixtures on Liquid and Solid Fragment Size Distributions

Distribution Statement A. Approved for public release; distribution is unlimited.

May 2016

HDTRA1-11-D-0004

Culbert B. Laney

Prepared by:
Engility Corporation
8211 Terminal Road
Suite 1000
Lorton, VA 22079

DESTRUCTION NOTICE:

Destroy this report when it is no longer needed.
Do not return to sender.

PLEASE NOTIFY THE DEFENSE THREAT REDUCTION
AGENCY, ATTN: DTRIAC/ J9STT, 8725 JOHN J. KINGMAN ROAD,
MS-6201, FT BELVOIR, VA 22060-6201, IF YOUR ADDRESS
IS INCORRECT, IF YOU WISH IT DELETED FROM THE
DISTRIBUTION LIST, OR IF THE ADDRESSEE IS NO
LONGER EMPLOYED BY YOUR ORGANIZATION.

REPORT DOCUMENTATION PAGE

Form Approved
OMB No. 0704-0188

Public reporting burden for this collection of information is estimated to average 1 hour per response, including the time for reviewing instructions, searching existing data sources, gathering and maintaining the data needed, and completing and reviewing this collection of information. Send comments regarding this burden estimate or any other aspect of this collection of information, including suggestions for reducing this burden to Department of Defense, Washington Headquarters Services, Directorate for Information Operations and Reports (0704-0188), 1215 Jefferson Davis Highway, Suite 1204, Arlington, VA 22202-4302. Respondents should be aware that notwithstanding any other provision of law, no person shall be subject to any penalty for failing to comply with a collection of information if it does not display a currently valid OMB control number. **PLEASE DO NOT RETURN YOUR FORM TO THE ABOVE ADDRESS.**

1. REPORT DATE (DD-MM-YYYY)		2. REPORT TYPE	3. DATES COVERED (From - To)		
4. TITLE AND SUBTITLE			5a. CONTRACT NUMBER		
			5b. GRANT NUMBER		
			5c. PROGRAM ELEMENT NUMBER		
6. AUTHOR(S)			5d. PROJECT NUMBER		
			5e. TASK NUMBER		
			5f. WORK UNIT NUMBER		
7. PERFORMING ORGANIZATION NAME(S) AND ADDRESS(ES)			8. PERFORMING ORGANIZATION REPORT NUMBER		
9. SPONSORING / MONITORING AGENCY NAME(S) AND ADDRESS(ES)			10. SPONSOR/MONITOR'S ACRONYM(S)		
			11. SPONSOR/MONITOR'S REPORT NUMBER(S)		
12. DISTRIBUTION / AVAILABILITY STATEMENT					
13. SUPPLEMENTARY NOTES					
14. ABSTRACT					
15. SUBJECT TERMS					
16. SECURITY CLASSIFICATION OF:			17. LIMITATION OF ABSTRACT	18. NUMBER OF PAGES	19a. NAME OF RESPONSIBLE PERSON
a. REPORT	b. ABSTRACT	c. THIS PAGE			19b. TELEPHONE NUMBER (include area code)

UNIT CONVERSION TABLE

U.S. customary units to and from international units of measurement*

U.S. Customary Units	Multiply by Divide by [†]	International Units
Length/Area/Volume		
inch (in)	2.54 × 10 ⁻²	meter (m)
foot (ft)	3.048 × 10 ⁻¹	meter (m)
yard (yd)	9.144 × 10 ⁻¹	meter (m)
mile (mi, international)	1.609 344 × 10 ³	meter (m)
mile (nmi, nautical, U.S.)	1.852 × 10 ³	meter (m)
barn (b)	1 × 10 ⁻²⁸	square meter (m ²)
gallon (gal, U.S. liquid)	3.785 412 × 10 ⁻³	cubic meter (m ³)
cubic foot (ft ³)	2.831 685 × 10 ⁻²	cubic meter (m ³)
Mass/Density		
pound (lb)	4.535 924 × 10 ⁻¹	kilogram (kg)
unified atomic mass unit (amu)	1.660 539 × 10 ⁻²⁷	kilogram (kg)
pound-mass per cubic foot (lb ft ⁻³)	1.601 846 × 10 ¹	kilogram per cubic meter (kg m ⁻³)
pound-force (lbf avoirdupois)	4.448 222	newton (N)
Energy/Work/Power		
electron volt (eV)	1.602 177 × 10 ⁻¹⁹	joule (J)
erg	1 × 10 ⁻⁷	joule (J)
kiloton (kt) (TNT equivalent)	4.184 × 10 ¹²	joule (J)
British thermal unit (Btu) (thermochemical)	1.054 350 × 10 ³	joule (J)
foot-pound-force (ft lbf)	1.355 818	joule (J)
calorie (cal) (thermochemical)	4.184	joule (J)
Pressure		
atmosphere (atm)	1.013 250 × 10 ⁵	pascal (Pa)
pound force per square inch (psi)	6.984 757 × 10 ³	pascal (Pa)
Temperature		
degree Fahrenheit (°F)	[T(°F) - 32]/1.8	degree Celsius (°C)
degree Fahrenheit (°F)	[T(°F) + 459.67]/1.8	kelvin (K)
Radiation		
curie (Ci) [activity of radionuclides]	3.7 × 10 ¹⁰	per second (s ⁻¹) [becquerel (Bq)]
roentgen (R) [air exposure]	2.579 760 × 10 ⁻⁴	coulomb per kilogram (C kg ⁻¹)
rad [absorbed dose]	1 × 10 ⁻²	joule per kilogram (J kg ⁻¹) [gray (Gy)]
rem [equivalent and effective dose]	1 × 10 ⁻²	joule per kilogram (J kg ⁻¹) [sievert (Sv)]

* Specific details regarding the implementation of SI units may be viewed at <http://www.bipm.org/en/si/>.

[†] Multiply the U.S. customary unit by the factor to get the international unit. Divide the international unit by the factor to get the U.S. customary unit.

Table of Contents

1. Introduction.....	1
2. Size Distributions	2
3. Average Fragment Sizes	4
4. Rosin-Rammler Size Distributions	6
4.1 Introduction.....	6
4.2 Weibull Size Distributions	8
4.3 Gamma Size Distributions	13
4.4 Exponential Power Law Size Distributions	16
5. Universal Size Distributions.....	21
6. Simple Fragmentation	23
7. Compound Simple Fragmentation	25
7.1 One Dimension ($m = 1$)	25
7.2 Two Dimensions ($m = 2$)	26
7.2.1 Case 1 ($n/m = -1/3$)	26
7.2.2 Case 2 ($n/m = -5/6$)	26
7.2.3 Case 3 ($n/m = -5/4$)	26
7.3 Three Dimensions ($m = 3$)	27
7.3.1 Case 1 ($n/m = -1/6$)	28
7.3.2 Case 2 ($n/m = -1/3$)	28
7.3.3 Case 3 ($n/m = -1/2$)	29
7.3.4 Case 4 ($n/m = -2/3$)	29
7.3.5 Case 5 ($n/m = \pm 5/6$)	30
7.3.6 Case 6 ($n/m = -7/6$)	31
7.3.7 Case 7 ($n/m = 5/12$)	32
7.4 Theory	33
8. Piecewise Simple and Piecewise Compound Simple Fragmentation	34
8.1 Introduction.....	34
8.2 Case 1	35
8.3 Case 2.....	35
8.4 Case 3.....	36
8.5 Case 4.....	37

9. Frequency Statistics	46
10. Conclusions.....	48
References	50
Appendix A: Algebraic Conservation Laws for Simple Fragmentation Events	58
A.1. Introduction.....	58
A.2. Algebraic Forms of Conservation of Energy	58
A.3. Case 1	60
A.4. Case 2.....	62
A.5. Case 3.....	64
A.6. Case 4.....	70
A.7. Case 5.....	71
A.8. Case 6.....	72
A.9. Tensile Strain Rates	73
A.10. Extensions to Low Strain Rates	74
A.11. Conclusions.....	77
References for Appendix A	78

Table of Figures

Figure 1. Type II Weibull distribution vs. test data for explosive-filled aluminum alloy cylindrical shells with an outer radius of 25mm as reported by Edwards & Deal (2011)	28
Figure 2. Type II Weibull distributions vs. test data for ball-milling of iron from Rosin & Rammler (1934)	35
Figure 3. Type II Weibull size distributions vs. modeling data for colliding spheres obtained by the Discrete Element Method by Wittel et.al. (2008) and Carmona et. al. (2008).	36
Figure 4. Type II Weibull size distributions vs. test data for impact fragmentation of molded gypsum discs dropped from heights of 0.75m and 7m taken from Åström et. al. (2004)	37
Figure 5. Type II Weibull size distribution vs. test data in a log-log plane for an explosively-fragmented iron cylindrical shell taken from Experiment 1 of Mock & Holt (1981, 1983)	39
Figure 6. Type II Weibull size distribution vs. test data in a log-log plane for an explosively-fragmented iron cylindrical shell taken from Experiment 2 of Mock & Holt (1981, 1983).....	40
Figure 7. Type II Weibull size distributions vs. test data in a plane in which F is linear or nearly-linear for an explosively-fragmented iron cylindrical shell taken from Experiment 2 of Mock & Holt (1981, 1983).....	41
Figure 8. Type II Weibull size distributions vs. test data in a plane in which F is linear or nearly-linear for an explosively-fragmented steel cylindrical shell taken from Experiment 4 of Mock & Holt (1981, 1983).....	43
Figure 9. Type II Weibull size distribution vs. test data in a log-log plane for an explosively-fragmented steel cylindrical shell taken from Experiment 5 of Mock & Holt (1981, 1983).....	44
Figure 10. Type II Weibull size distributions vs. test data in a plane in which F is linear or nearly-linear for an explosively-fragmented steel cylindrical shell taken from Experiment 5 of Mock & Holt (1981, 1983)	45
Figure 11. Exponents in Type II Weibull size distributions (equivalently power laws) obtained in the six studies listed in Table 15	47
Figure A.1. Multiplicative constant vs. exponent n in a Type II Weibull size distribution for spherical fragments	69

Table of Tables

Table 1. Parameters for Rosin-Rammler size distributions assuming the first self-similarity condition applies	7
Table 2. Ratios of average fragment diameters for Rosin-Rammler size distributions assuming the self-similarity conditions apply.....	8
Table 3. Parameters for Type II Weibull size distributions assuming the first self-similarity condition applies	9
Table 4. Ratios of average fragment diameters for Type II Weibull size distributions assuming the self-similarity conditions apply.....	9
Table 5. Parameters for Type I Weibull size distributions assuming the first self-similarity condition applies	11
Table 6. Examples of Type II Weibull size distributions derived from geometric proofs.....	13
Table 7. Parameters for Type II Gamma size distributions.....	14
Table 8. Fundamental size distributions for integer m	21
Table 9. Examples of restrictions on reference sizes implied by universal size distributions for coagulation	22
Table 10a. Fragment size distributions for tests of solid uniformly-expanding thin rings with $m=1$	24
Table 10b. Fragment size distributions for tests of solid uniformly-expanding thin cylindrical shells with $m=2$	24
Table 10c. Fragment size distributions for tests of solid uniformly-expanding thin cylindrical shells with $m=3$	24
Table 11. Fragment size distributions for various tests involving liquids with $m=3$	24
Table 12. Universal size distributions for various compound simple fragmentation tests with $m = 3$	27
Table 13. Fragment size distributions based on curve fits to test data reported by Edwards & Deal (2011)	29
Table 14. Summary of fragments size distributions vs. material strength for two Armco Iron and four HF-1 steel cylindrical shells tested by Mock & Holt (1981, 1983).	38
Table 15. Type II Weibull size distributions (equivalently power laws) obtained in six studies of fragmentation with $m=3$	46

Effects of Mixtures on Liquid and Solid Fragment Size Distributions

Culbert B. Laney¹

Engility Corp., 8211 Terminal Rd, Lorton, VA 22079 U.S.A.

Abstract: *This paper discusses the effects of mixing diverse fragment populations. Such mixing naturally occurs when the tensile strain rates that drive fragmentation vary with time and/or space. Understanding such mixtures requires understanding the ingredients, i.e., simple fragmentation driven by steady uniform strain rates in a fixed dimension. Theoretical proofs are given showing that simple fragmentation – as well as its inverse, simple coagulation – leads to an infinite but discrete set of universal size distributions. This conclusion is a middle ground between previous studies which found one universal, two universals, or an infinite continuum of non-universals. This paper finds that complex multi-stage fragmentation events may often be treated, in aggregate, as virtual simple single-stage fragmentation events.*

Key Words: Fragmentation, coagulation, universal size distributions, Rosin-Rammler distributions, Weibull distributions, Gamma distributions, Mott-Linfoot distributions, Grady-Kipp distributions, Simmons root normal distribution, maximum entropy theory, Grady’s law, mining, milling, orbital debris, hypervelocity impact, weapon effects, atomization and sprays

1. Introduction

Fragmentation occurs in many different applications including: rock blasting for mining and excavation; materials processing such as milling, grinding, and crushing; orbital debris from artificial satellites including collisional cascades; hypervelocity impacts and collisional evolution of asteroids and meteorites; cratering, ejecta, dust, and debris from high-explosive and nuclear weapon detonations; cased munitions including sympathetic detonations; debris from high-speed projectile penetration; bubble-bearing magmatic ejecta from volcanic eruptions; burn rates in fluidized-bed combustors; and liquid atomization and sprays.

Researchers have found that manifestly-different fragmentation events may obtain the same or similar outcomes. For example, Domokos et. al. (2015) report that “fragmenting various types of materials by slowly proceeding weathering and by rapid breakup due to explosion and hammering” produces fragments size distributions and shapes with “astonishing universality ... in spite of the strongly different cracking mechanisms governing fragment formation in dynamic fragmentation initiated by explosion and hammering and in weathering induced spallation.” For another example, in a literature survey, Laney (2016) found a number of cases where liquids and solids obtained identical or nearly-identical fragment size distributions. This was true despite the fact that liquids and solids fragment in entirely different ways. In particular, liquids typically fragment via stable and unstable flows followed by secondary breakup and coagulation, while solids typically fragment via crack propagation.

Other researchers have found that seemingly-similar fragmentation events may obtain radically different outcomes. For example, in a comprehensive survey of “size distributions of asteroid

¹ E-mail address: Bert.Laney@engilitycorp.com

families ... [believed to be] remnants of parent bodies that broke into fragments,” Parker et. al. (2008) found size distributions with power law exponents ranging continuously from -0.1 to -1.04 . On this basis, they concluded that the “size distribution varies significantly [and] ... cannot be described by a universal function.” In addition, they found that many “size distributions ... display a well-defined change of slope and can [only] be modeled as a ‘broken’ double power law.”

This paper attempts to explain these divergent findings by distinguishing between simple events that produce a single type of fragment and compound events that produce mixtures of different fragments formed under different conditions at different times, in different places, and in different dimensions. Following Laney (2016), this paper draws freely on results previously obtained for various solids, liquids, and hypothetical materials, such as those studied in Discrete Element Methods (DEMs), Molecular Dynamics (MD), and other types of models. Thus this paper benefits from the progress made in a wide variety of different communities.

2. Size Distributions

Suppose fragment sizes can be described as follows:

$$X = c_i D^i \tag{1}$$

where i and c_i are constants. Notice that $c_i=1$ for $i = 1$ and $i > 3$. Also notice that $c_{-i}=1/c_i$. The three most common choices of X are as follows:

$i = 1$	$X = D$	diameter
$i = m - 1$	$X = \mathcal{A}$	surface area
$i = m$	$X = M = \rho \mathcal{V}$	mass

where $1 \leq m \leq 3$ is the fragment dimension, ρ is density, and \mathcal{V} is volume. Less common but still important choices of X are as follows:

$i = -1$	$X = 1/D$	inverse diameter
$i = -(m - 1)$	$X = 1/\mathcal{A}$	inverse surface area
$i = -m$	$X = 1/M$	inverse mass

In general, liquids produce spherical or nearly-spherical fragments; thus liquid fragments are usually characterized by $X = D$ (or D^{-1}). By contrast, in general, solids produce rough irregular fragments. Thus solid fragments are usually characterized by $X = M$ (or M^{-1}).

Because it is difficult measure directly, the surface area \mathcal{A} is rarely used to characterize either liquid or solid fragments. However, as discussed in Appendix A, \mathcal{A} is a natural choice, because the work required to create fragments is proportional to \mathcal{A} .

For example, for spherical fragments such as liquid droplets:

$$m = 3; \quad c_2 = \pi; \quad c_3 = \rho\pi/6$$

For another example, for solids such as rock, Domokos et. al. (2015) found that “above a characteristic size the overall shape of all fragments can be well approximated by rectangles of dimensions 1: 1.56 : 2.32.” Let D be the middle dimension and let:

$$AR_1 = 1/1.56 = 0.641 \text{ and } AR_2 = 2.32/1.56 = 1.487$$

be the aspect ratios. Then:

$$m = 3; \quad c_2 = 2(AR_1 + AR_2 + AR_2AR_1) = 6.163; \quad c_3 = AR_2AR_1\rho = 0.953\rho$$

For comparison, perfectly square fragments obtain:

$$m = 3; \quad c_2 = 6.; \quad c_3 = \rho$$

As a final example, Wittel et. al. (2006) measured “regular isotopic” solid shell fragments to find $m = 2$ and “needle-like” plate glass fragments to find $m = 1.5$, which “implies that fragments have a self-affine character, meaning that the larger they are, the more elongated they get.”

Because researchers rarely specify m , it must usually be estimated from experimental photographs or written descriptions of fragment shapes. More specifically, if the aspect ratio does not depend on fragment size, and if the fragments retain two parallel surfaces from the original body, then $m = 2$. Alternatively, if the aspect ratio does not depend on fragment size, and if the fragments do not retain any surfaces from the original body, then $m = 3$.

Fragment size distributions may be described by $f(X)$, i.e., the number fraction of fragments in a range dX centered on X divided by dX . In standard probability theory, $f(X)$ is called the *probability density function (PDF)*. Notice that $f(X)$ is always non-negative such that:

$$\int_0^{\infty} f(X)dX = 1 \tag{2a}$$

Alternatively, fragment size distributions may be described by $f_Y(X)$, i.e., the Y fraction of fragments in a range dX centered on X divided by dX where $Y = c_j D^j$. Notice that $f_Y(X)$ is always non-negative such that:

$$\int_0^{\infty} f_Y(X) dX = 1 \quad (2b)$$

Also notice that:

$$f_Y(X) = \frac{Yf(X)}{\int_0^{\infty} Yf(X) dX} \quad (3)$$

3. Average Fragment Sizes

Consider the following averages based on diameter, surface area, mass, and so forth:

$$X_{avg} = \int_0^{\infty} Xf(X) dX \quad (4)$$

$$X_{Y avg} = \int_0^{\infty} Xf_Y(X) dX = \frac{\int_0^{\infty} XYf(X) dX}{\int_0^{\infty} Yf(X) dX} \quad (5)$$

where $X = c_i D^i$ and $Y = c_j D^j$. The best known examples are as follows:

$$D_{avg} = \int_0^{\infty} Df(D) dD \quad (6)$$

$$D_{M avg} = \int_0^{\infty} Df_M(D) dD \quad (7)$$

which are known as the *count mean diameter (CMD)* and the *mass mean diameter (MMD)*, respectively. Less common but still important, consider the following averages based on inverse diameter, inverse surface area, inverse mass, and so forth:

$$\frac{1}{X'_{avg}} = \int_0^{\infty} \frac{f(X)}{X} dX \quad (8)$$

$$\frac{1}{X'_{Y avg}} = \int_0^{\infty} \frac{f_Y(X)}{X} dX = \frac{\int_0^{\infty} \frac{Yf(X)}{X} dX}{\int_0^{\infty} Yf(X) dX} \quad (9)$$

The best known example is as follows:

$$\frac{1}{D'_{M avg}} = \int_0^{\infty} \frac{f_M(D)}{D} dD \quad (10a)$$

or equivalently:

$$D'_{M avg} = \frac{1}{\int_0^{\infty} \frac{f_M(D)}{D} dD} \quad (10b)$$

which is called the *Sauter mass mean diameter (SMD)*.

Consider the following ratios of average fragment diameters:

$$Q_X = \frac{D_{X avg}}{D_{avg}} \quad Q'_X = \frac{D'_{X avg}}{D'_{avg}} \quad (11)$$

$$R = \frac{D_{avg}}{D'_{avg}} \quad (12)$$

$$R_X = \frac{D_{X avg}}{D'_{X avg}} \quad (13)$$

For Equation (13), the best known example is R_M as seen in, e.g., Simmons (1977), Wu et. al. (1991), Chou & Faeth (1998), and Sallam et. al. (2006).

Finally, consider the following ratio of average fragment sizes:

$$S_X \equiv \frac{X_{ref}}{c_i D_{ref}^i} \quad (14)$$

where X_{ref} may be X_{avg} , X'_{avg} , $X_{Y avg}$, or $X'_{Y avg}$ and D_{ref} may be D_{avg} , D'_{avg} , $D_{Y avg}$, or $D'_{Y avg}$.

4. Rosin-Rammler Size Distributions

4.1 Introduction

Rosin-Rammler size distributions may be defined as follows:

$$f(D) = \frac{1}{AD_{ref}} \left(\frac{D}{D_{ref}} \right)^l \exp \left[-|a| \left(\frac{D}{D_{ref}} \right)^n \right] \quad (15a)$$

where a , A , l , and n are parameters and D_{ref} is a reference diameter. If $Y = c_j D^j$, Equation (15a) can be rewritten as follows:

$$f_Y(D) = \frac{1}{A_Y D_{ref}} \left(\frac{D}{D_{ref}} \right)^{l+j} \exp \left[-|a| \left(\frac{D}{D_{ref}} \right)^n \right] \quad (15b)$$

If $X = c_i D^i$, Equations (15a) and (15b) can be rewritten as follows:

$$f(X) = \frac{S_X}{iAX_{ref}} \left(\frac{S_X X}{X_{ref}} \right)^{\frac{l+1}{i}-1} \exp \left[-|a| \left(\frac{S_X X}{X_{ref}} \right)^{\frac{n}{i}} \right] \quad (16a)$$

$$f_Y(X) = \frac{S_X}{iA_Y X_{ref}} \left(\frac{S_X X}{X_{ref}} \right)^{\frac{l+j+1}{i}-1} \exp \left[-|a| \left(\frac{S_X X}{X_{ref}} \right)^{\frac{n}{i}} \right] \quad (16b)$$

By Equation (2):

$$A = \frac{1}{|n|} |a|^{-\frac{l+1}{n}} \Gamma \left(\frac{l+1}{n} \right) \quad (17)$$

$$A_Y = \frac{1}{|n|} |a|^{-\frac{l+j+1}{n}} \Gamma \left(\frac{l+j+1}{n} \right) \quad (18)$$

Laney (2015b) suggested three self-similarity conditions:

1. When a size distribution is expressed in terms of a given average size, it should actually obtain that average size.
2. When a size distribution is expressed in terms of a given average size, and that average size changes, key free parameters in the size distribution should remain the same.
3. When a size distribution is expressed in terms of a given average size, and that average size changes, the size distribution should stay the same.

Table 1 shows parameters for Rosin-Rammler size distributions. This table assume that the first self-similarity condition applies and that $Z = c_k D^k$.

Table 1. Parameters for Rosin-Rammler size distributions assuming the first self-similarity condition applies.

	$D_{ref} = D_{avg}$	$D_{ref} = D_{Z_{avg}}$	$D_{ref} = D'_{avg}$	$D_{ref} = D'_{Z_{avg}}$
$ a $	$\frac{\Gamma\left(\frac{l+2}{n}\right)^n}{\Gamma\left(\frac{l+1}{n}\right)^n}$	$\frac{\Gamma\left(\frac{l+k+2}{n}\right)^n}{\Gamma\left(\frac{l+k+1}{n}\right)^n}$	$\frac{\Gamma\left(\frac{l+1}{n}\right)^n}{\Gamma\left(\frac{l}{n}\right)^n}$	$\frac{\Gamma\left(\frac{l+k+1}{n}\right)^n}{\Gamma\left(\frac{l+k}{n}\right)^n}$
S_X	$\frac{\Gamma\left(\frac{l+i+1}{n}\right)}{ a ^{i/n} \Gamma\left(\frac{l+1}{n}\right)}$	$\frac{\Gamma\left(\frac{l+i+k+1}{n}\right)}{ a ^{i/n} \Gamma\left(\frac{l+k+1}{n}\right)}$	$\frac{\Gamma\left(\frac{l+1}{n}\right)}{ a ^{i/n} \Gamma\left(\frac{l-i+1}{n}\right)}$	$\frac{\Gamma\left(\frac{l+k+1}{n}\right)}{ a ^{i/n} \Gamma\left(\frac{l-i+k+1}{n}\right)}$

The second self-similarity condition is true for Rosin-Rammler size distributions if:

$$l = l_1 = l_2 \quad (19a)$$

$$n = n_1 = n_2 \quad (19b)$$

where the subscripts 1 and 2 refer to any two reference diameters. As it turns out, Equation (19) also ensures the third self-similarity condition, at least for the averages described in Section 3.

To prove this, notice that the second and third self-similarity conditions are both true if:

$$f(D) = \frac{1}{A_1 D_{ref1}} \left(\frac{D}{D_{ref1}} \right)^l \exp \left[-|a_1| \left(\frac{D}{D_{ref1}} \right)^n \right] = \frac{1}{A_2 D_{ref2}} \left(\frac{D}{D_{ref2}} \right)^l \exp \left[-|a_2| \left(\frac{D}{D_{ref2}} \right)^n \right]$$

This is true if:

$$A_1 D_{ref1}^{l+1} = A_2 D_{ref2}^{l+1}$$

$$|a_1| D_{ref1}^{-n} = |a_2| D_{ref2}^{-n}$$

Multiply the first equation by the second equation taken to the $(l+1)/n$ power to obtain:

$$A_1 |a_1|^{\frac{l+1}{n}} = A_2 |a_2|^{\frac{l+1}{n}}$$

By Equation (17), this is true because:

$$A_1 |a_1|^{\frac{l+1}{n}} = A_2 |a_2|^{\frac{l+1}{n}} = \frac{1}{|n|} \Gamma\left(\frac{l+1}{n}\right)$$

Table 2 shows expressions for the ratios of fragment diameters assuming the self-similarity conditions apply. As before, Table 2 assumes $X = c_i D^i$.

Table 2. Ratios of average fragment diameters for Rosin-Rammler size distributions assuming the self-similarity conditions apply.

$Q_x = \frac{\Gamma\left(\frac{l+1}{n}\right)\Gamma\left(\frac{l+i+2}{n}\right)}{\Gamma\left(\frac{l+2}{n}\right)\Gamma\left(\frac{l+i+1}{n}\right)}$	$R = \frac{\Gamma\left(\frac{l+2}{n}\right)\Gamma\left(\frac{l}{n}\right)}{\Gamma\left(\frac{l+1}{n}\right)^2}$	$R_x = \frac{\Gamma\left(\frac{l+i+2}{n}\right)\Gamma\left(\frac{l+i}{n}\right)}{\Gamma\left(\frac{l+i+1}{n}\right)^2}$
---	---	---

The following subsections focus on three specific classes of Rosin-Rammler size distributions that have proven physical meanings.

4.2 Weibull Size Distributions

As defined here, a Weibull size distribution can be written in the following form:

$$\text{const. } x^{b-1} \exp[-\text{const. } x^b]$$

where x is some measure of fragment size. As one special case, consider Rosin-Rammler size distributions with $l = n-1$ and $a > 0$:

$$f(D) = \frac{1}{AD_{ref}} \left(\frac{D}{D_{ref}}\right)^{n-1} \exp\left[-a\left(\frac{D}{D_{ref}}\right)^n\right] \quad (20a)$$

or equivalently:

$$f_Y(D) = \frac{1}{A_Y D_{ref}} \left(\frac{D}{D_{ref}}\right)^{n+j-1} \exp\left[-a\left(\frac{D}{D_{ref}}\right)^n\right] \quad (20b)$$

where, as usual, $Y = c_j D^j$. Equations (20a) and (20b) can be rewritten as follows:

$$f(X) = \frac{S_X}{iAX_{ref}} \left(\frac{S_X X}{X_{ref}}\right)^{\frac{n}{i}-1} \exp\left[-a\left(\frac{S_X X}{X_{ref}}\right)^{\frac{n}{i}}\right] \quad (21a)$$

$$f_Y(X) = \frac{S_X}{iA_Y X_{ref}} \left(\frac{S_X X}{X_{ref}} \right)^{\frac{n+j}{i}-1} \exp \left[-a \left(\frac{S_X X}{X_{ref}} \right)^{\frac{n}{i}} \right] \quad (21b)$$

where, as usual, $X = c_i D^i$. By Equations (17) and (18):

$$A = \frac{1}{a|n|} \quad (22)$$

$$A_Y = \frac{1}{|n|} a^{-\left(1+\frac{j}{n}\right)} \Gamma\left(1+\frac{j}{n}\right) \quad (23)$$

Table 3 shows results for other parameters assuming that $l = n-1$ and that the first self-similarity condition applies. As before, $Z = c_k D^k$.

Table 3. Parameters for Type II Weibull size distributions assuming the first self-similarity condition applies.

	$D_{ref} = D_{avg}$	$D_{ref} = D_{Zavg}$	$D_{ref} = D'_{avg}$	$D_{ref} = D'_{Zavg}$
a	$\Gamma\left(1+\frac{1}{n}\right)^n$	$\frac{\Gamma\left(1+\frac{k+1}{n}\right)^n}{\Gamma\left(1+\frac{k}{n}\right)^n}$	$\Gamma\left(1-\frac{1}{n}\right)^{-n}$	$\frac{\Gamma\left(1+\frac{k}{n}\right)^n}{\Gamma\left(1+\frac{k-1}{n}\right)^n}$
S_X	$\frac{\Gamma\left(1+\frac{i}{n}\right)}{a^{i/n}}$	$\frac{\Gamma\left(1+\frac{k+i}{n}\right)}{a^{i/n} \Gamma\left(1+\frac{k}{n}\right)}$	$\frac{1}{a^{i/n} \Gamma\left(1-\frac{i}{n}\right)}$	$\frac{\Gamma\left(1+\frac{k}{n}\right)}{a^{i/n} \Gamma\left(1+\frac{k-i}{n}\right)}$

Table 4 shows expressions ratios of fragment diameters assuming the self-similarity condition applies. As before, $X = c_i D^i$.

Table 4. Ratios of average fragment diameters for Type II Weibull size distributions assuming the self-similarity conditions apply.

$Q_x = \frac{\Gamma\left(1+\frac{i+1}{n}\right)}{\Gamma\left(1+\frac{1}{n}\right)\Gamma\left(1+\frac{i}{n}\right)}$	$R = \Gamma\left(1+\frac{1}{n}\right)\Gamma\left(1-\frac{1}{n}\right)$	$R_x = \frac{\Gamma\left(1+\frac{i+1}{n}\right)\Gamma\left(1+\frac{i-1}{n}\right)}{\Gamma\left(1+\frac{i}{n}\right)^2}$
---	--	---

As another special case, consider Rosin-Rammler size distributions with $l = n - j - 1$ and $a > 0$:

$$f_Y(D) = \frac{1}{A_Y D_{ref}} \left(\frac{D}{D_{ref}} \right)^{n-1} \exp \left[-a \left(\frac{D}{D_{ref}} \right)^n \right] \quad (24a)$$

or equivalently:

$$f(D) = \frac{1}{AD_{ref}} \left(\frac{D}{D_{ref}} \right)^{n-j-1} \exp \left[-a \left(\frac{D}{D_{ref}} \right)^n \right] \quad (24b)$$

where, as usual, $Y = c_j D^j$. Equations (24a) and (24b) can be rewritten as follows:

$$f_Y(X) = \frac{S_X}{iA_Y X_{ref}} \left(\frac{S_X X}{X_{ref}} \right)^{\frac{n}{i}-1} \exp \left[-a \left(\frac{S_X X}{X_{ref}} \right)^{\frac{n}{i}} \right] \quad (25a)$$

$$f(X) = \frac{S_X}{iAX_{ref}} \left(\frac{S_X X}{X_{ref}} \right)^{\frac{n-j}{i}-1} \exp \left[-a \left(\frac{S_X X}{X_{ref}} \right)^{\frac{n}{i}} \right] \quad (25b)$$

where, as usual, $X = c_i D^i$ and $Y = c_j D^j$. By Equations (17) and (18):

$$A = \frac{1}{|n|} a^{-\left(1-\frac{j}{n}\right)} \Gamma\left(1-\frac{j}{n}\right) \quad (26)$$

$$A_Y = \frac{1}{a|n|} \quad (27)$$

Table 5 shows results for other parameters assuming that $l = n - j - 1$ and that the first self-similarity condition applies. As before, $Z = c_k D^k$.

Table 5. Parameters for Type I Weibull size distributions assuming the first self-similarity condition applies.

	$D_{ref} = D_{avg}$	$D_{ref} = D_{Zavg}$	$D_{ref} = D'_{avg}$	$D_{ref} = D'_{Zavg}$
a	$\frac{\Gamma\left(1 - \frac{j-1}{n}\right)^n}{\Gamma\left(1 - \frac{j}{n}\right)^n}$	$\frac{\Gamma\left(1 - \frac{j-k-1}{n}\right)^n}{\Gamma\left(1 - \frac{j-k}{n}\right)^n}$	$\frac{\Gamma\left(1 - \frac{j}{n}\right)^n}{\Gamma\left(1 - \frac{j+1}{n}\right)^n}$	$\frac{\Gamma\left(1 - \frac{j-k}{n}\right)^n}{\Gamma\left(1 - \frac{j-k+1}{n}\right)^n}$
S_X	$\frac{\Gamma\left(1 - \frac{j-i}{n}\right)}{a^{i/n} \Gamma\left(1 - \frac{j}{n}\right)}$	$\frac{\Gamma\left(1 - \frac{j-k-i}{n}\right)}{a^{i/n} \Gamma\left(1 - \frac{j-k}{n}\right)}$	$\frac{\Gamma\left(1 - \frac{j}{n}\right)}{a^{i/n} \Gamma\left(1 - \frac{j+i}{n}\right)}$	$\frac{\Gamma\left(1 - \frac{j-k}{n}\right)}{a^{i/n} \Gamma\left(1 - \frac{j-k+i}{n}\right)}$

With the parameter choices shown in Tables 3 and 5, Weibull size distributions satisfy all three self-similarity conditions. In particular, the key parameter n does not depend on D_{ref} .

Not all combinations of i, j, k , and n are allowed. For example, suppose $D_{ref} = D_{avg}$ and $j = k = 0$. Then Tables 3 and 5 give the following:

$$a = \Gamma\left(1 + \frac{1}{n}\right)^n$$

which is valid if and only if $n < -1$ or $n > 0$. For another example, suppose $D_{ref} = D'_{avg}$ and $j = k = 0$. Then Tables 3 and 5 give the following:

$$a = \Gamma\left(1 - \frac{1}{n}\right)^{-n}$$

which is valid if and only if $n < 0$ or $n > 1$.

Notice that, for $n < 0$, Weibull size distribution become power law size distributions when $D \gg D_{ref}$. *This treatment assumes that power law size distributions are, in fact, the large size limit of Weibull size distributions with $n < 0$; see also Laney (2015b).*

As seen in Laney (2015b), the most common Weibull forms can be designated as Types I and II. More specifically, Type I Weibull size distributions can be written as follows:

$$f_M(D) = \frac{1}{AD_{ref}} \left(\frac{D}{D_{ref}}\right)^{n-1} \exp\left[-a \left(\frac{D}{D_{ref}}\right)^n\right] \quad (28a)$$

$$f_M(M) = \frac{S_M}{mAM_{ref}} \left(\frac{S_M M}{M_{ref}} \right)^{\frac{n}{m}-1} \exp \left[-a \left(\frac{S_M M}{M_{ref}} \right)^{\frac{n}{m}} \right] \quad (28b)$$

and Type II Weibull size distributions can be written as follows:

$$f(D) = \frac{1}{AD_{ref}} \left(\frac{D}{D_{ref}} \right)^{n-1} \exp \left[-a \left(\frac{D}{D_{ref}} \right)^n \right] \quad (29a)$$

$$f(M) = \frac{S_M}{mAM_{ref}} \left(\frac{S_M M}{M_{ref}} \right)^{\frac{n}{m}-1} \exp \left[-a \left(\frac{S_M M}{M_{ref}} \right)^{\frac{n}{m}} \right] \quad (29b)$$

The Type I is obtained from Equations (24) and (25) with $X = Y = M$ or, equivalently, $i = j = m$. The Type II is obtained from Equations (20) and (21) with $X = M$ or, equivalently, $i = m$.

Weibull size distributions with $n > 0$ are often associated with ductile materials while those with $n < 0$ are often associated with brittle shatter-prone materials. However, as seen later, any material – including simple liquids like water – can fragment with either $n > 0$ or $n < 0$. Instead of ductile vs. brittle, which can change with strain rate, this treatment distinguishes $n > 0$ from $n < 0$ based on fragment geometry.

As seen in Table 6, there is an association between Type II Weibull size distributions and geometry, a.k.a., perfect packing theory. More specifically, Type II Weibull distributions with $n > 0$ are associated with cases where adjacent fragments meet along extended lines or surfaces, so that the parts to fit together like jigsaw puzzle pieces, e.g., tessellations, subdivisions. Similarly, Type II Weibull size distributions with $n < 0$ are associated with cases where adjacent fragments meet only at a single point, e.g., fractals, Apollonian sphere packings.

Table 6. Examples of Type II Weibull size distributions derived from geometric proofs. Cowan (2010) and Gilvarry (1961) are exact while the others are numerical approximations. For negative n , the original results are power laws.

n/m	n	m	Description	Reference
1	2	2	Various random subdivisions by straight lines based on Poisson distributions.	Grady & Kipp (1985) Cowan (2010)
-1/2 to -1	-1 to -2	2	Various random 2D circle, triangle, square, and diamond packings. The most common value of n is ~ -1.3 .	Aste (1996)
-2/3	-2	3	Random subdivision by arbitrary surfaces, lines, and points based on mutually-independent Poisson distributions assuming the fragments are “geometrically similar.”	Gilvarry (1961) Gilvarry & Bergstrom (1961)
-2/3 to -1	-2 to -3	3	Various random 3D Apollonian sphere packings. The most common value of n is ~ -2.5	Lind et. al. (2008)

As shown by Laney (2015b), Type I, Type II, and other types of Weibull size distribution mimic each other, except for very large or very small fragments. As a result, without exact solutions, it is hard to distinguish the real size distributions from their close approximations. Fortunately, there is at least one exact solution. More specifically, for certain kinds of linear subdivisions, Cowan (2010) proved that a Type II Weibull distribution – and not any other type of Weibull size distribution – is an exact geometric solution.

More importantly, Brown & Woheltz (1995) gave an exact semi-geometric proof for Type II Weibull distributions in general. First, they introduced a simplified form of the Population Balance Equation (PBE) involving a “single-event particle distribution function;” see also, e.g., Hamilton et al. (2003) and Kostoglou & Karabelas (2004). Next, based on geometric theory, they argued that the single-event particle distribution function is a power law; see also, e.g., Turcotte (1986). Finally, they proved that Type II Weibull distributions are the exact analytic solutions of their simplified Population Balance Equation.

Based on the available evidence, it will be assumed that *Type II Weibull size distributions uniquely represent fragment geometries.*

4.3 Gamma Size Distributions

As defined here, a Gamma size distribution can be written in the following form:

$$\text{const. } x^{b-1} \exp[-|b|x^n]$$

where x is some measure of fragment size. As one special case, consider Rosin-Rammler size distributions with $l = a - 1$:

$$f(D) = \frac{1}{AD_{ref}} \left(\frac{D}{D_{ref}} \right)^{a-1} \exp \left[-|a| \left(\frac{D}{D_{ref}} \right)^n \right] \quad (30a)$$

or equivalently:

$$f_Y(D) = \frac{1}{A_Y D_{ref}} \left(\frac{D}{D_{ref}} \right)^{a+j-1} \exp \left[-|a| \left(\frac{D}{D_{ref}} \right)^n \right] \quad (30b)$$

Equations (30a) and (30b) can be rewritten as follows:

$$f(X) = \frac{S_X}{iAX_{ref}} \left(\frac{S_X X}{X_{ref}} \right)^{\frac{a}{i}-1} \exp \left[-|a| \left(\frac{S_X X}{X_{ref}} \right)^{\frac{n}{i}} \right] \quad (31a)$$

$$f_Y(X) = \frac{S_X}{iA_Y X_{ref}} \left(\frac{S_X X}{X_{ref}} \right)^{\frac{a+j}{i}-1} \exp \left[-|a| \left(\frac{S_X X}{X_{ref}} \right)^{\frac{n}{i}} \right] \quad (31b)$$

where, as usual, $X = c_i D^i$ and $Y = c_j D^j$. These will be called Type II Gamma size distributions; see also Laney (2015b). Notice that earlier treatments, including Laney (2015b), were limited to positive a . However, this treatment allows both negative and positive a .

Section 4.1 gives expressions for n , A , A_Y and S_X as functions of a and X_{ref} . For example, see Table 7. As shown by Laney (2015b), with the parameter choices given in Table 7, Type II Gamma size distributions satisfy the first and third self-similarity conditions, but not the second self-similarity condition. In other words, the key parameter a depends on the choice of D_{ref} .

Table 7. Parameters for Type II Gamma size distributions.

	$D_{ref} = D_{avg}$	$D_{ref} = D_{Zavg}$	$D_{ref} = D'_{avg}$	$D_{ref} = D'_{Zavg}$
$ a $	$\frac{\Gamma\left(\frac{a+1}{n}\right)^n}{\Gamma\left(\frac{a}{n}\right)^n}$	$\frac{\Gamma\left(\frac{a+k+1}{n}\right)^n}{\Gamma\left(\frac{a+k}{n}\right)^n}$	$\frac{\Gamma\left(\frac{a}{n}\right)^n}{\Gamma\left(\frac{a-1}{n}\right)^n}$	$\frac{\Gamma\left(\frac{a+k}{n}\right)^n}{\Gamma\left(\frac{a+k-1}{n}\right)^n}$
S_X	$\frac{\Gamma\left(\frac{a+i}{n}\right)}{ a ^{i/n} \Gamma\left(\frac{a}{n}\right)}$	$\frac{\Gamma\left(\frac{a+i+k}{n}\right)}{ a ^{i/n} \Gamma\left(\frac{a+k}{n}\right)}$	$\frac{\Gamma\left(\frac{a}{n}\right)}{ a ^{i/n} \Gamma\left(\frac{a-i}{n}\right)}$	$\frac{\Gamma\left(\frac{a+k}{n}\right)}{ a ^{i/n} \Gamma\left(\frac{a-i+k}{n}\right)}$

Table 7 gives implicit expressions for n as a function of a . In general, these must be solved iteratively. However, if $a > 0$ and $D_{ref} = D_{avg}$, there is a simple analytical solution:

$$n = 1$$

which follows from $\Gamma(a+1) = a\Gamma(a)$. Similarly, if $a < 0$ and $D_{ref} = D'_{avg}$, there is a simple analytical solution:

$$n = -1$$

As another special case, consider Rosin-Rammler size distributions with $l = iaS_X^{n/i} - 1$:

$$f(X) = \frac{S_X^{aS_X^{n/i}}}{iAX_{ref}} \left(\frac{X}{X_{ref}} \right)^{aS_X^{n/i} - 1} \exp \left[-|a| S_X^{n/i} \left(\frac{X}{X_{ref}} \right)^{n/i} \right] \quad (32a)$$

or equivalently:

$$f_Y(X) = \frac{S_X^{aS_X^{n/i}}}{iA_Y X_{ref}} \left(\frac{X}{X_{ref}} \right)^{aS_X^{n/i} + j/i - 1} \exp \left[-|a| S_X^{n/i} \left(\frac{X}{X_{ref}} \right)^{n/i} \right] \quad (32b)$$

If $X = M$, these will be called Type IV Gamma size distributions. This is a short but opaque definition. Laney (2015b) gives a longer but clearer definition of Type IV Gamma size distributions.

More generally, every X is associated with a different type of Gamma size distribution. However, regardless of type, Gamma size distributions satisfy the first and third self-similarity conditions, but not the second self-similarity condition. In other words, the key parameter a always depends on D_{ref} .

Similar to Weibull size distributions, there is a strong association between Gamma size distributions and geometrical theory. In fact, the research literature suggests the three possible geometrical interpretations:

1. Kiang (1966) argued that Type IV Gamma size distributions approximate fragment size distributions. As evidence, he showed that Type IV Gamma size distributions approximate the results of Voronoi tessellation. The association between Gamma size distributions and Voronoi tessellation has been confirmed by numerous subsequent researchers, e.g., Ferenc & Néda (2007). However, the association between Voronoi tessellation and fragmentation has not been confirmed. To the contrary, Grady & Kipp (1985) observed that while “Kiang has very strongly stated his belief that the Voronoi method is at the foundation of random fragmentation, ... we personally feel that the Voronoi construction introduces too much correlation among neighboring points to

provide a good description of fragmentation.” Having said this, there is limited evidence that Voronoi tessellation represents cases where both fragmentation and its inverse, coagulation, occur; see, e.g., Appendix A.1 in Laney (2016).

2. Melzak (1953) argued that Type IV Gamma size distributions are the natural initial conditions for coagulation. More specifically, he showed that the Smoluchowski coagulation equation has an analytical solution if the initial size distribution is a Type IV Gamma size distribution; see also Friedlander & Wang (1966), Scott (1968), and Lindblad (2005, 2007).

3. Villiermaux et. al. (2004) and Marmottant & Villiermaux (2004) argued that Type II Gamma size distributions are the natural final conditions for the Smoluchowski coagulation equation. The proof is similar to that given by Brown & Woheltz (1995), as discussed above.

This treatment will adopt the third and most modern interpretation. In fact, the proof given by Villiermaux et. al. (2004) and Marmottant & Villiermaux (2004) appears to be equally valid for Gamma size distributions associated with diameter (Type II), inverse diameter, surface area, inverse surface area, mass (Type IV), inverse mass, and so forth. In other words, based on the available evidence, it will be assumed that *various types of Gamma size distributions represent coagulation geometries*.

Recent research has shown that, in some cases, fragmentation is inextricably linked with coagulation. For example, Villiermaux et. al. (2004) argued that a common liquid “fragmentation mechanism . . . , somewhat surprisingly, consists of a coalescence process.” Similarly, Marmottant & Villiermaux (2004) note that liquid “blobs, just before breakup, interact, and that the interaction is of a coalescence or aggregation type.” Less commonly, solids can experience something like coagulation due to surface deformation such as occurs in explosive consolidation of powders, surface melting, surface wetness, electrostatic forces, magnetic forces, chemical forces, gravitational forces, van der Waals forces, and so forth; see, e.g., Brilliantov (2015), Vledouts et. al. (2015, 2016a).

4.4 Exponential Power Law Size Distributions

As defined here, an exponential power law size distribution can be written in the following form:

$$\text{const.} \exp[-\text{const.} x^b]$$

where x is some measure of fragment size. As one special case, consider Rosin-Rammler size distributions with $l = i - 1$ and $a > 0$:

$$f(X) = \frac{S_x}{iAX_{ref}} \exp \left[-a \left(\frac{S_x X}{X_{ref}} \right)^{\frac{n}{i}} \right] \quad (33a)$$

$$f_Y(X) = \frac{S_X}{iA_Y X_{ref}} \left(\frac{S_X X}{X_{ref}} \right)^{\frac{j}{i}} \exp \left[-a \left(\frac{S_X X}{X_{ref}} \right)^{\frac{n}{i}} \right] \quad (33b)$$

where, as usual, $X = c_i D^i$ and $Y = c_j D^j$. Section 4.1 gives expressions for a , A , A_Y and S_X as functions of n and X_{ref} . For example, by Equations (17) and (18):

$$A = \frac{1}{|n|} a^{-\frac{i}{n}} \Gamma\left(\frac{i}{n}\right) \quad (34)$$

$$A_Y = \frac{1}{|n|} a^{-\frac{i+j}{n}} \Gamma\left(\frac{i+j}{n}\right) \quad (35)$$

As another special case, consider Rosin-Rammler size distributions with $l = i - j - 1$ and $a > 0$:

$$f_Y(X) = \frac{S_X}{iA_Y X_{ref}} \exp \left[-a \left(\frac{S_X X}{X_{ref}} \right)^{\frac{n}{i}} \right] \quad (36a)$$

or equivalently:

$$f(X) = \frac{S_X}{iAX_{ref}} \left(\frac{S_X X}{X_{ref}} \right)^{-\frac{j}{i}} \exp \left[-a \left(\frac{S_X X}{X_{ref}} \right)^{\frac{n}{i}} \right] \quad (36b)$$

where, as usual, $X = c_i D^i$ and $Y = c_j D^j$. As before, Section 4.1 gives expressions for a , A , A_Y and S_X as functions of n and X_{ref} . For example, by Equations (17) and (18):

$$A = \frac{1}{|n|} a^{-\frac{i-j}{n}} \Gamma\left(\frac{i-j}{n}\right) \quad (37)$$

$$A_Y = \frac{1}{|n|} a^{-\frac{i}{n}} \Gamma\left(\frac{i}{n}\right) \quad (38)$$

With the parameter choices shown in Tables 1 and 2, exponential power law size distributions satisfy all three self-similarity conditions. In other words, the key parameter n does not depend on D_{ref} .

The following is a generalization of a maximum entropy proof given by Cousin et. al. (1996). Entropy is defined as follows:

$$S = -\text{const.} \int_0^{\infty} f(X) \ln[f(X)] dX \quad (39)$$

Based on Equation (2), two possible constraints are as follows:

$$\int_0^{\infty} f(X) dX = 1 \quad (40)$$

$$\int_0^{\infty} f_Y(X) dX = 1 \quad (41)$$

where, as usual, $X = c_i D^i$ and $Y = c_j D^j$. Using Lagrange multipliers to maximize entropy subject to these two constraints:

$$f(X) = \text{const.} \exp(-\text{const.} X^{j/i}) \quad (42)$$

Notice that Equation (42) is the same as Equation (33a) if $n = j$. Also notice that Equation (42) does not automatically ensure Equations (40) and (41). Rather, the two constants must be chosen specifically to ensure Equations (40) and (41). While Equation (40) is usually enforced, Equation (41) is rarely enforced.

As one example, suppose that:

$$X = Y = M$$

Then Equations (40) and (41) become:

$$\int_0^{\infty} f(M) dM = 1 \quad (43)$$

$$\int_0^{\infty} M f(M) dM = M_{\text{avg}} \quad (44)$$

In addition, Equation (42) becomes:

$$f(M) = \text{const.} \exp(-\text{const.} M) \quad (45a)$$

or equivalently:

$$f(D) = \text{const.} D^{m-1} \exp(-\text{const.} D^m) \quad (45b)$$

Notice that Grady & Kipp (1985) obtained Equation (45a) for $m = 2$ while Li & Tankin (1987) obtained Equation (45b) for $m = 3$.

As alternatives to Equations (40) and (41), two possible constraints are as follows:

$$\int_0^{\infty} f(X) dX = 1 \quad (46)$$

$$\int_0^{\infty} f_{\frac{1}{Y}}(X) dX = 1 \quad (47)$$

Using Lagrange multipliers to maximize entropy subject to these two constraints:

$$f(X) = \text{const.} \exp(-\text{const.} X^{-j/i}) \quad (48)$$

Notice that this is the same as Equation (33a) if $n = -j$. As one example, suppose that:

$$X = Y = M$$

Then Equations (46) and (47) become:

$$\int_0^{\infty} f(M) dM = 1 \quad (49)$$

$$\int_0^{\infty} \frac{f(M)}{M} dM = \frac{1}{M'_{avg}} \quad (50)$$

In addition, Equation (48) becomes:

$$f(M) = \text{const.} \exp\left(-\frac{\text{const.}}{M}\right) \quad (51)$$

Finally, suppose the two constraints are as follows:

$$\int_0^{\infty} f_Y(X) dX = 1 \quad (52)$$

$$\int_0^{\infty} f_{YZ^{\pm 1}}(X) dX = 1 \quad (53)$$

where, as usual, $X = c_i D^i$, $Y = c_j D^j$, and $Z = c_k D^k$. Using Lagrange multipliers to maximize entropy subject to these two constraints:

$$f_Y(X) = \text{const.} \exp(-\text{const.} X^{\pm k/i}) \quad (54)$$

This is the same as Equation (36a) if $n = \pm k$.

Suppose that more than two constraints are imposed. For example, Ahmadi & Sellens (1993) imposed four constraints as follows:

$$\int_0^{\infty} f(D) dD = 1 \quad (55)$$

$$\int_0^{\infty} f_{1/D}(D) dD = \text{const.} \int_0^{\infty} \frac{1}{D} f(D) dD = 1 \quad (56)$$

$$\int_0^{\infty} f_{D^2}(D) dD = \text{const.} \int_0^{\infty} D^2 f(D) dD = 1 \quad (57)$$

$$\int_0^{\infty} f_{D^3}(D) dD = \text{const.} \int_0^{\infty} D^3 f(D) dD = 1 \quad (58)$$

and obtained:

$$f(D) = \text{const.} \exp\left(-\frac{\text{const.}}{D} - \text{const.} D^2 - \text{const.} D^3\right) \quad (59)$$

In this case, and in general, multiple constraints lead to exponentials of linear combinations of powers of D . Notice that Equation (59) does not automatically ensure Equations (55) to (58). Rather, the four constants must be chosen specifically to ensure Equations (55) to (58), which requires solving a 4×4 system of equations.

For more information on maximum entropy theory see, e.g., the surveys by Englman (1996), Babinsky & Sojka (2002), Dumouchel (2009), and Déchelette et. al. (2011). Based on the available evidence, it will be assumed that *exponential power laws satisfy maximum entropy constraints and are equally relevant to fragmentation and coagulation.*

5. Universal Size Distributions

As defined here, *universal size distributions for fragmentation* are those size distributions which are both Type II Weibull and exponential power laws. As seen in Section 4.2, Type II Weibull size distributions satisfy constraints imposed by fragmentation geometry while exponential power law size distributions satisfy constraints imposed by maximum entropy theory. Thus *universal size distributions for fragmentation satisfy both geometric and maximum entropy constraints simultaneously*.

In addition to exponential power laws, maximum entropy theory yields all sorts of other size distributions, e.g., Equation (59). However, only exponential power laws intersect Type II Weibull size distributions. For earlier discussions of the intersections between Type II Weibull and exponential power law size distributions – or, equivalently, the intersections between fragment geometry and maximum entropy theory – see, for example, Grady & Kipp (1985), Brown & Wohletz (1995), and Kumar & Kumaran (2005).

By Equations (20) and (33), Type II Weibull size distributions are the same as exponential power law size distributions if and only if $l = i - 1 = n - 1$ or:

$$n = i \tag{60}$$

Thus the problem becomes one of selecting $X = c_i D^i$. As seen in Section 2, the most common and physical choices of X are as follows:

$$i = \pm 1 \quad \text{or} \quad X = D^{\pm 1}$$

$$i = \pm(m - 1) \quad \text{or} \quad X = \mathcal{A}^{\pm 1}$$

$$i = \pm m \quad \text{or} \quad X = M^{\pm 1}$$

Type II Weibull size distributions with $n = i = \pm 1$, $\pm(m - 1)$, and $\pm m$ will be called the *fundamental size distributions*.

Table 8 summarizes the fundamental size distributions for integer m . For $m = 2$, $D = \mathcal{A}$ and thus there are only two fundamental size distributions. Similarly, for $m = 1$, $\mathcal{A} = \text{const.}$ and $D = M$ and thus there is only one fundamental size distribution.

Table 8. Fundamental size distributions for integer m .

	$m = 3$	$m = 2$	$m = 1$
$n = \pm 1$	$n/m = \pm 1/3$ Mott & Linfoot (1943)	$n/m = \pm 1/2$ Mott & Linfoot (1943)	$n/m = \pm 1$ Lineau (1936)
$n = \pm 2$	$n/m = \pm 2/3$ Gilvarry (1961)	$n/m = \pm 1$ Grady & Kipp (1985)	
$n = \pm 3$	$n/m = \pm 1$ Li & Tankin (1987)		

Notice that all of the references given in Table 8 concern positive fundamentals, except for Gilvarry (1961), which concerns a negative fundamental. In addition, all of the references in Table 8 provide full theoretical proofs, except for Mott & Linfoot (1943), who provide only a partial proof. These earlier proofs generally differ from the one given here.

Some rows and columns in Table 8 have been known for decades. For example, Tucker et. al. (1965) described the first row of Table 8. More specifically, they noted that a Type II Weibull size distribution with $n/m = 1$ “applies for random or semi-random breakup of a bar,” $n/m = 1/2$ “applies for breakup of a thin metal shell and is observed to hold for two-dimensional breakup,” and $n/m = 1/3$ “applies for a very thick metal shell and is observed to hold for three-dimensional breakup [and] ... may be expected to hold for the smallest fragments.” For another example, Gilvarry (1961) described something similar to the first column of Table 8. More specifically, for $m = 3$, he suggested Type I Weibull size distributions with $n = 1, 2$, and 3 . However, he is best remembered for deriving a Type II Weibull size distribution with $n = -2$.

Turning from fragmentation to coagulation, *universal size distributions for coagulation* are those size distributions which are both Gamma and exponential power laws. As seen in Section 4.3, Gamma size distributions satisfy constraints imposed by coagulation geometry while exponential power law size distributions satisfy constraints imposed by maximum entropy theory. Thus *universal size distributions for coagulation satisfy both geometric and maximum entropy constraints simultaneously.*

By Equations (31) and (33), Type II Gamma size distributions are the same as exponential power law size distributions if and only if $l = i - 1 = a - 1$ or:

$$a = i$$

As for fragmentation, the three most physical choices of i are 1 , $m - 1$, and m . However, using Table 7, it can be shown that there is a solution for n if and only if:

$$a = i = n = 1 \tag{62}$$

and:

$$D_{ref} = D_{avg} \tag{63}$$

Using the same approach on other types of Gamma size distributions, the *universal size distributions for coagulation are the same as those for fragmentation.* The only difference is that coagulation, unlike fragmentation, restricts the reference size; see Table 9.

Table 9. Examples of restrictions on reference sizes implied by universal size distributions for coagulation.

$n = 1$	$D_{ref} = D_{avg}$	$n = -1$	$D_{ref} = D'_{avg}$
$n = m - 1$	$\bar{\mathcal{A}}_{ref} = \bar{\mathcal{A}}_{avg}$	$n = -(m - 1)$	$\bar{\mathcal{A}}_{ref} = \bar{\mathcal{A}}'_{avg}$
$n = m$	$M_{ref} = M_{avg}$	$n = -m$	$M_{ref} = M'_{avg}$

The restrictions given in Table 9 resolve an inherent ambiguity with Gamma size distributions. More specifically, Gamma size distributions no longer violate the second self-similarity condition because the key parameter a no longer depends on an arbitrary reference size but rather on a single clearly-defined reference size.

The remainder of this paper is limited to integer m . If the fundamentals are $n = \pm 1, \dots, \pm m$, then the *overtones* are Type II Weibull size distributions where:

$$n = \pm(m+1), \pm(m+2), \pm(m+3), \dots$$

In addition, the *semitones* or *half tones* are Type II Weibull size distributions where:

$$n = \pm 1/2, \pm 3/2, \pm 5/2, \dots$$

The following sections argue that, for $m = 3$, the universal size distributions consist of the fundamentals, overtones, and semitones. In other words:

$$n = \pm 1/2, \pm 1, \pm 3/2, \pm 2, \pm 5/2, \pm 3, \pm 7/2, \dots$$

or equivalently:

$$\frac{n}{m} = \pm \frac{1}{6}, \pm \frac{1}{3}, \pm \frac{1}{2}, \pm \frac{2}{3}, \pm \frac{5}{6}, \pm 1, \pm \frac{7}{6} \dots$$

Because these values are integer multiples of one sixth, this may be called the *law of sixths*. The law of sixths also seems to apply for $m = 1$ and 2. In other words, only the classification of the universals changes with m , e.g., $n/m = 1/2$ is a fundamental for $m = 2$ but a semitone for $m = 3$.

6. Simple Fragmentation

As defined here, *simple fragmentation* occurs when the tensile strain rate $\dot{\epsilon}$ and fragment dimension m are constants. This assumes that the tensile strain rate drives fragmentation and that it can be expressed as a scalar rather a full tensor. As seen in Section A.9, examples include radially-expanding thin cylindrical shells, radially-expanding thin spherical shells, radially-expanding thin rings, stretched straight rods, stretched linear filaments, and so forth.

Appendix A shows that simple fragmentation leads to simple algebraic expressions for average fragments sizes. In addition, it will be argued, simple fragmentation leads to universal size distributions about those average fragment sizes. Mott & Linfoot (1943) were the first to make the association between universal size distributions and simple algebraic expressions for average fragment sizes.

As noted in the introduction, many communities study fragmentation. However, only two communities routinely study *simple* fragmentation, namely, the conventional weapons effects

community in terms of cased munitions, and the liquid atomization and sprays community in terms of round jets, planar jets, air bubbles, rings, ligaments, and so forth.

Table 10 gives examples of size distributions taken from the research literature on cased munitions where n/m , n , and m refer to parameters in Type II Weibull size distributions. In these examples, the cylindrical shells obtain fundamentals while the rings obtain overtones. As described in Appendix A, simple fragmentation only occurs for sufficiently thin rings and shells. This not very common; see sections 7.3.2 and 8.5 for examples involving thick shells.

Table 10a. Fragment size distributions for tests of solid uniformly-expanding thin rings with $m=1$.

n/m	n	m	Reference	Notes
2	2	1	Zhou et. al. (2006)	Various tests found in a literature survey
4	4	1	Moxnes & Børve (2015)	25mm-thick steel rings cut from warheads

Table 10b. Fragment size distributions for tests of solid uniformly-expanding thin cylindrical shells with $m=2$.

n/m	n	m	Reference	Notes
1/2	1	2	Bess (1975)	10 to 17mm-thick SAE 1050 steel
"	"	"	Arnold & Rottenkolber (2008)	2mm-thick steel; $n/m = 0.48, 0.55$
-1/2	-1	2	Bannikova et. al. (2014)	2mm-thick alumina; $n/m = -0.47 \pm 0.02$

Table 10c. Fragment size distributions for tests of solid uniformly-expanding thin cylindrical shells with $m=3$.

n/m	n	m	Reference	Notes
1/3	1	3	Arnold & Rottenkolber (2008)	6mm-thick steel; $n/m = 0.29, 0.31, 0.35$
2/3	2	3	Grady et. al. (2001)	8%-thick heat-treated steel; $n/m = 0.67$

Table 11 gives examples of size distributions taken from the research literature on atomization and sprays where n/m , n , and m refer to the parameters in Type II Weibull size distributions as converted from the Type I root normal and Type II Gamma size distributions originally given in most of the references; see Laney (2015a, 2016). Notice that all the tests obtained fundamentals except the last, which obtained an overtone.

Table 11. Fragment size distributions for various tests involving liquids with $m=3$.

n/m	n	m	Reference	Notes (% of tests obtaining distribution)
1/3	1	3	Spielbauer et. al. (1989)	Sheet jets (60%)
2/3	2	3	Wu et. al. (1991)	Cylindrical jets (16.6%)
2/3	2	3	Marmottant & Villermaux (2004)	Stretched ligaments (33.3%)
1	3	3	Bremond & Villermaux (2006)	Sheet jets (16.6%)
1	3	3	Lhuissier & Villermaux (2012)	Spherical shells ("air bubbles") (100%)
-1	-3	3	Lhuissier et. al. (2013)	Radial ligaments from drop impact (100%)
2	6	3	Chou & Faeth (1998)	Semi-spherical bags (50%)

In summary, *the available experimental evidence indicates that simple fragmentation always obtains either a fundamental or an overtone.*

7. Compound Simple Fragmentation

As defined here, *compound simple fragmentation* is any non-simple case that results in a single overall Type II Weibull size distribution. Two common outcomes are universal size distributions, as discussed earlier, and *compound size distributions*. For universal size distributions, n/m tends to remain constant regardless of the exact conditions. When it does change, it jumps from one discrete value to another. By contrast, for compound size distributions, n/m changes continuously as the exact conditions change. Sections 7.1 to 7.4 give examples of universal and compound size distributions based on a literature survey. Section 7.5 gives a basic theory, involving mixing and the integral mean value theorem, for why universal and compound size distributions occur in compound simple fragmentation.

7.1 One Dimension ($m = 1$)

One-dimensional objects such as bars, rings, rods, etc. can be loaded in various different ways including: axially in tension; axially in compression; and laterally. As seen Section 6, simple axial tension results in simple fragmentation, i.e., fundamentals and overtones with $n/m = \pm 1, \pm 2, \pm 3, \dots$

As an example of axial compression, Gladden et. al. (2005) studied “dynamic buckling and fragmentation of slender rods axially impacted by a projectile ... for a range of materials including teflon, dry pasta, glass, and steel.” They obtained an expression for average fragment size similar to those given in Appendix A. However, while the results are similar, the proofs are different. More specifically, Appendix A assumes fragmentation is governed by the tensile component of the usual conservation laws, while Gladden et. al. (2005) assumes fragmentation is driven by unstable oscillatory bending modes. Gladden et. al. (2005) give experimental size distributions that appear to be, at best, piecewise compound simple and possibly completely non-simple.

As an example of lateral loading, Ching et. al. (2000) studied impact fragmentation of long thin glass rods with lengths of 2m and diameters of 2mm. When the glass rods were dropped horizontally onto the ground from heights of 1.2 or 2.0m, they found that: (a.) the fragments formed in one-dimension and (b.) a single power law (equivalently, a single Type II Weibull size distribution with $n < 0$) provided a good fit for entire fragment size distribution. When the glass rods were dropped from larger heights up to 23.6m, they found that the smallest fragments formed in three dimensions and obeyed one power law, while the largest fragments formed in one dimension and obeyed another power law. Of the seven power law indices reported, five approximately agree with the law of sixths. More specifically, two have $n/m \approx -1/3$ and three have $n/m \approx -1/2$. This indicates that when fragments form in a full three-dimensional space, they tend to obtain fragment size distributions typical of three-dimensions, regardless of the fact that $m = 1$.

7.2 Two Dimensions ($m = 2$)

7.2.1 Case 1 ($n/m = -1/3$)

To simulate space debris, Wittel et. al. (2004, 2005, 2006) studied fragmentation due to small hydrogen gas explosions inside eggshells. In all cases tested, they obtained a power law (equivalently a Type II Weibull size distribution) with $m = 2$ and $n/m \approx -1/3$. According to Figure 1 in Wittel et. al. (2005), “the ignition took place at the top of the egg,” causing the top of the eggshell to fragment first and relieving overpressure on the bottom of the eggshell. Since the top experienced a higher strain rate than the bottom, as opposed to the uniform strain rates characteristic of simple fragmentation, this is an example of compound simple fragmentation.

As another way to simulate space debris, Wittel et. al. (2004, 2005, 2006) studied “intact eggshells ... catapulted onto the ground at a high speed using a simple setup of rubber bands.” In all cases tested, they obtained $m = 2$ and $n/m \approx -1/3$. According to Figure 2 in Wittel et. al. (2005), when an “egg [shell] hits the ground in the direction of its longer axis ... [the] egg [shell] suffers gradual collapse as it moves forward, making the impact process relatively long ...” The timing between sequential experimental photographs indicates that the eggshell front experiences higher strain rates than the back. In addition, the eggshell experiences primarily lateral loading on the front and back, and compressive loading on the sides, as opposed to tensile loading in explosive cases. The fact that such radically different loading conditions – both explosive and impact – always obtained $n/m \approx -1/3$ implies that this is a true universal size distribution.

In addition to tests, Wittel et. al. (2004, 2005, 2006) modeled egg shell fragmentation using a Discrete Element Method (DEM) for a hypothetical material composed of “pointlike material elements [with] ... bonds between nodes ... assumed to be springs having linear elastic behavior up to failure.” This model obtained $n/m = -0.35 \pm 0.03$ for impact fragmentation and $n/m = -0.55 \pm 0.03$ for explosive fragmentation, which approximately follows the law of sixths.

7.2.2 Case 2 ($n/m = -5/6$)

In an early study of space debris, Bess (1975) used a light gas gun to fire a 1.65g steel cylinder at 3.0km/s and a 0.37g aluminum cylinder at 4.5 km/s into a simulated spacecraft wall consisting of an “insulated fiberglass wall in back of which were a number of electronic boxes containing resistors, capacitors, etc.” Despite the complex geometry and the variety of different wall materials, the two tests each obtained a single fragment size distribution. More specifically, the wall fragments obeyed a power law with $n/m \approx -0.80$ for the steel test and $n/m \approx -0.84$ for the aluminum test. Bess described the wall fragments as “irregularly shaped, flat plates,” which implies $m = 2$. Based on these and four subsequent tests, the NASA Standard Breakup Model assumes $n = -1.71$ for collisions involving satellites or, equivalently, $n/m \approx -0.855$; see, e.g., Johnson et. al. (2001), Sakuraba et. al. (2008). This approximately obeys the law of sixths.

7.2.3 Case 3 ($n/m = -5/4$)

The previous cases approximately obeyed the law of sixths, which assumes the same set of universal size distributions occur regardless of whether $m = 1, 2$, or 3. However, this is only true

when fragmentation occurs in a full three-dimensional space. As an example that does not obey the law of sixths, Kun & Herrmann (1999) modeled collisions between two-dimensional disks using a Molecular Dynamics (MD) model. This model treats each disk as a hypothetical material composed of “unbreakable, undeformable ... randomly shaped convex polygons” connected by breakable elastic beams. Because this model confined fragmentation to two dimensions, it obtained a two- rather than a three-dimensional semitone. More specifically, all but the largest fragments obtained a Type II Weibull size distribution with $n/m = -1.27 \pm 0.05 \approx -5/4$ or, equivalently, $n \approx -5/2$. This is a semitone for $m = 2$, i.e., it is halfway between the fundamental $n = -2$ and the overtone $n = -3$.

7.3 Three Dimensions ($m = 3$)

This section considers six cases that obey the law of sixths, as summarized in Table 12, and one case that violates the law of sixths.

Table 12. Universal size distributions for various compound simple fragmentation tests with $m=3$.

	n/m	m	Reference	Notes
1	-0.20 ± 0.06	3	Timár et. al. (2010)	Impact fragmentation of small (4mm) polypropylene spheres.
	-0.15 -0.17 -0.20	3	Oddershedde et. al. (1993)	Impact fragmentation of thin (4mm) gypsum plates.
2	$-1/3$	3	Edwards & Deal (2011)	Explosive fragmentation of 9.25mm-thick aluminum alloy cylindrical shell.
3	-0.48	3	Oddershedde et. al. (1993)	Impact fragmentation of frozen 7.5cm cubes of gypsum, stearic paraffin, soap, and potato
	-0.49 ± 0.18	3	Onose & Fujiwara (2004)	Porous gypsum spheres impacted by nylon spheres fired from a light gas gun.
4	$-2/3$	3	Gilvarry & Bergstrom (1961) Yamakoshi et. al. (1981) Inaoka & Takayasu (1996, 99) Hooper (2012)	Impact fragmentation of glass spheres, asteroids, meteorites, planetesimals, and consolidated aluminum powder spheres.
5	-0.83 ± 0.03	3	Seebaugh (1977) Schoutens (1979) Ivanov et. al. (1983) O’Keefe & Ahrens (1985, 87) Turcotte (1986)	Rubbleized and ejected rock from high-speed impact, high-explosive and nuclear tests such as Flat Top, Pile Driver, and Danny Boy.
	0.84^1	3	Vledouts et. al. (2016b)	Explosive fragmentation of thin roughly-spherical water-glycerol shells
6	$-7/6$	3	Kaminski & Jaupert (1998)	Explosive volcanic eruptions of bubble-bearing magma.
	-1.15 ± 0.08	3	Durand & Soulard (2012, 13)	Shock-loaded metal melts resulting in planar jets.

1. Converted from Type II Gamma size distributions as in Laney (2015b, 2016)

7.3.1 Case 1 ($n/m = -1/6$)

This subsection concerns Case 1 in Table 12. As one example, to model “industrial processes related to mining and ore processing,” Timár et. al. (2010) studied isotactic polypropylene spheres with diameters of 4mm impacting a hard wall. Based on experimental results for impact velocities of 40, 60, and 75 m/s, they suggested a Type II Weibull size distribution (equivalently a power law) with $n/m = -0.2 \pm 0.06$. As another example, Oddershedde et. al. (1993) studied 4mm-thick gypsum plates “thrown horizontally onto the floor [or] ... thrown vertically down” and obtained $n/m = -0.15$ to -0.20 . In all these cases, $n/m = -1/6$ to within the experimental error. These examples concern impact fragmentation. Here and in general, impact fragmentation tends to produce highly unsteady and non-uniform tensile strain rates. A possible exception is when the flat face of a rectangular object impacts a flat surface.

7.3.2 Case 2 ($n/m = -1/3$)

This subsection concerns Case 2 in Table 12. Edwards & Deal (2011) studied explosive-filled 7075-T6 cylindrical aluminum alloy shells. The as-received (“AR”) shells were heat-treated in two different ways (“OA” and “ST”) to reduce their strength and hardness. The outer radius of the shells varied while all other parameters were kept fixed. More specifically, all shells had a length of 33mm, an inner diameter of 6.5mm, and were fragmented by detonating a 35mm-long 1.05g granulated pellet of tetryl. Figure 1 shows a typical result.

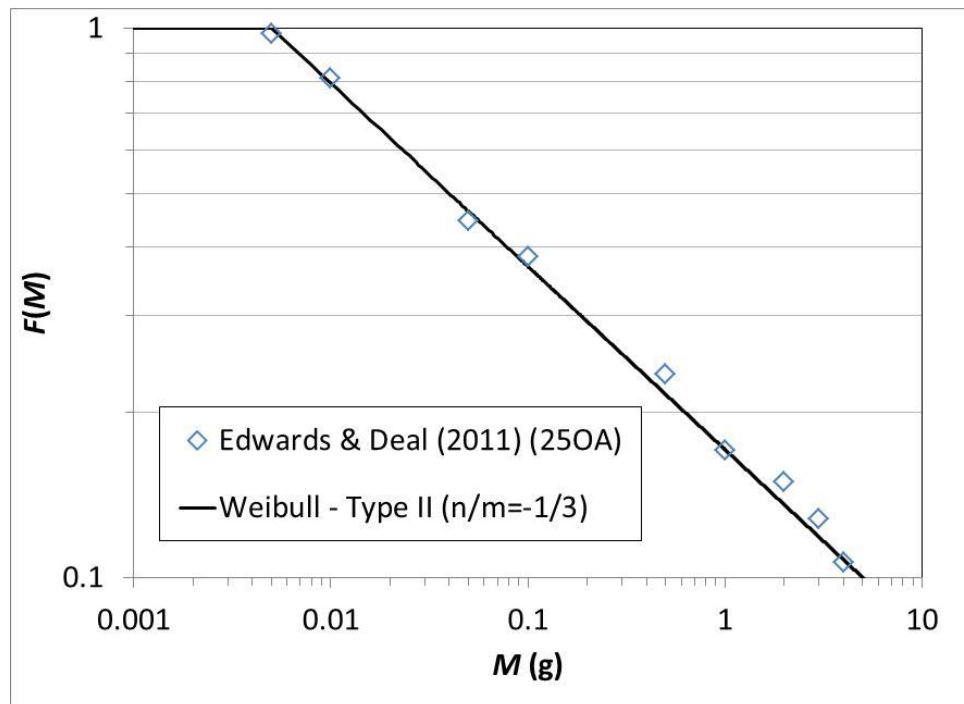


Figure 1. Type II Weibull distribution vs. test data for explosive-filled aluminum alloy cylindrical shells with an outer radius of 25mm as reported by Edwards & Deal (2011).

Table 13 summarizes the best-fit Type II Weibull size distributions (equivalently power laws). Notice that all size distributions obey the law of sixths. However, the values given in the shaded cells are somewhat uncertain due to the coarse binning used in the tests. More specifically,

Edwards & Deal (2011) used only 12 size bins with fixed limits, meaning that as few as four size bins were actually occupied in any given test.

Table 13. Fragment size distributions based on curve fits to test data reported by Edwards & Deal (2011).

Case	Strength (MPa)		Outer Diameter (mm) [Explosive-to-Metal Mass Ratio]			
	Yield	Tensile	33 [0.0130]	25 [0.0231]	20 [0.0382]	15 [0.0752]
“OA”	274±41	343±1.4	$n/m = -2/3$	$n/m = -1/3$	$n/m = -1/2$	$n/m = -1/2$
“ST”	401±15	551±22	$n/m = -2/3$	$n/m = -1/3$	$n/m = -1/2$	$n/m = -1/2$
“AR”	519±13	578±12	$n/m = -2/3$	$n/m = -1/2$	$n/m = -1/2$	$n/m = -1/2$

In addition to the cases shown in Table 13, Edwards & Deal (2011) also tested thicker shells with outer radii of 42mm, 50mm, and 100mm. In the 42mm case, the strongest shell produced eight fragments, the middling shell produced three fragments, and weakest shell cracked but did not fragment. The 50mm and 100mm shells did not fragment regardless of material strength.

Due to the thick shell walls, the explosive charge-to-shell mass ratio in Edwards & Deal (2011) was much smaller than in most similar tests. For example, the ratio was 2 to 11 times smaller than in Mock & Holt (1981, 1983). This may explain why Mock & Holt (1981, 1983) obtained $n/m > 0$, as discussed in Section 8.5, while Edwards & Deal obtained $n/m < 0$.

7.3.3 Case 3 ($n/m = -1/2$)

This subsection concerns Case 3 in Table 12. To simulate high-speed collisions involving asteroids and planetesimals, Onose & Fujiwara (2004) studied 64%-porous gypsum spheres impacted by nylon spheres fired from a two-stage light gas gun. They found $n/m = -0.49 \pm 0.18 \approx 1/2$ for early-time fragments “ejected conically within a few msec after the impact” and $n/m = -1.49 \pm 0.09 \approx 3/2$ for late-time fragments “consisting of hundreds of slow, small fragments ejected almost perpendicular to the target.” Separating fragments in time is rare – most experiments mix early- and late-time fragments together. The early-time results agree with those obtained by Oddershede et. al. (1993) when “stearic paraffin, soap, and potato were frozen in liquid nitrogen before being fragmented by a hammer.” Oddershede et. al. (1993) concluded that “within the accuracy of the determination of the exponents no significant dependence on material was observed.” This insensitivity implies that $n/m = -1/2$ is a true universal size distribution.

7.3.4 Case 4 ($n/m = -2/3$)

This subsection concerns Case 4 in Table 12. As an early example, Gilvarry & Bergstrom (1961, 1962) obtained $n/m = -2/3$ for fragmentation of small glass spheres impacted by a piston. They included gelatin “to prevent the fragments from colliding with the walls of the retaining chamber; otherwise, they will undergo secondary fracture by virtue of their large kinetic energy.” In this regard, they noted that “... experimental [results] ... for single fracture were virtually nonexistent in the literature” at that time.

As another example, Yamakoshi et. al. (1981) obtained $n/m = -2/3$ for asteroid break up, planetesimal fragmentation, and fragmentation of iron meteorites; see also Grady & Kipp (1987).

As a third example, based on a literature survey and a three-dimensional impact fracture model, Inaoka & Takayasu (1996, 1999) concluded that $n/m = -2/3$ “seems to be a very universal value.” As a fourth example, Hooper (2012) obtained $n/m = -2/3$ for “fragmentation of brittle, granular aluminum spheres following high velocity impact (0.5–2.0 km/s) on thin steel plates.” More specifically, he studied “spherical porous aluminum projectiles 2.51 cm in diameter ... cut from a cylinder of Valimet H-2 aluminum powder which had been isostatically pressed into a monolith.” As a final example, Domokos et. al. (2015) found $n/m = -2/3$ in seven different fragmentation experiments involving rocks and minerals such as limestone, dolomite, and gypsum. The fragmentation was done in substantially different ways including gradual weathering, hammering, and explosions. Domokos et. al. (2015) observe that “it is astonishing that the same universality class is recovered” in all cases.

Åström et. al. (2004) noted that “within the mining engineering community, ... [this] scale-invariant fragment-size distribution has long been known.” However, modern mainstream mining engineering practice typically involves an infinite continuum of compound size distributions rather than universal size distributions; see, e.g., Cunningham (2005).

7.3.5 Case 5 ($n/m = \pm 5/6$)

This subsection concerns Case 5 in Table 12. Seebaugh (1977), Schoutens (1979), Ivanov et. al. (1983), O’Keefe & Ahrens (1985, 1987), and Turcotte (1986) surveyed test results for rock fragmentation due to high-velocity impacts, large chemical explosions, and nuclear tests. In most cases, they found power laws with $\alpha \approx 0.5$ where:

$$\alpha = n + m.$$

In other words, in most cases they found Type II Weibull size distributions with $n/m \approx -5/6$. In one case, O’Keefe & Ahrens (1985) found that the smallest fragments obtained $n/m \approx -0.633$ while the largest fragments obtained $n/m \approx -0.827$. Notice that the former value is approximately a fundamental while the latter value is approximately a semitone.

For an essentially unbounded fragmenting object such as the earth, the majority of fragments will be produced in peripheral regions where the fragmentation forces barely exceed the material strength, while only a minority of fragments will be produced in the core regions where the fragmentation forces greatly exceed the material strength. This is true regardless of how large the fragmenting forces may be. This means that negative size distributions characteristic of brittle fragmentation will tend to be observed rather than the positive distributions characteristic of ductile fragmentation, even in the most extreme cases, such as high-yield nuclear weapon detonations.

O’Keefe & Ahrens (1987) speculated that “additional comminution” including “grinding and crushing ... occurs after the initial shock has passed” leading to a “broader size distribution in impact ejecta as compared to that obtained in simple brittle failure experiments.” While trying to verify a similar hypothesis, Kaminski & Jaupart (1998) repeatedly dropped a piston onto samples of rhyolitic pumice. Regardless of the number of piston strikes, they found that the fragment “population always keeps the same power law exponent of $n = -2.6 \pm 0.1$.” Assuming $m = 3$, this

approximately corresponds to $n/m = -5/6$. Finally, out of frustration, they put the fragments through a rotating grinder, either with or without a small steel ball. Not surprisingly, this reduced the fragment size spread and increased the absolute value of the power law exponent. The fact that $n/m = -5/6$ appears in so many different kinds of tests, and persists through multiple stages of fragmentation, implies that it is a true universal value.

As a final example, Vledouts et. al. (2016b) used rapid exothermic gaseous reactions to drive expansion of thin, roughly-spherical liquid shells. They found that hydrodynamic instability leads to “holes [that] grow in radius by capillary retraction, accumulating the liquid of the shell into their rim, which merge with the rim of the neighboring hole, finally leaving the shell as a web of ligaments, which break by capillary instability;” see also their Figure 4. The various circular rims and ligaments probably each experiences simple fragmentation. However, because the different rims and ligaments form at different times and places, and thus experience different strain rates, the net result is compound simple fragmentation with $n/m \approx 5/6$. While $n/m = 5/6$ may seem to be very different than $n/m = -5/6$, the results given in Sections 8.2 and 8.3 imply that they are actually closely related.

7.3.6 Case 6 ($n/m = -7/6$)

This subsection concerns Case 6 in Table 12. Kaminski & Jaupert (1998) note that “explosive volcanic eruptions eject a large mass of magma fragments, ranging from meter-sized blocks to micron-sized ash particles dispersed at high altitudes in the atmosphere.” In a literature survey, Kaminski & Jaupert (1998) found eleven instances of powers laws with $n \approx -3$ and six instances of power laws with $n \approx -3.5$. Assuming $m = 3$, these correspond to $n/m \approx -1$ and $n/m \approx -7/6$, respectively, where the former is a fundamental and the latter is a semitone.

Although bubble-bearing liquid magma might seem to be classically ductile, Kaminski & Jaupert (1998) found only power laws, which are typically indicative of brittle fragmentation. Indeed, Clarke (2013) notes that “high magma acceleration rates can generate large strain rates that may result in a rheological transition from ductile to brittle behavior ... causing the magma to behave in a brittle fashion, and leading to fragmentation.”

As another example, Durand & Soulard (2012, 2013) studied fragmentation of shock loaded metal melts. More specifically, the specified loading conditions created three sheet jets:

“During the expansion of the sheets, holes/cracks, randomly distributed, begin to appear... Once the void has percolated, a complementary network of ligaments of liquid metal between the pores appears ... In the late times, the oblique views of the whole systems show that the ligaments previously created in the three sheets have broken up and have reached a final spherical form.”

The various liquid metal ligaments probably each experience simple fragmentation. However, because they fragment at different strain rates, the net result is compound simple fragmentation. A computational approach, based on large-scale molecular dynamics, found power laws with $n/m = -1.15 \pm 0.08 \approx -7/6$ over a range of one or two orders-of-magnitude in fragment mass.

7.3.7 Case 7 ($n/m = 5/12$)

Unlike the previous six cases, this final case violates the law of sixths. Simmons (1977) considered spray atomization in “a subset of 200 tests selected almost at random ... [from] over 2,000 separate tests on about 100 different nozzle designs;” see also Spielbauer et. al. (1989). As seen in Laney (2016), Simmons’ Type I root normal size distribution approximately corresponds to a Type II Weibull distribution with:

$$\frac{n}{m} = \frac{5}{12} = \frac{1}{2} \left(\frac{1}{3} + \frac{1}{2} \right) = 0.41666$$

which is an average of a fundamental and a semitone. Put another way, Simmons approximately obtained a *quarter tone*. This has long been considered a universal size distribution. However, as described below, the available evidence indicates that, by the definitions introduced here, it may be better described as a compound size distribution.

At each fixed downstream station, round liquid jets typically experience simple fragmentation, i.e., thin cylindrical surface layers form ligaments that fragment to produce universal size distributions about averages obtained as in Appendix A. As a result, spray atomization can and often does produce true universal size distributions; see also Laney (2015a,b, 2016).

Away from the jet surface, liquid fragments tend to experience breakup due to aerodynamic forces and coagulation due to random collisions; see, e.g., Ruff et. al. (1992), Hsiang & Faeth (1992, 1993), Chou et. al. (1997). Such events introduce compounding. In addition, as described by Laney (2016), each downstream station tends to fragment differently. This is because the jet radius – and thus the surface strain rate – tends to increase linearly with distance from the nozzle exit. As a result, averaging results across different stations will, in many cases, yield compound size distributions. More specifically, when n is different at different stations, the average \bar{n} will change continuously depending on the exact choice of stations used to form the average.

In Simmons (1977), many if not most of the test results measured the spray characteristics away from the jet surface, averaged across various downstream stations. This implies that compounding occurs in many if not most of the individual tests. However, even if that were not the case, and even if all the individual tests involved simple fragmentation, averaging across different tests with different outcomes yields compound rather than universal size distributions. In other words, when n is different in different tests, the average \bar{n} changes continuously depending on the exact choice of tests used to form the average.

While numerous papers have appeared in the research literature providing additional evidence that supports Simmons’ size distribution, these almost all involve averages across multiple tests rather than specific tests; see, e.g., Spielbauer et. al. (1989), Ruff et. al. (1992), Hsiang & Faeth (1992, 1993), Chou et. al. (1997), and Laney (2015a). In other words, the available evidence indicates that Simmons (1977) obtained a compound size distribution rather than a true universal size distribution. Like most compound size distributions, Simmons’ size distribution violates the law of sixths.

7.4 Theory

Suppose a compound simple event can be subdivided into local regions in time and space where the fragmentation is approximately simple, i.e., where $\dot{\epsilon}$ and m are approximately constant. Suppose the probability density function for each such local sub-event is as follows:

$$f(X; \dot{\epsilon}; m) \quad (64)$$

Assuming the fragments originating in different regions in time and space are thoroughly mixed together, and assuming m is constant, then the probability density function for the overall fragmentation event is as follows:

$$\int w(\dot{\epsilon}) f(X; \dot{\epsilon}; m) d\dot{\epsilon} \quad (65)$$

where w is a positive weighting function such that:

$$\int w(\dot{\epsilon}) d\dot{\epsilon} = 1 \quad (66)$$

By the integral mean value theorem, Equation (65) can be written as follows:

$$\int w(\dot{\epsilon}) f(X; \dot{\epsilon}; m) d\dot{\epsilon} = f(X; \bar{\dot{\epsilon}}; m) \quad (67)$$

where $\bar{\dot{\epsilon}}$ is an average strain rate. This assumes that $w > 0$ over the limits of integration and that f and w are continuous functions of $\dot{\epsilon}$; see, e.g., Theorem 7.2 of Sahoo & Riedel (1998). Notice that, because there is no mean value theorem for double integrals, this proof does not apply if m and $\dot{\epsilon}$ vary simultaneously.

For example, if the probability density function for each local event is a Type II Weibull distribution, then Equation (67) says that the probability density function for the overall mixture is also a Type II Weibull distribution with:

$$\bar{D}_{ref} = D_{ref}(\bar{\dot{\epsilon}}, m) \quad (68)$$

and:

$$\bar{n} = n(\bar{\dot{\epsilon}}, m) \quad (69)$$

where \bar{n} is a either discrete or a continuous function of $\bar{\dot{\epsilon}}$. Put another way, compound simple fragmentation produces either universal or compound size distributions.

8. Piecewise Simple and Piecewise Compound Simple Fragmentation

8.1 Introduction

Piecewise simple and piecewise compound simple fragmentation occurs when different size ranges obtain different universal or compound size distributions. Section 7.5 found that compound simple fragmentation occurs when m is constant and $w > 0$. Conversely, piecewise simple or piecewise compound simple fragmentation occurs when m varies and/or when strain rate regions with $w = 0$ separate regions with $w > 0$.

As one example, consider multimode breakup of liquid droplets; see, e.g., Pilch & Erdman (1987), Chou & Faeth (1998), Dai & Faeth (2001). In such cases, aerodynamic forces cause droplets to distort until they form semi-spherical bags attached to semi-circular rims; optionally, a semi-linear stamen may extend from the center rear of the bag through the center of the rim. The bag, rim, and stamen probably each experiences simple fragmentation. However, because each feature experiences different strain rates, and the weighting function w is zero except for those three discrete strain rates, the net result is piecewise simple fragmentation.

As another example, consider explosive fragmentation of thin cylindrical shells. In many cases, the largest fragments form in two-dimensions while the smallest fragments form in three-dimensions. Then the universal size distribution changes when the fragment dimension m changes. As one specific case, suppose the universal changes from $n/m = 1/3$ when $m = 3$ to $n/m = 1/2$ when $m = 2$. These are typically reported as a single average, e.g., Cohen (1981) found:

$$0.433 \approx \frac{1}{2} \left(\frac{1}{3} + \frac{1}{2} \right)$$

This is about the same as Simmons (1977), as discussed earlier in Section 7.3.7. However, because m is fixed at 3 in Simmons (1977), it occurs for different reason. As another specific case, suppose the universal changes from $n/m = 2/3$ when $m = 3$ to $n/m = 1$ when $m = 2$. Again, these are typically reported as a single average, e.g., Grady et. al. (2001) found:

$$0.85 \approx \frac{1}{2} \left(\frac{2}{3} + 1 \right)$$

This is easily confused with the semitone $n/m = 5/6 \approx 0.83$.

As a third example, as discussed earlier in Section 7.6, Onose & Fujiwara (2004) studied porous gypsum spheres impacted by nylon spheres. In each of six reported tests, they found that the fragment size distributions had “three regions [separated] by two inflections,” which they called Region I, II, and III for the “largest,” “intermediate” and “finest” sizes, respectively. They reported n/m for each size region separately. In general, n/m was substantially different in different size regions. The following subsections provide more examples of piecewise simple and piecewise compound simple fragmentation.

8.2 Case 1

Figure 2 plots two Type II Weibull size distributions versus test data from Rosin & Rammler (1934). The smallest fragments have $n/m = -2/3$ while the largest fragments have $n/m = 2/3$. Brown & Woheltz (1995) suggest that “the data consist of two populations: fines that experienced a single fragmentation event and remained unaffected in spaces among larger particles that were repeatedly fragmented during milling.”

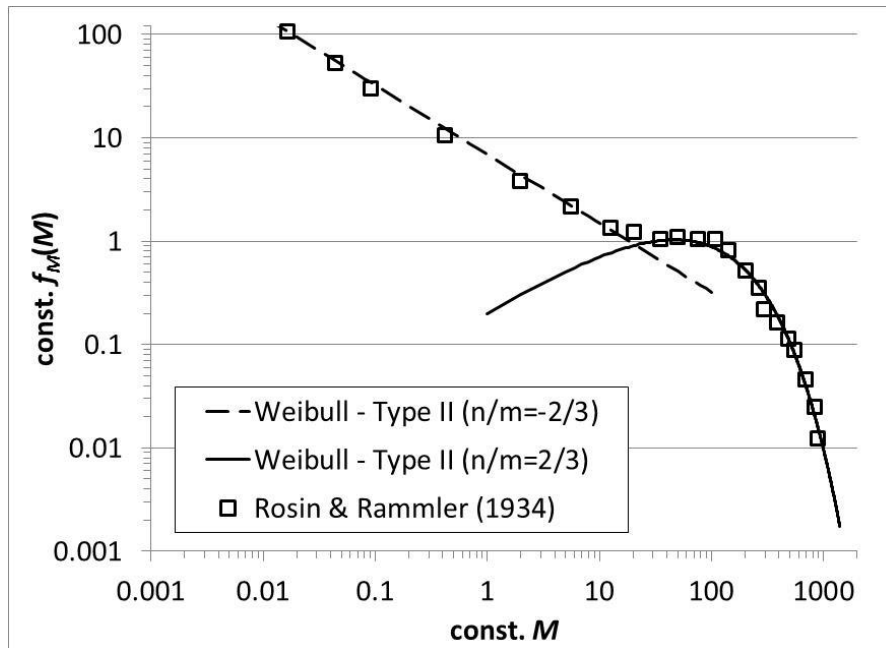


Figure 2. Type II Weibull distributions vs. test data for ball-milling of iron from Rosin & Rammler (1934). A similar figure appeared in Brown & Wohletz (1995).

8.3 Case 2

Wittel et.al. (2008) and Carmona et. al. (2008) modeled collisions between three-dimensional spheres using a Discrete Element Method (DEM), where each sphere was composed of a hypothetical material consisting of smaller “spheres of two different sizes ... connected by beam-truss elements that can elongate, shear, bend, ... torque” and break. As seen in Figure 3, in one possible fitting scheme, the largest fragments obtained $n/m \approx 2$, the middling fragments obtained $n/m \approx -2$, and the smallest fragments obtained $n/m \approx -1$.

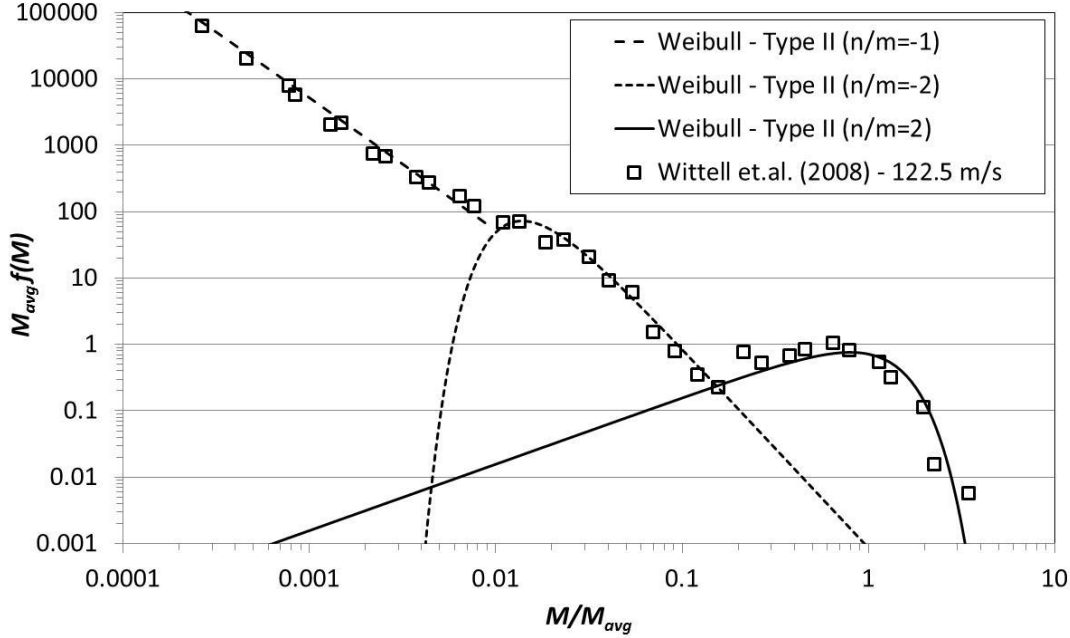


Figure 3. Type II Weibull size distributions vs. modeling data for colliding spheres obtained by the Discrete Element Method by Wittell et.al. (2008) and Carmona et. al. (2008).

8.4 Case 3

The complementary cumulative distribution function F is defined in terms of the probability density function f as follows:

$$F(X) = -\int_X^{\infty} f(x)dx ; f(X) = -\frac{dF}{dX} \quad (70)$$

This and the following example will use the time-proven technique of viewing F in a plane in which it is linear or nearly-linear. This view tends to expose differences between size distributions better than other views. In Sections 8.2 and 8.3, the size distribution shifted from positive to negative. Such dramatic shifts are obvious in almost any view. Here and in Section 8.5, the size distribution shifts between two positive size distributions, such that n/m changes by as little as $1/12$, which is not apparent in many views.

To model “large-scale quarry blastings of granitic gneiss,” Åström et. al. (2004) studied impact fragmentation of molded gypsum disks dropped onto flat surfaces from heights of 0.25m to 10m. Each gypsum disk had a diameter of 10.65cm and a thickness of 2.28cm. As shown in Figure 4, for a drop height of 0.75m, the smallest fragments approximately obey a Type II Weibull size distribution (equivalently a power law) with $n/m = -1/3$ while most of the remaining fragments approximately obey a Type II Weibull size distribution (equivalently a power law) with $n/m = -1/6$. Similarly, for a drop height of 7m, most of the fragments approximately obey a Type II Weibull size distribution (equivalently a power law) with $n/m = -1/3$. However, the larger fragments are piecewise compound simple or possibly completely non-simple. Notice that the fits suggested here differ from those suggested by Åström et. al. (2004).

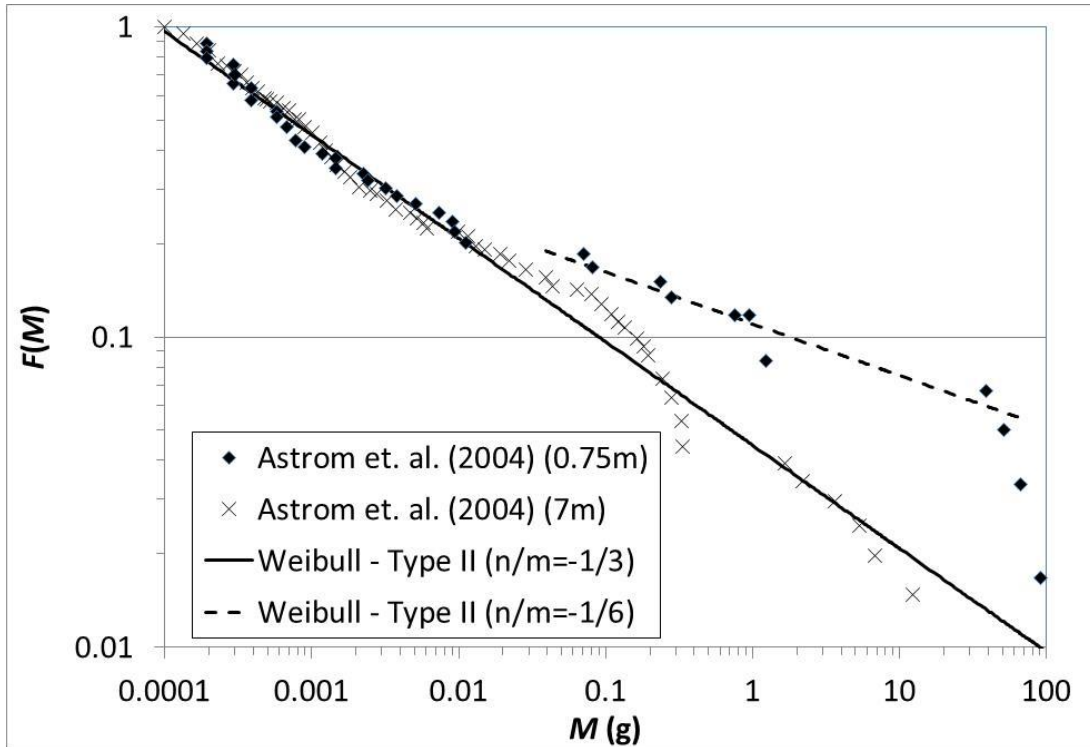


Figure 4. Type II Weibull size distributions vs. test data for impact fragmentation of molded gypsum discs dropped from heights of 0.75m and 7m taken from Åström et. al. (2004).

8.5 Case 4

Mock & Holt (1981, 1983) gave highly-detailed results for six tests involving explosively-driven cylindrical metal shells. Two of these tests involved Armco iron shells, two of these tests involved weak HF-1 steel shells, and two of these tests involved strong HF-1 steel shells. The difference in the strengths of the steel shells is due to a difference in the heat treatment. The iron shells had an outer diameter of 4.5 inches, an inner diameter of 3 inches, a wall thickness of 0.75 inches, and a length of 8 inches. The steel shells had an outer diameter of 4.75 inches, an inner diameter of 3 inches, a wall thickness of 0.875 inches, and a length of 8 inches. Notice that the ratio of the wall thickness to the outer radius is 0.333 for iron and 0.368 for steel, making these relatively thick shells. The shells were fragmented by detonating 2.75kg cylinder of cast-in-place Composition B, with 57% inside the metal shells and 43% outside of the metal shells. The charge-to-shell mass ratio was 0.17 for iron and 0.15 for steel.

Table 14 summarizes the results of the six tests. Notice that the curve fits given in Table 14 differ from those given by Mock & Holt (1981, 1983).

Table 14. Summary of fragments size distributions vs. material strength for two Armco Iron and four HF-1 steel cylindrical shells tested by Mock & Holt (1981, 1983).

Exp.	Casing Mat'l	Casing Strength (MPa)		No. Size Bins	Type II Weibull Size Distribution				
		Yield	Tensile		Smallest Frags ($m = 3$)		Largest Frags ($m = 2$)		Best Overall
					n/m	n	n/m	n	
1	Iron	180	300	18	1/3	1	1/2	1	1/3
2	"	"	"	144	1/3	1	1/2	1	1/3
3	Steel	980-1040	1105-1320	15	1/2	3/2	1/2	1	1/2
4	"	"	"	65	1/2	3/2	2/3	4/3	0.58
5	Steel	857	882	67	1/2	3/2	2/3	4/3	0.58
6	"	"	"	67	1/2	3/2	2/3	4/3	0.58

Figures 5 and 6 show the results of Experiments 1 and 2 in a log-log plane. Notice that the two experiments are identical, except for the number of bins and random shot-to-shot variation. In Figure 5, a Type II Weibull distribution with $n/m = 1/3$ appears to provide a good fit regardless of fragment size. However, in Figure 6, with eight times as many bins, a Type II Weibull distribution $n/m = 1/3$ provides a good fit for fragments less than 600gr, a mediocre fit for fragments between 600 and 2,000gr, and a poor fit for fragments greater than 2,000gr.

As an alternative to Figure 6, Figure 7 shows the results of Experiment 2 in a plane in which F is linear or nearly-linear. In this view, the size distribution clearly transitions from $n/m = 1/3$ for the smallest fragments with $m = 3$ to $n/m = 1/2$ for the largest fragments with $m = 2$. During the transition, the size distribution briefly assumes the average:

$$\frac{n}{m} \approx \frac{1}{2} \left(\frac{1}{3} + \frac{1}{2} \right) = 0.41666$$

On the surface, Experiments 1 and 2 appear to be textbook cases of simple fragmentation with a dimensional transition. However, because the iron shell is fairly thick, there is actually a significant compounding effect. According to lower plot in Figure 7, most of the fragments between about 600 and 2,000gr are two-dimensional, i.e., they retain two parallel smooth surfaces from the original shell. According to upper plot in Figure 7, these midrange two-dimensional fragments obtain $n/m = 1/3$ just like the smallest three-dimensional fragments.

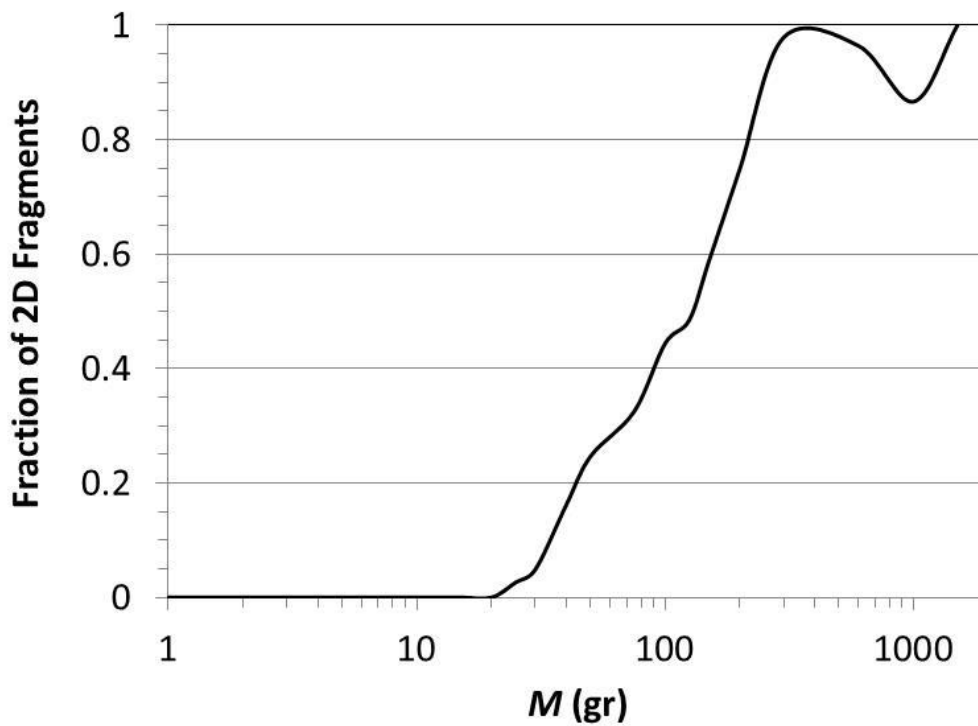
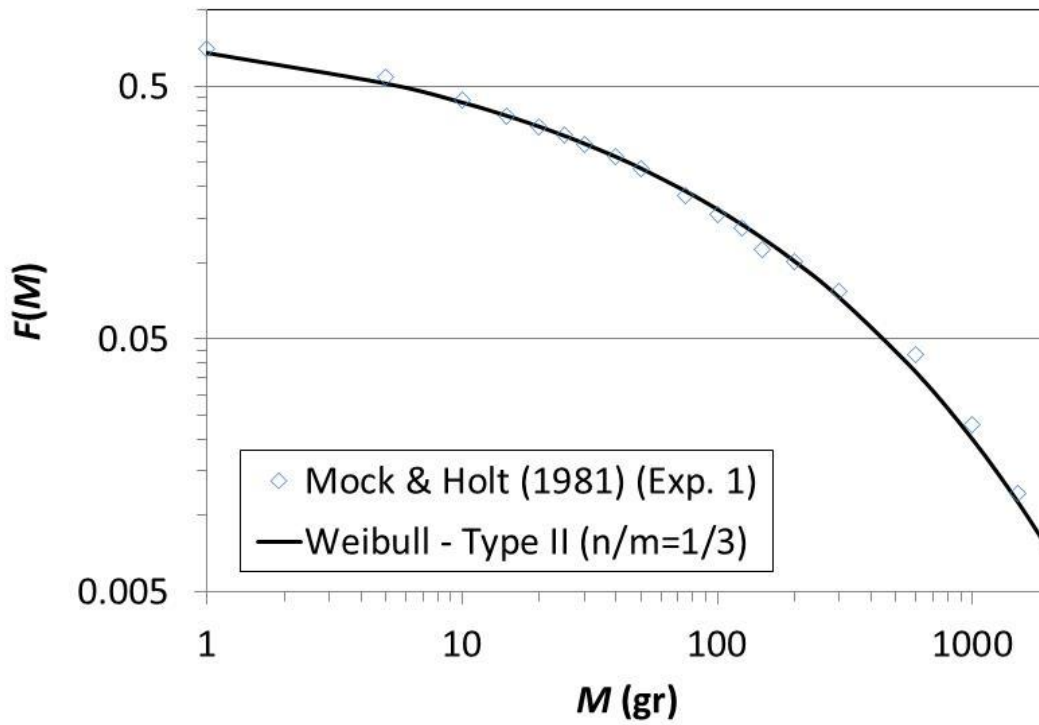


Figure 5. Type II Weibull size distribution vs. test data in a log-log plane for an explosively-fragmented iron cylindrical shell taken from Experiment 1 of Mock & Holt (1981, 1983). The lower plot shows the fraction of fragments retaining portions of both the inner and outer surface of the original iron shell, which are called Type 1 by Mock & Holt (1981, 1983).

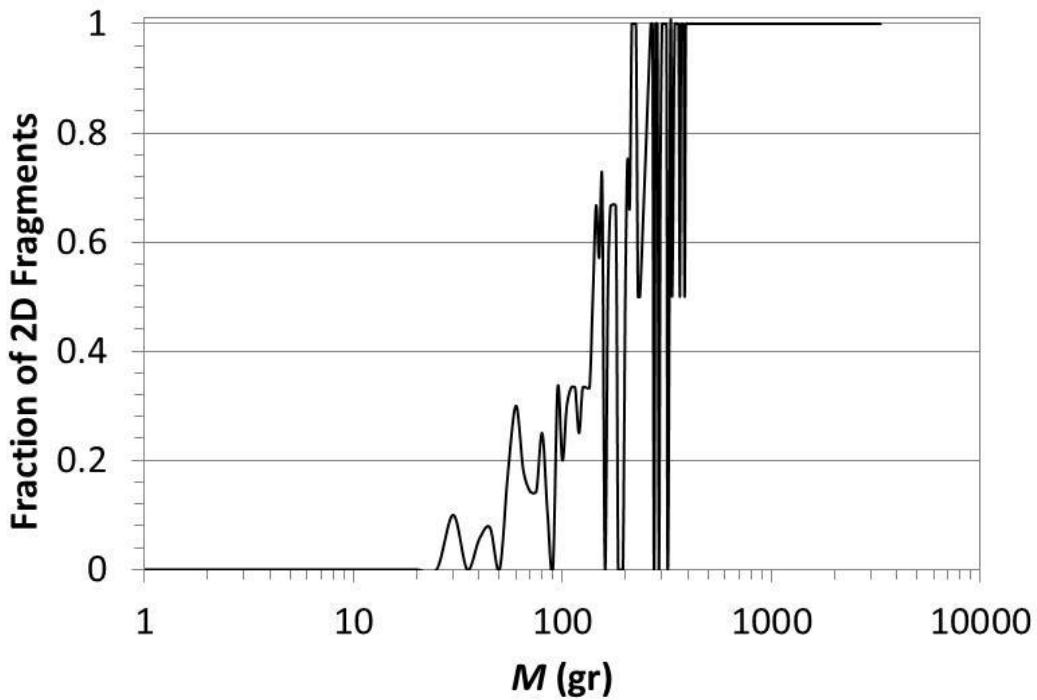
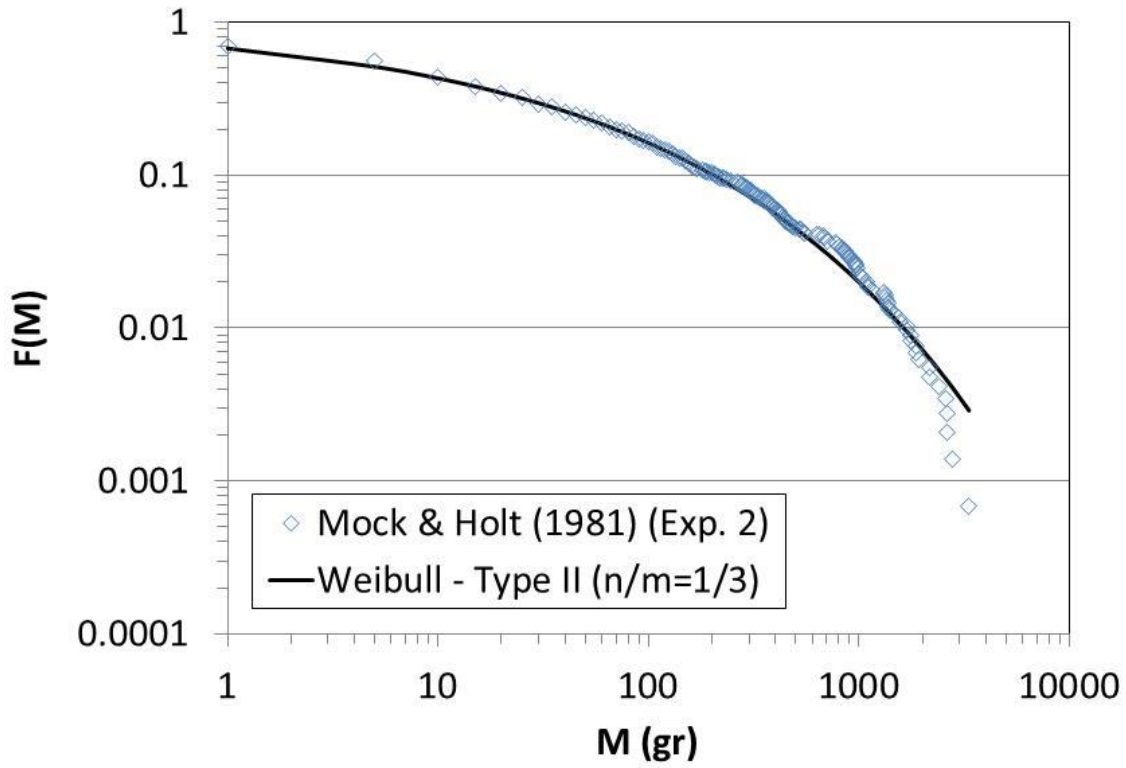


Figure 6. Type II Weibull size distribution vs. test data in a log-log plane for an explosively-fragmented iron cylindrical shell taken from Experiment 2 of Mock & Holt (1981, 1983). The lower plot shows the fraction of fragments retaining portions of both the inner and outer surface of the original iron shell, which are called Type 1 by Mock & Holt (1981, 1983).

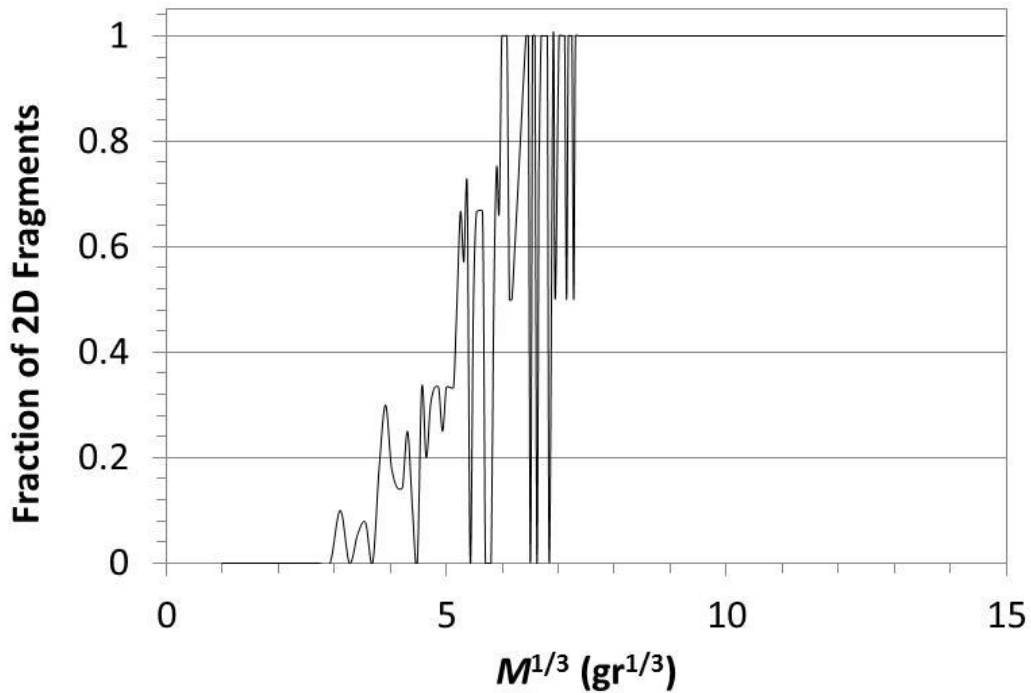
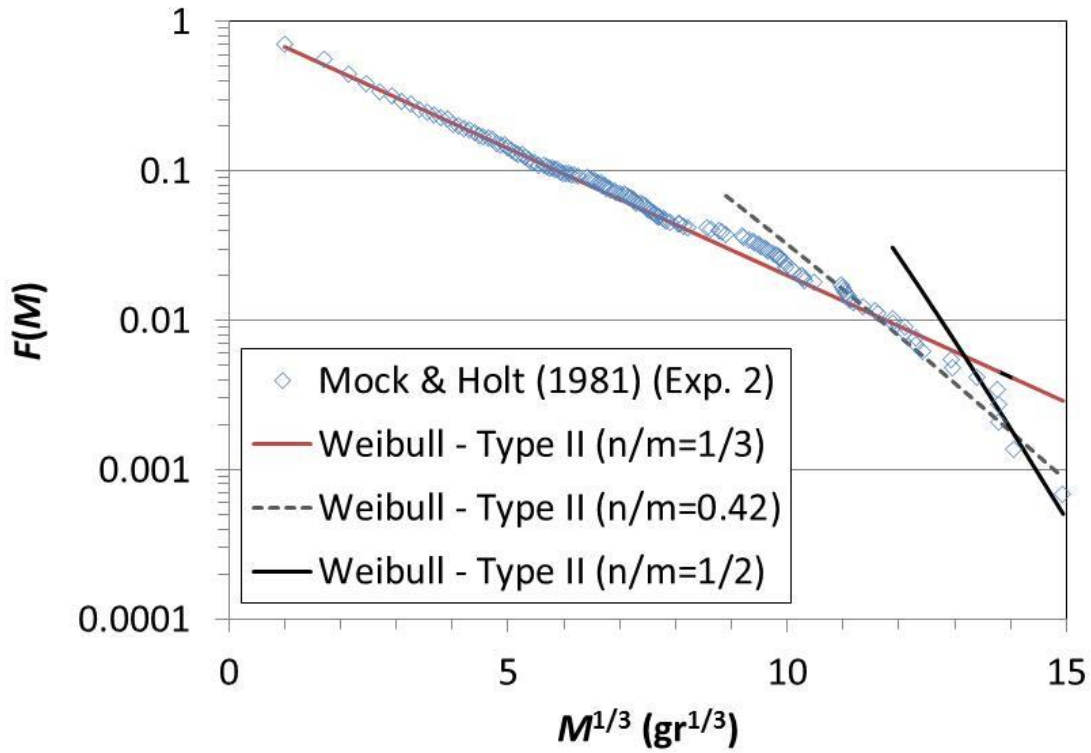


Figure 7. Type II Weibull size distributions vs. test data in a plane in which F is linear or nearly-linear for an explosively-fragmented iron cylindrical shell taken from Experiment 2 of Mock & Holt (1981, 1983). The lower plot shows the fraction of fragments retaining portions of both the inner and outer surface of the original steel shell, which are called Type 1 by Mock & Holt (1981, 1983).

Figure 8 shows the results of Experiment 4 in a plane in which F is linear or nearly-linear. The casing thickness is slightly larger, and the casing strength is much larger, than in Experiments 1 and 2. As a result, compounding effects are more pronounced. In fact, the smallest fragments with $m = 3$ have $n/m = 1/2$ and the largest fragments with $m = 2$ have $n/m = 2/3$, reversing expectations based on simple fragmentation. Notice that, during the dimensional transition, the size distribution briefly assumes the average:

$$\frac{n}{m} \approx \frac{1}{2} \left(\frac{1}{2} + \frac{2}{3} \right) = 0.58333$$

Figure 9 shows the results of Experiment 5 in a log-log plane. In this view, it appears that a Type II Weibull distribution with $n/m = 0.58$ provides a good fit, except for a few of the largest size bins. In other words, Experiment 5 appears to violate the law of sixths. For a clearer view, Figure 10 shows the results of Experiment 5 in a plane in which F is linear or nearly-linear. In this view, the size distribution clearly transitions from $n/m = 1/2$ for the smallest fragments to $n/m = 2/3$ for the largest fragments, without assuming any intermediate values such as $n/m = 0.58$. In this view, it is apparent that Experiment 5 satisfies the law of sixths, in a piecewise fashion. The material strength in Experiment 5 is somewhat less than that in Experiment 4. Comparing Figures 8 and 10, the main effect seems to be eliminating the transition region where $n/m = 0.58$.

In general, a *view* is a specific combination of the following:

- (a.) a size distribution such as $f(X)$, $f_Y(X)$, $F(X)$, or $F_Y(X)$ for some X and Y
- (b.) a plane such as the linear-linear plane, the log-log plane, or a plane in which $f(X)$, $f_Y(X)$, $F(X)$, or $F_Y(X)$ is linear, piecewise-linear, or nearly so
- (c.) upper and lower bounds on each axis.

Comparing Figures 6 and 7, or Figures 9 and 10, shows how much difference the view can make on the perceived goodness of fit; see also Laney (2015a, b, 2016). The *sensitivity* or *discrimination* of a given view can be determined by varying key parameters such as n/m . In discriminating views, small changes in n/m lead to large changes in the size distribution.

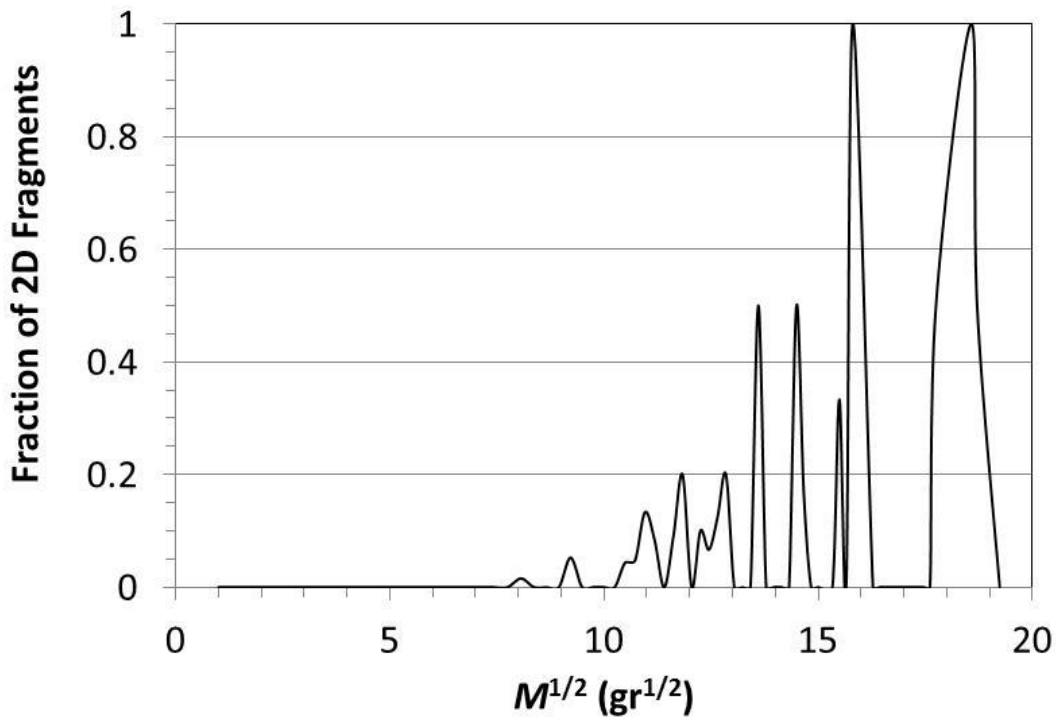
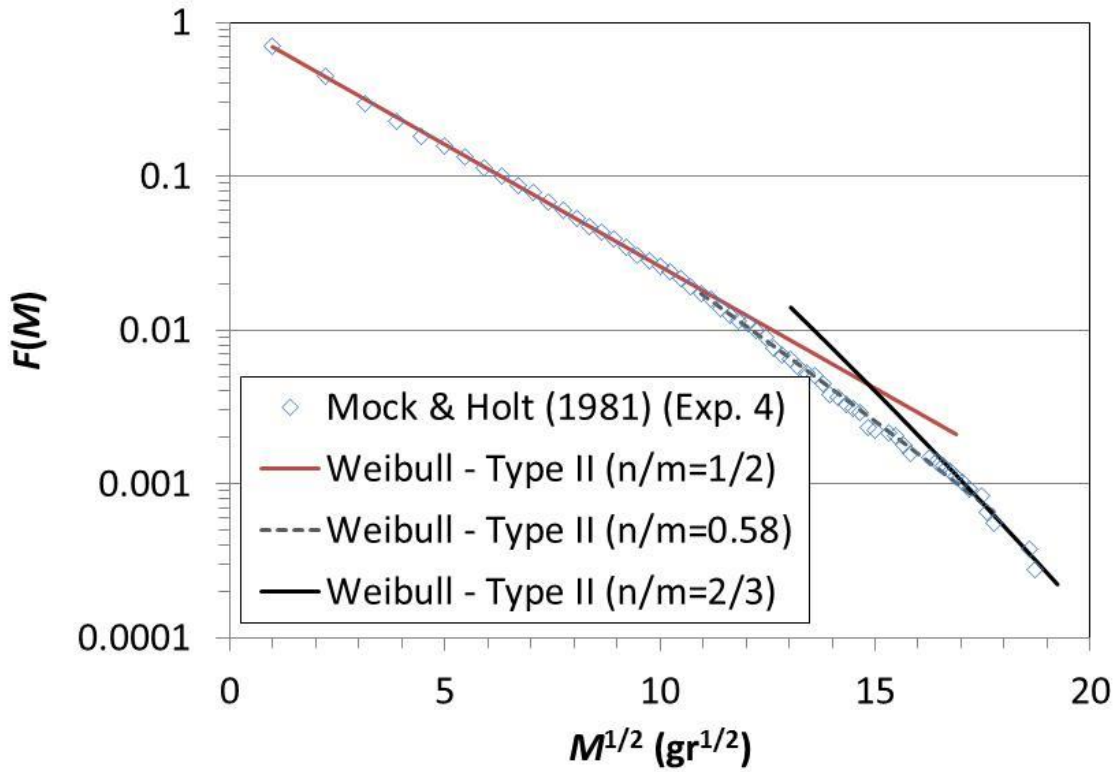


Figure 8. Type II Weibull size distributions vs. test data in a plane in which F is linear or nearly-linear for an explosively-fragmented steel cylindrical shell taken from Experiment 4 of Mock & Holt (1981, 1983). The lower plot shows the fraction of fragments retaining portions of both the inner and outer surface of the original steel shell, which are called Type 1 by Mock & Holt (1981, 1983).

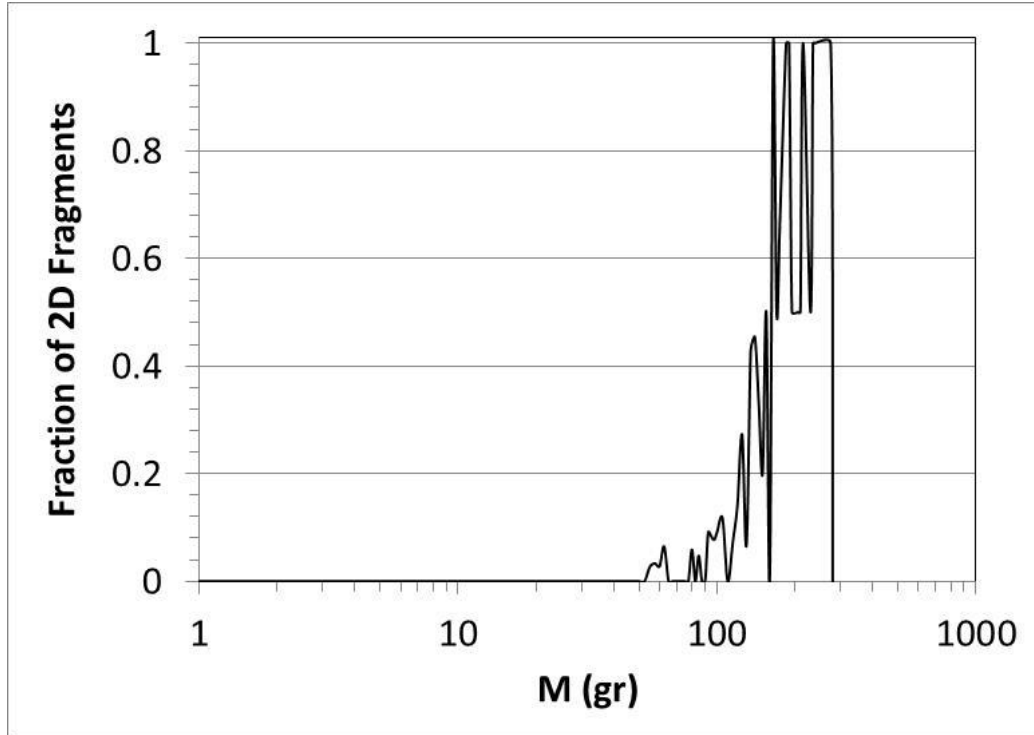
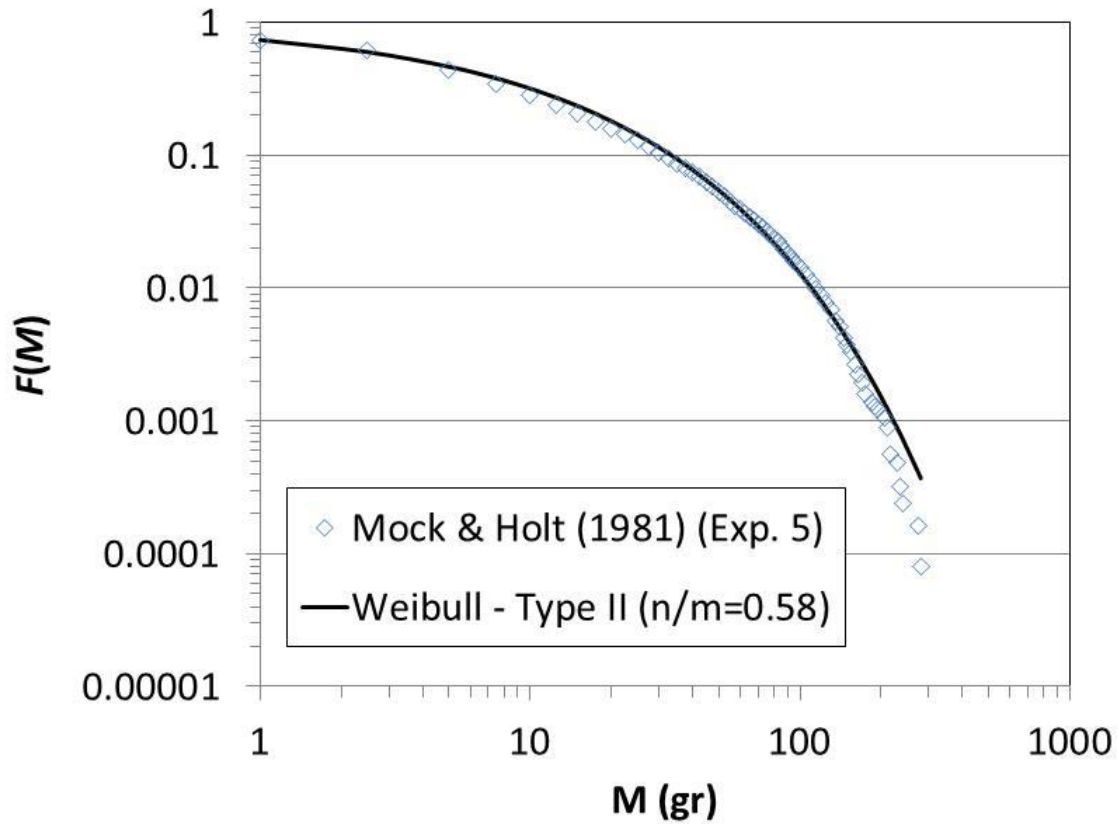


Figure 9. Type II Weibull size distribution vs. test data in a log-log plane for an explosively-fragmented steel cylindrical shell taken from Experiment 5 of Mock & Holt (1981, 1983). The lower plot shows the fraction of fragments retaining portions of both the inner and outer surface of the original steel shell, which are called Type 1 by Mock & Holt (1981, 1983).

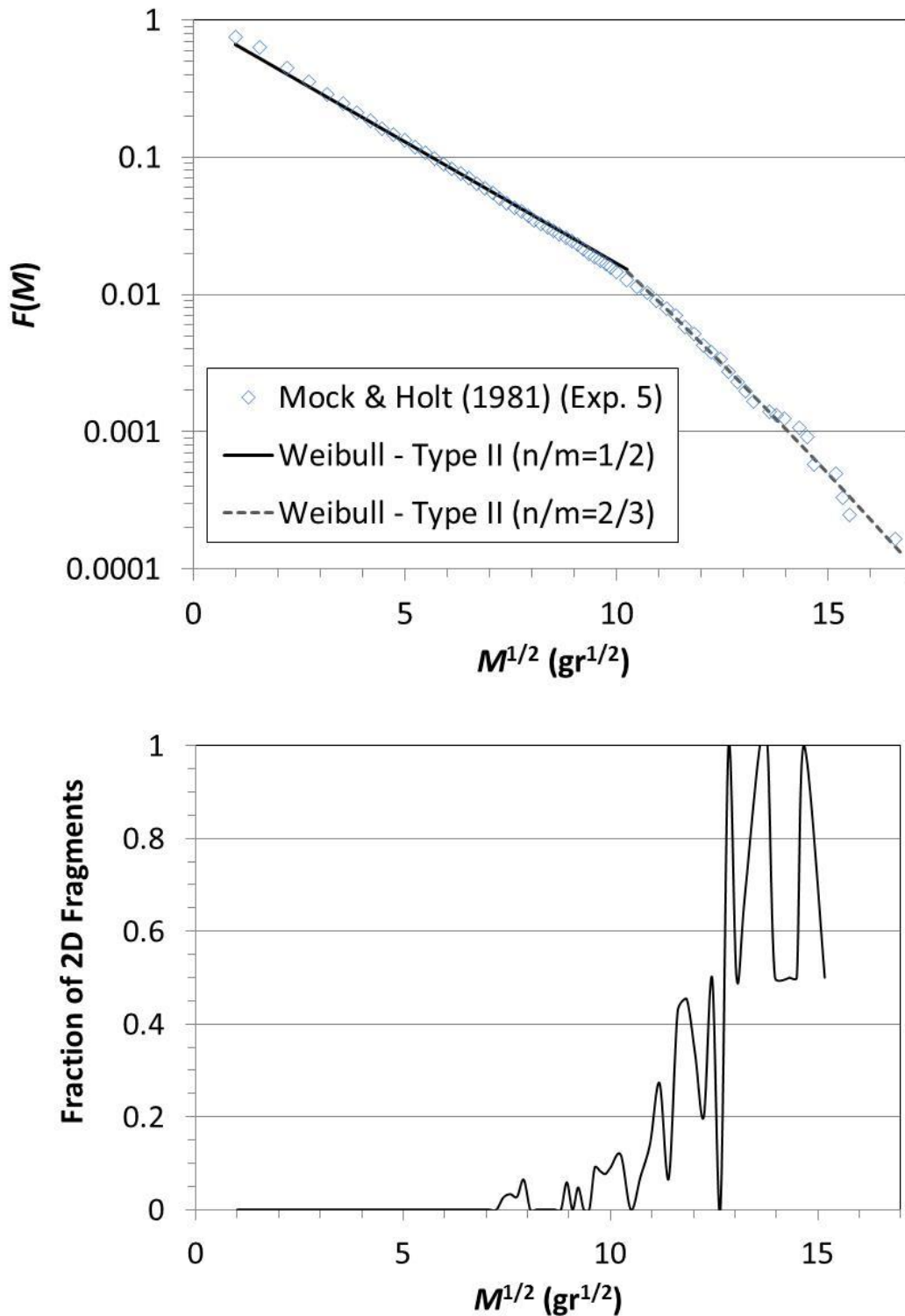


Figure 10. Type II Weibull size distributions vs. test data in a plane in which F is linear or nearly-linear for an explosively-fragmented steel cylindrical shell taken from Experiment 5 of Mock & Holt (1981, 1983). The lower plot shows the fraction of fragments retaining portions of both the inner and outer surface of the original steel shell, which are called Type 1 by Mock & Holt (1981, 1983).

9. Frequency Statistics

To give a sense for how often various universal and compound size distributions occur, Table 15 summarizes the results of six fragmentation studies, each of which reported 20 or more Type II Weibull size distributions (equivalently power laws).

Table 15. Type II Weibull size distributions (equivalently power laws) obtained in six studies of fragmentation with $m=3$.

Reference	Materials	Type	$-n_{\min}$	$-n_{\max}$	No.
Hartmann (1969)	Geological	Original Results	1.80	3.60	20
Turcotte (1986)	Geological Asteroids Meteorites	Literature Survey	1.44	3.54	21
Oddershede et. al. (1993) (*)	Gypsum Frozen Soap Etc.	Original Results	0.4	1.9	20
Kaminski & Jaupart (1998)	Magma	Literature Survey	2.9	3.9	64
Onose & Fujiwara (2004)	Gypsum	Original Results	0.93	8.46	28
Yanovsky, Tur, & Kuklina (2010)	Geological Asteroids Meteorites Glass	Literature Survey	1.44	4.0	21
Total Number of Observed Fragment Size Distributions					174

(*) Four size distributions were excluded because they concerned thin plates that do not necessarily experience three-dimensional fragmentation. Two size distributions were excluded because they were influenced by an exponential roll-off applied to the standard power law.

At first glance, the exponent n in these six studies seem to be uniformly random. However, upon closer examination, universals occur significantly more frequently than other size distributions; see Figure 11. More specifically, for $1 \leq -n \leq 3.5$, universals occur about 30% of the time. Rounding n to the nearest 0.1, universals should occur 20% of the time simply by random chance, according to the law of sixths. Thus, for $1 \leq -n \leq 3.5$, universals occur about 50% more often than would be expected simply by random chance. For $-n > 3.5$, the sample size is small, and universals occur no more often than would be expected by random chance.

Due to common curve fitting practices, many studies obtain compound size distributions when they should have obtained universal size distributions and, vice versa, many studies obtain universal size distributions when they should have obtained compound size distributions. The most reliable studies are those where conditions vary, e.g., Tables 13 and 14. If the fragment size distributions change continuously with changing conditions, they are likely to be compound size distributions. If the fragment size distributions stay the same or jump with changing conditions, they are likely to be universals.

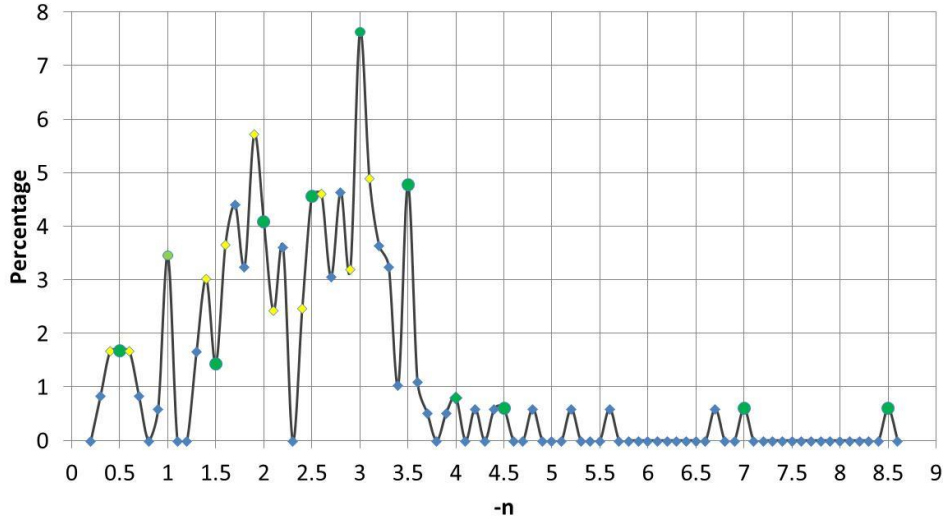


Figure 11. Exponents in Type II Weibull size distributions (equivalently power laws) obtained in the six studies listed in Table 15. The percentages were computed separately for each of the six studies. The final percentage was obtained by equally weighting the six studies to obtain something akin to an average PDF.

Some questionable fitting practices have already been discussed, e.g., using a single size distribution when two or more are actually required, fitting in a single low-discrimination view, etc. As another example, researchers sometimes assume the wrong kind of size distributions, e.g., negative instead of positive size distributions. For example, Ghosh et. al. (1990) gave 26 power law indices for rock fragmentation in open-pit copper mines. Only one is approximately a universal, far less than one would expect simply from random chance. The likely source of the problem is seen in their Figure 2, where the chosen power law fit is linear in the log-log plane while the as-measured size distribution is highly non-linear, i.e., the power law is essentially a tangent line to the true size distribution.

As another example, closely related to the previous one, the vast majority of fits are done with simple least squares fitting, rather than more rigorous statistical procedures such as Maximum Likelihood Estimation (MLE), Pearson’s chi-square test, the Kolmogorov–Smirnov test, or the Wald–Wolfowitz runs test; see, e.g., Clauset et. al. (2009), Gritsevich et. al. (2014).

As another example, fits may be unduly influenced by measurement errors at the extremes. In particular, many experiments fail to obtain fully-adequate statistics for the largest and rarest fragments, because this may require painstaking and costly repetition of the same test. Also, many experiments impose a soft lower limit on fragment size, meaning they obtain only an arbitrary fraction of the fragments below a given threshold.

Finally, fits may use too many size bins, too few size bins, fixed bin widths, or inadequately-varying bin widths. Overpopulated bins – which typically occur for smaller fragments – obscure the characteristics that distinguish one size distribution from another. Underpopulated bins – which typically occur for larger fragments – tend to exaggerate natural random variations. In the ideal, bin widths should vary so that all bins have nearly the same number of fragments or, more realistically, the number of fragments does not change dramatically between adjacent bins.

10. Conclusions

This paper explains why some studies have found that different fragmentation events have similar outcomes, while other studies have found that similar fragmentation events have different outcomes. More specifically, simple fragmentation events – those with simple geometries and steady, uniform strain rates – tend to produce universal size distributions. By contrast, complex fragmentation events – those with complex geometries and unsteady, non-uniform strain rates – tend not to produce universal size distributions. Having said this, naturally-occurring mixing may cause complex fragmentation to resemble simple fragmentation, the main difference being that the key size parameters may vary continuously rather than discretely with changing conditions.

To explain further, this paper finds that simple fragmentation is governed by Type II Weibull size distributions with two free parameters, namely,

$$n = \pm 1, \pm 2, \pm 3, \dots$$

and

$$D_{ref} \sim \dot{\epsilon}^{-2/k}, \quad k = 1, 2, 3, \dots$$

The expression for n is obtained from the three-way intersection of Weibull size distributions, Gamma size distributions, and exponential power law size distributions. Weibull and Gamma size distributions ensure geometric properties for fragmentation and coagulation, respectively, while exponential power law size distributions ensure maximum entropy properties. The expression for k is obtained from conservation laws and constitutive relations.

Simple fragmentation is rarely seen in practice. Fortunately, expressions developed for simple fragmentation often apply to non-simple fragmentation, after straightforward modifications. The following list gives the five conditions required to achieve simple fragmentation and, in most cases, the extension to non-simple fragmentation:

1. The fragment size can be described by a single diameter, such that mass and surface area are constant integer powers of this diameter. Counter-examples include the stringy highly-distended fragments produced by non-Newtonian liquids. This assumption can be relaxed; see, e.g., the discussion of non-integer m in Section 5 and non-constant m in Section 8.
2. Material properties such as density, surface tension, and fracture toughness are approximately constant throughout the fragmentation event.
3. Fragmentation is driven by a constant scalar tensile strain rate. As seen in Appendix A.9, this occurs for thin uniformly-radially-expanding cylindrical and spherical shells, uniformly-stretched bars, uniformly-stretched ligaments, and so forth. This assumption can be relaxed. In particular, Sections 7, 8, and 9 show that mixtures resulting from variable strain rates, tensor strain rates, and non-tensile strain rates often produce Type II Weibull size distributions with:

$$\frac{n}{m} = \pm \frac{1}{6}, \pm \frac{1}{3}, \pm \frac{1}{2}, \pm \frac{2}{3}, \pm \frac{5}{6}, \pm 1, \dots$$

Since these are all integer multiples of one sixth, this may be called the law of sixths.

4. Fragmentation forces overwhelm cohesive strength, i.e., the tensile strain rate is sufficiently large. This assumption can be relaxed; see Section A.10.
5. Fragmentation occurs in a single stage. In other words, fragmentation is not followed by coagulation or additional fragmentation. This assumption can be relaxed; see, e.g., the discussion of universal size distributions for coagulation in Section 5 and the discussion of multi-stage fragmentation in Section 7.3.5.

The non-simple cases covered by the various extensions listed above can be categorized as either compound simple, piecewise simple, or piecewise compound simple.

The last item on the above list merits further discussion. Villermaux et. al. (2004) argued that liquid fragmentation is often dominated by coagulation. More specifically, they say “the fragmentation mechanism ... , somewhat surprisingly, consists of a coalescence process [that] ... is in fact, generic of all situations where drops come from the capillary destabilization of a strongly corrugated ligament.” Their experimental results obtained a Type II Gamma size distribution with $b = 3.5$. As shown by Laney (2016), this approximately corresponds to Type II Weibull distribution with $n/m = 1/2$ and $m = 3$, i.e., it is universal just like fragmentation alone typically obtains.

Similarly, Michel et. al. (2002) argue that certain types of solid fragmentation events may also be dominated by coagulation. More specifically, they used a Smooth Particle Hydrodynamics (SPH) code to simulate fragmentation of monolithic basalt bodies, meant to represent large asteroids, and an N-body code to simulate coagulation. They conclude “that the parent body is first completely shattered at the end of the fragmentation phase, and then subsequent gravitational reaccumulations lead to the formation of an entire family of large and small objects ...” They obtained ten power laws (equivalently Type II Weibull size distributions with $n < 0$), three of which are approximately fundamentals and four of which are approximately semitones, much greater than would be expected by random chance. Again, the combination of fragmentation and coagulation obtains the same universal size distributions as fragmentation alone.

Many researchers have stressed the role of secondary, tertiary, etc. fragmentation, in which the original ‘parent’ fragments break up into smaller ‘child’ fragments due to collisions, aerodynamic forces, and so forth. Similarly, there may be multiple stages of coagulation. This treatment helps to explain why multiple stages of fragmentation and coagulation often produce universal size distributions just like simple one-stage fragmentation.

In short, this paper finds that complex multistage events – which produce a diverse mixture of fragments formed at different times, in different places, in different dimensions, and under

different conditions – may often be treated, in aggregate, as a single virtual event governed by a single universal or compound size distribution.

Where universal size distributions apply, a key unsolved problem is choosing n and k . One common approach is to assume frequently-observed values such as $n = 1$ or 2 and $k = 2$ or 3 . A better but less common approach is to estimate n and k from experimental databases or curve fits to experimental results, e.g. Cunningham (2005). A third possible approach is stability analysis, as discussed briefly in Section 7.1. This is common when easily-visible oscillations occur prior to fragmentation but may apply more generally.

References

M. Ahmadi and R. W. Sellens, A Simplified Maximum-Entropy-Based Drop-Size Distribution, *Atomization and Sprays*, 3(3), 291-310, 1993

W. Arnold and E. Rottenkolber. Fragment Mass Distribution of Metal Cased Explosive Charges, *International Journal of Impact Engineering*, 35(12), 1393-1398, 2008

T. Aste, Circle, Sphere, and Drop Packings, *Physical Review E*, 53(3), 2571-2579, 1996

J. A. Åström, R.P. Linna, J. Timonen, P. F. Møller, and L. Oddershede, Exponential and Power-Law Mass Distributions in Brittle Fragmentation, *Physical Review E*, 70, 026104, 2004

E. Babinsky and P. E. Sojka, Modeling Drop Size Distributions, *Progress in Energy and Combustion Science*, 28(4), 303-329, 2002

I. Bannikova, S. Uvarov, M. Davydova, and O. Naimark, Study of Ceramic Tube Fragmentation under Shock Wave Loading, *Procedia Materials Science*, 3, 592 – 597, 2014

T. D. Bess, *Mass Distribution of Orbiting Man-Made Space Debris*, NASA Technical Note TN D-8108, December 1975

N. Bremond and E. Villermaux, Atomization by Jet Impact, *Journal of Fluid Mechanics*, 549, 273-306, 2006

N. Brilliantov, P. L. Krapivsky, A. Bodrovac, F. Spahn, H. Hayakawa, V. Stadnichuk, and J. Schmidt, Size Distribution of Particles in Saturn's Rings from Aggregation and Fragmentation, *Proceedings of the National Academy of Sciences*, 112(31), 9536–9541, 2015

W. K. Brown and K. H. Wohletz, Derivation of the Weibull Distribution Based on Physical Principles and Its Connection to the Rosin–Rammler and Lognormal Distributions, *Journal of Applied Physics*, 78(4), 2758-2763, 1995

H. A. Carmona, F. K. Wittel, F. Kun, and H. J. Herrmann, Fragmentation Processes in Impact of Spheres, *Physical Review E*, 77, 051302, 2008

- E. S. C. Ching, S. L. Liu, and K.-Q. Xia, Energy Dependence of Impact Fragmentation of Long Glass Rods, *Physica A*, 287(1-2), 83-90, 2000
- W.-H. Chou, L.-P. Hsiang, and G. M. Faeth, Temporal Properties of Drop Breakup in the Shear Breakup Regime, *International Journal of Multiphase Flow*, 23(4), 651-669, 1997
- W.-H. Chou and G. M. Faeth, Temporal Properties of Secondary Drop Breakup in the Bag Breakup Regime, *International Journal of Multiphase Flow*, 24(6), 889-912, 1998
- A. B. Clarke, Unsteady Explosive Activity: Vulcanian Eruptions, In S. Fagents, T. Gregg, R. Lopes, Editors, *Modeling Volcanic Processes: The Physics and Mathematics of Volcanism*, Cambridge University Press, 2013
- A. Clauset, C. R. Shalizi, and M. E. J. Newman, Power-Law Distributions in Empirical Data, *SIAM Review*, 51(4), 661-703, 2009
- E. A. Cohen, New Formulas for Predicting the Size Distribution of Warhead Fragments, *Mathematical Modeling*, 2(1), 19-32, 1981
- J. Cousin, S. J. Yoon, and C. Dumouchel, Coupling of Classical Linear Theory and Maximum Entropy Formalism for Prediction of Drop-Size Distribution in Sprays: Application to Pressure Swirl Atomizers, *Atomization and Sprays*, 6(5), 601-622, 1996
- R. Cowan, New Classes of Random Tessellations Arising from Iterative Division of Cells, *Advances in Applied Probability*, 42(1), 26-47, 2010
- C. V. B. Cunningham, The Kuz-Ram Fragmentation Model – 20 Years On, In R. Holmberg et al., Editors, *Proceedings of the 3rd World Conference on Explosives and Blasting*, European Federation of Explosives Engineers, 2005
- Z. Dai and G. M. Faeth, Temporal Properties of Secondary Drop Breakup in the Multimode Breakup Regime, *International Journal of Multiphase Flow*, 27(2), 217-236, 2001
- A. Déchelette, E. Babinsky, and P. E. Sojka, Drop Size Distributions, In N. Ashgriz, Editor, *Handbook of Atomization and Sprays: Theory and Application*, Springer, 2011
- G. Domokos, F. Kun, A. Árpád, and T. Szabó, Universality of Fragment Shapes, *Scientific Reports*, 5, 9147, 2015
- C. Dumouchel, The Maximum Entropy Formalism and the Prediction of Liquid Spray Drop-Size Distribution, *Entropy*, 11, 713-747, 2009
- O. Durand and L. Souldard, Large-Scale Molecular Dynamics Study of Jet Breakup and Ejecta Production from Shock-Loaded Copper with a Hybrid Method, *Journal of Applied Physics*, 111, 044901, 2012

- O. Durand and L. Soulard, Power Law and Exponential Ejecta Size Distributions from the Dynamic Fragmentation of Shock-loaded Cu and Sn Metals under Melt Conditions, *Journal of Applied Physics*, 114, 194902, 2013
- M. R. Edwards and C. Deal, Effect of Heat Treatment on Small Scale Fragmentation of Aluminium Alloy, *Materials Science and Technology*, 27(1), 332-338, 2011
- R. Engelman, Maximum Entropy Principles in Fragmentation Data Analysis, In L. Davison, D. E. Grady, and M. Shahinpoor, Editors, *High-Pressure Shock Compression of Solids II*, Springer-Verlag, 1996
- J.-S. Ferenc and Z. Néda, On the Size Distribution of Poisson Voronoi Cells, *Physica A*, 385(2), 518-526, 2007
- S. K. Friedlander and C. S. Wang, The Self-Preserving Particle Size Distribution for Coagulation by Brownian Motion, *Journal of Colloid and Interface Science*, 22(2), 126-132, 1966
- A. Ghosh, J. J. K. Daemen, and D. van Zyl, Fractal-Based Approach to Determine the Effect of Discontinuities on Blast Fragmentation, In W. A. Hustrulid and G. A. Johnson, *Rock Mechanics: Contributions and Challenges*, A. A. Balkema Publishers, 1990
- J. J. Gilvarry, Fracture of Brittle Solids. I. Distribution Function for Fragment Size in Single Fracture (Theoretical), *Journal of Applied Physics*, 32(3), 391-399, 1961
- J. J. Gilvarry and B. H. Bergstrom, Fracture of Brittle Solids. II. Distribution Function for Fragment Size in Single Fracture (Experimental), *Journal of Applied Physics*, 32(3), 400-410, 1961
- J. J. Gilvarry and B. H. Bergstrom, Fracture of Brittle Solids. III. Experimental Results on the Distribution of Fragment Size in Single Fracture, *Journal of Applied Physics*, 33 (11), 3211-3213, 1962
- J. R. Gladden, N. Z. Handzy, A. Belmonte, and E. Villermaux, Dynamic Buckling and Fragmentation in Brittle Rods, *Physical Review Letters*, 94, 035503, 2005
- D. E. Grady and M. E. Kipp, Geometric Statistics and Dynamic Fragmentation, *Journal of Applied Physics*, 58(3), 1985
- D. E. Grady and M. E. Kipp, Dynamic Rock Fragmentation, In B. K. Atkinson, Editor, *Fracture Mechanics of Rock*, Academic Press, 429-475, 1987
- D. E. Grady, L. T. Wilson, D. R. Reedal, L. D. Kuhns, M. E. Kipp, and J. W. Black, Comparing Alternate Approaches in the Scaling of Naturally Fragmenting Munitions, In I. R. Crewther, Editor, *Proceedings of the 19th International Symposium on Ballistics*, IBS, 2001

- M. Gritsevich, V. Vinnikov, T. Kohout, J. Tóth, J. Peltoniemi, L. Turchak, and J. Virtanen, A Comprehensive Study of Distribution Laws for the Fragments of Košice Meteorite, *Meteoritics & Planetary Science*, 49(3), 328–345, 2014
- R. A. Hamilton, J. S. Curtis, and D. Ramkrishna, Beyond Log-Normal Distributions: Hermite Spectra for Solving Population Balances, *AIChE Journal*, 49(9), 2328-2343, 2003
- W. K. Hartmann, Terrestrial, Lunar, and Interplanetary Rock Fragmentation, *Icarus*, 10(2), 201-213, 1969
- J. P. Hooper, Impact Fragmentation of Aluminum Reactive Materials, *Journal of Applied Physics*, 112, 043508, 2012
- L.-P. Hsiang and G. M. Faeth, Near-Limit Drop Deformation and Secondary Breakup, *International Journal of Multiphase Flow*, 18(5), 635-652, 1992
- L.-P. Hsiang and G. M. Faeth, Drop Deformation and Breakup Due to Shock Wave and Steady Disturbances, *International Journal of Multiphase Flow*, 21(4), 545-560, 1993
- H. Inaoka and H. Takayasu, Universal Fragment Size Distribution in a Numerical Model of Impact Fracture, *Physica A*, 229(1), 5-25, 1996
- H. Inaoka and H. Takayasu, Application of Statistical Physics to Impact Fragmentation, *Physica A*, 274(1), 300-309, 1999
- B. A. Ivanov, A. T. Basilevsky, and O. Y. Schmidt, On the Fragment-Size Distribution of Ejecta of Impact Craters, *Lunar and Planetary Science*, XIV, 345-346, 1983
- N. L. Johnson, P. H. Krisko, J.-C. Liou, and P. D. Anz-Meador, NASA's New Breakup Model of EVOLVE 4.0, *Advances in Space Research*, 28(8), 1377–1384, 2001
- E. Kaminski and C. Jaupart, The Size Distribution of Pyroclasts and the Fragmentation Sequence in Explosive Volcanic Eruptions, *Journal of Geophysical Research*, 103(B12), 29,759-29,779, 1998
- T. Kiang, Random Fragmentation in Two and Three Dimensions, *Zeitschrift für Astrophysik*, 64, 433-439, 1966
- M. Kostoglou and A.J. Karabelas, Optimal Low Order Methods of Moments for Solving the Fragmentation Equation, *Powder Technology*, 143– 144, 280– 290, 2004
- V. S. Kumar and V. Kumaran, Voronoi Cell Volume Distribution and Configurational Entropy of Hard-Spheres, *The Journal of Chemical Physics*, 123(11), 114501, 2005
- F. Kun and H. J. Herrmann, Transition from Damage to Fragmentation in Collision of Solids, *Physical Review E*, 59(3), 2623-2632, 1999

C. B. Laney, *Improved Root Normal Size Distributions for Liquid Atomization*, Defense Threat Reduction Agency Technical Report DTRA-TR-16-003, November 2015a

C. B. Laney, *Transformation and Self-Similarity Properties of Gamma and Weibull Fragment Size Distributions*, Defense Threat Reduction Agency Technical Report DTRA-TR-16-006, December 2015b

C. B. Laney, *On the Relationships Between Liquid and Solid Fragmentation*, Defense Threat Reduction Agency Technical Report DTRA-TR-16-19, January 2016

H. Lhuissier and E. Villermaux, Bursting Bubble Aerosols, *Journal of Fluid Mechanics*, 696, 5-44, 2012

H. Lhuissier, C. Sun, A. Prosperetti, and D. Lohse, Drop Fragmentation at Impact onto a Bath of an Immiscible Liquid, *Physical Review Letters*, 110, 264503, 2013

X. Li and R. S. Tankin, Droplet Size Distribution: A Derivation of a Nukiyama-Tanasawa Type Distribution Function, *Combustion Science and Technology*, 56(1), 65-76, 1987

P. G. Lind, R. M. Baram, and H. J. Herrmann, Obtaining the Size Distribution of Fault Gouges with Polydisperse Bearings, *Physical Review E*, 77, 021304, 2008

U. Lindblad, Extension of the Parameter Range of the Power Series Expressions and Asymptotes of the Exact Solutions to Smoluchowski's Coagulation Equation with Gamma Distributions as Initial Size Spectra, *Journal of Colloid and Interface Science*, 283(1), 267-273, 2005

U. Lindblad, Asymptotic Solutions to the Smoluchowski's Coagulation Equation with Singular Gamma Distributions as Initial Size Spectra, *Journal of Colloid and Interface Science*, 309(2), 440-444, 2007

C. C. Lineau, Random Fracture of a Brittle Solid, *Journal of the Franklin Institute*, 221(4), 485-494, 1936

S. S. Manna and H. J. Herrmann, Precise Determination of the Fractal Dimensions of Apollonian Packing and Space-Filling Bearings, *Journal of Physics A: Mathematical and General*, 24 (L481-L490), 1991

P. Marmottant and E. Villermaux, Fragmentation of Stretched Liquid Ligaments, *Physics of Fluids*, 16(8), 2732-2741, 2004

Z. A. Melzak, The Effects of Coalescence in Certain Collision Processes, *Quarterly Journal of Applied Mathematics*, 11, 231-236, 1953

P. Michel, P. Tanga, W. Benz, and D. C. Richardson, Formation of Asteroid Families by Catastrophic Disruption: Simulations with Fragmentation and Gravitational Reaccumulation, *Icarus*, 160(1), 10-23, 2002

- W. Mock and W. H. Holt, *Computational and Experimental Determination of Fragmentation for Naturally Fragmenting Warheads*, U.S. Naval Surface Warfare Center Technical Report, NSWC TR 80-238, May 1981
- W. Mock and W. H. Holt, Fragmentation Behavior of Armco Iron and HF-1 Steel Explosive-Filled Cylinders, *Journal of Applied Physics*, 54(5), 2344-2351, 1983
- N. F. Mott and E. H. Linfoot, *A Theory of Fragmentation*, U. K. Ministry of Supply, AC3348, January 1943 (see also D. E Grady, *Fragmentation of Rings and Shells: The Legacy of N. F. Mott*, Springer, 2006)
- J. F. Moxnes and S. Børve, Simulation of Natural Fragmentation of Rings Cut from Warheads, *Defence Technology*, 11(4), 319-329, 2015
- L. Oddershede, P. Dimon, and J. Bohr, Self-Organized Criticality in Fragmenting, *Physical Review Letters*, 71(19), 3107-3110, 1993
- J. D. O'Keefe and T. J. Ahrens, Impact and Explosion Crater Ejecta, Fragment Size, and Velocity, *Icarus*, 62, 328-338, 1985
- J. D. O'Keefe and T. J. Ahrens, The Size Distribution of Fragments Ejected at a Given Velocity from Impact Craters, *International Journal of Impact Engineering*, 5, 493-499, 1987
- N. Onose and A. Fujiwara, Mass-Velocity Distributions of Fragments in Oblique Cratering on Gypsum, *Meteoritics and Planetary Science*, 39(2), 321-331, 2004
- A. Parker, Ž. Ivezić, M. Jurić, R. Lupton, M.D. Sekora and A. Kowalski, The Size Distributions of Asteroid Families in the SDSS Moving Object Catalog 4, *Icarus*, 198, 138–155, 2008
- M. Pilch and C. A. Erdman, Use of Breakup Time Data and Velocity History Data to Predict the Maximum Size of Stable Fragments for Acceleration-Induced Breakup of a Liquid Drop, *International Journal of Multiphase Flows*, 13(6), 741-757, 1987
- P. Rosin and E. Rammner, Die Kornzusammensetzung des Mahlgutes im Lichte der Wahrscheinlichkeitslehre, *Kolloid-Zeitschrift*, 67(1), 16-26, 1934
- G. A. Ruff, P.-K. Wu, L. P. Bernal and G. M. Faeth, Continuous- and Dispersed-Phase Structure of Dense Nonevaporating Pressure-Atomized Sprays, *Journal of Propulsion and Sprays*, 8(2), 1992
- P. K. Sahoo and T. Riedel, *Mean Value Theorems and Functional Equations*, World Scientific, 1998
- K. A. Sallam, C. Aalburg, G.M. Faeth, K.-C. Lin, C.D. Carter, and T.A. Jackson, Primary Breakup of Aerated-Liquid Jets in Supersonic Crossflows, *Atomization and Sprays*, 16(6), 657-672, 2006

- J. E. Schoutens, Empirical Analysis of Nuclear and High-Explosive Cratering and Ejecta, In *Nuclear Geoplosics Sourcebook*, IV(II), U.S. Defense Nuclear Agency, DNA 6501H-4-2, 1979
- W. T. Scott, Analytic Studies on Cloud Droplet Coalescence, *Journal of Atmospheric Sciences*, 25(1), 54-65, 1968
- W. R. Seebaugh, A Dynamic Crater Ejecta Model, In D. J. Roddy, R. O. Pepin, and R. B. Merrill, Editors, *Impact and Explosion Cratering*, Pergammon Press, 1977
- H. C. Simmons, The Correlation of Drop-Size Distributions in Fuel Nozzle Spray, Parts I and II, *Journal of Engineering for Power*, 99(3), 309-319, 1977
- T. M. Spielbauer, T. N. Adams, J. E. Monacelli, and R. T. Bailey, Droplet Size Distribution of Black Liquor Sprays, *Proceedings of International Chemical Recovery Conference*, Ottawa, Canada, TAPPI/CPPA, 1989
- K. Sakuraba, Y. Tsuruda, T. Hanada, J.-C. Liou, and Y. Akahoshi, Investigation and Comparison Between New Satellite Impact Test Results and NASA Standard Breakup Model, *International Journal of Impact Engineering*, 35(12), 1567–1572, 2008
- G. Timár, J. Blömer, F. Kun, and H. J. Herrmann, New Universality Class for the Fragmentation of Plastic Materials, *Physical Review Letters*, 104, 095502, 2010
- D. C. Tucker, W. R. Orr, and C. R. Hoggatt, *Prediction of the Theoretical Behavior and Energy Transfer when Solids are Subjected to Explosive Loading*, Denver Research Institute Summary Report, U.S. Defense Technical Information Service, AD0613697, January 1965
- D. L. Turcotte, Fractals and Fragmentation, *Journal of Geophysical Research*, 91(B2), 1921–1926, 1986
- E. Villermaux, Ph. Marmottant, and J. Duplat, Liquid-Mediated Spray Formation, *Physical Review Letters*, 92(7), 074501, 2004
- A. Vledouts, N. Vandenberghe, and E. Villermaux, Fragmentation as an Aggregation Process, *Proceedings of the Royal Society A: Mathematical, Physical and Engineering Sciences*, 471, 20150678, 2015
- A. Vledouts, N. Vandenberghe, and E. Villermaux, Fragmentation as an Aggregation process: The Role of Defects, *Proceedings of the Royal Society A: Mathematical, Physical and Engineering Sciences*, 472, 20150679, 2016a
- A. Vledouts, J. Quinard, N. Vandenberghe, and E. Villermaux, *Journal of Fluid Mechanics*, 788, 246-273, 2016b

- F. K. Wittel, F. Kun, H. J. Herrmann, and B. H. Kröplin, Fragmentation of Shells, *Physical Review Letters*, 93(3), 035504, 2004
- F. K. Wittel, F. Kun, H. J. Herrmann, and B. H. Kröplin, Breakup of Shells Under Explosion and Impact, *Physical Review E*, 71(1), 016108, 2005
- F. K. Wittel, F. Kun, B. H. Kröplin, and H. J. Herrmann, Study on the Fragmentation of Shells, *International Journal of Fracture*, 140(1), 243, 2006
- F. K. Wittel, H. A. Carmona, F. Kun, and H. J. Herrmann, Mechanisms in Impact Fragmentation, *International Journal of Fracture*, 154(1-2), 105-117, 2008
- P.-K. Wu, G. A. Ruff, and G. M. Faeth, Primary Breakup in Liquid-Gas Mixing Layers, *Atomization and Sprays*, 1(4), 421-440, 1991
- K. Yamakoshi, K. Nogami, and T. Shimamura, Size Distribution of Siderophile Element Concentrations in Black Magnetic Spherules from Deep-Sea Sediments, *Journal of Geophysical Research*, 86(B4), 3129–3132, 1981
- V. V. Yanovsky, A. V. Tur, and O. V. Kuklina, Universal Elements of Fragmentation, *Journal of Experimental and Theoretical Physics*, 110(5), 863-876, 2010
- F. Zhou, J.-F. Molinari, and K. T. Ramesh, Characteristic Fragment Size Distributions in Dynamic Fragmentation, *Applied Physics Letters*, 88, 261918, 2006

Appendix A. Algebraic Conservation Laws for Simple Fragmentation Events

A.1 Introduction

This appendix derives simple algebraic expressions for average fragment sizes from conservation of mass, momentum, and energy, plus constitutive relations. This treatment assumes that fragmentation is driven by a scalar tensile component of the strain rate or, alternatively, the tensile component of the kinetic energy. This treatment builds on earlier proofs including the following:

Spherical Geometries	Grady & Kipp (1993)
Cylindrical Geometries	Mott & Linfoot (1943); Grady (1982); Wu et. al. (1992)
Cartesian Geometries	Lefebvre (1992a,b); Kirane et. al. (2015)

The current approach has several advantages over earlier approaches. First, earlier approaches usually did not commit to a particular average fragment size, such as the mass mean diameter; the current approach is specific. Second, earlier approaches usually assumed that the original fragmenting body was a solid or hollow cylinder, sphere, cube, and so forth; this approach makes no such assumption. Third, earlier approaches usually assumed that the fragments were spheres, cubes, and so forth; this approach makes no such assumptions. Finally, earlier approaches assumed a constant multiplicative factor; this approach shows that the multiplicative factor is not constant but rather depends on the fragment size distribution, fragment shape, the choice of average fragment diameter, and the minimum fragment size inherent in most experimental measurements.

A.2 Algebraic Forms of Conservation of Energy

If the two primary forms of energy are kinetic energy and surface energy, conservation of energy requires:

$$\iiint_{\text{body}} \frac{1}{2} V^2 dM + \Gamma \mathcal{A} = \sum_{i=1}^N \left(\frac{1}{2} U_i^2 M_i + \Gamma_i \mathcal{A}_i \right) \quad (\text{A.1})$$

where V is the tensile component of velocity before fragmentation measured in units such as cm/s, U_i is the tensile component of velocity of fragment i measured in units such as cm/s, \mathcal{A} is the surface area before fragmentation measured in units such as cm^2 , \mathcal{A}_i is the surface area of fragment i measured in units such as cm^2 , M_i is the mass of fragment i measured in units such as g, Γ_i is the surface energy per unit area of fragment i measured in units such as dyne/cm, and N is the total number of fragments. Notice that:

$$\iiint_{\text{body}} \frac{1}{2} V^2 dM = \sum_{j=1}^N \frac{1}{2} V_j^2 M_j \quad (\text{A.2})$$

In other words, the tensile kinetic energy of the whole is equal to the tensile kinetic energy of its parts. Also assume that:

$$\mathcal{A} \ll \sum_{i=1}^N \mathcal{A}_i \quad (\text{A.3})$$

In other words, assume the surface energy of the whole is much less than the surface energy of its parts. Finally assume that:

$$U_j \ll V_j \quad (\text{A.4})$$

In other words, assume that the vast majority of tensile kinetic energy is converted to surface energy. Notice that Equation (A.4) concerns only the *tensile* component of velocity. Fragments generally retain a substantial *non-tensile* component of velocity; see, e.g., Kennedy (1998). With the above assumptions, Equation (A.2) can be written as follows

$$\sum_{j=1}^N \frac{1}{2} M_j V_j^2 = \sum_{i=1}^N \Gamma_i \mathcal{A}_i \quad (\text{A.5})$$

Equation (A.5) allows simple analytical solutions if V_j is a power of D_j and Γ_i is a power of D_i . More specifically, suppose:

$$V_j = V_0 D_j^\nu \quad (\text{A.6})$$

$$\Gamma_i = \Gamma_0 D_i^\gamma \quad (\text{A.7})$$

where V_0 , ν , Γ_0 and γ are constants. In addition, Equation (1) says:

$$\mathcal{A}_j = c_{m-1} D_j^{m-1} \quad (\text{A.8})$$

$$M_j = \rho c_m D_j^m \quad (\text{A.9})$$

Notice that if $m=1$, then $c_{m-1} = c_0 = 2\mathcal{A}_0$. In other words, $\mathcal{A}_i = 2\mathcal{A}_0$ where \mathcal{A}_0 is a fixed cross-sectional area. Equation (A.5) becomes:

$$\sum_{j=1}^N D_j^{2\nu-\gamma+1} \frac{D_j^{\gamma+m-1}}{\sum_{i=1}^N D_i^{\gamma+m-1}} = \frac{2c_{m-1}\Gamma_0}{c_m\rho V_0^2} \quad (\text{A.10})$$

By Equation (5), this becomes:

$$X_{Y \text{ avg}} = \frac{2c_{m-1}\Gamma_0}{c_m\rho V_0^2} \quad \text{for} \quad 2\nu - \gamma + 1 > 0, \quad \gamma + m - 1 \geq 0 \quad (\text{A.11a})$$

$$X'_{Y \text{ avg}} = \frac{c_m\rho V_0^2}{2c_{m-1}\Gamma_0} \quad \text{for} \quad 2\nu - \gamma + 1 < 0, \quad \gamma + m - 1 \geq 0 \quad (\text{A.11b})$$

where:

$$X = D^{|2\nu-\gamma+1|} \quad (\text{A.12})$$

$$Y = D^{\gamma+m-1} \quad (\text{A.13})$$

If $\gamma + m - 1 = 0$ then $X_{Y \text{ avg}}$ is replaced by $X_{\text{ avg}}$ and $X'_{Y \text{ avg}}$ is replaced by $X'_{\text{ avg}}$.

This is the final result. Notice that Equation (A.11a) applies primarily to positive size distributions, e.g., Type II Weibull distributions with $n > 0$. Similarly, Equation (A.11b) applies primarily to negative size distributions, e.g., Type II Weibull distributions with $n < 0$.

A.3 Case 1

Starting with the easiest case, suppose that:

$$V_j = V_0 = \text{const.} \quad (\text{A.14})$$

$$\Gamma_i = \Gamma_0 = \text{const.} \quad (\text{A.15})$$

Using conservation of momentum, Equation (A.14) can be written as follows:

$$V_j = V_0 = \frac{1}{2} \dot{\epsilon} D_0 \quad (\text{A.16})$$

where D_0 is a fixed geometric length scale measured in units such as cm and $\dot{\epsilon}$ is a tensile strain rate measured in units such as 1/s. For example, Grady (1981) suggests $D_0 = L$ where L is the initial length of a linear body. Other possibilities include: the thickness of a cylindrical shell, e.g., Mott et. al. (1944); the thickness of a flat sheet, e.g., Lefebvre (1992a, b); and the

characteristic size of or spacing between pre-existing or strain-induced features such as flaws, cracks, voids, bubbles, or instability-driven oscillations, e.g., Curran & Seaman (1996), Zhou et al. (2005).

Using constitutive equations, Equation (A.15) can be written as follows:

$$\Gamma_0 = \sigma \quad (\text{A.17})$$

for inviscid liquids where σ is the surface tension measured in units such as dyne/cm; see, e.g., Grady (1982) and Grady & Kipp (1982). Similarly:

$$\Gamma_0 = \frac{1}{2} G_s \quad (\text{A.18})$$

for solids where G_c is the work of fracture measured in units such as dyne/cm. Zhou et al. (2005) describe G_c as the “fracture energy dissipated by the crack.” Notice that:

$$G_c = K_c^2 / E$$

$$E = \rho c_s^2$$

where K_c is the fracture toughness measured in units such as $\text{g}/(\text{cm}^{1/2}\text{s}^2)$, E is the Young’s modulus measured in units such as dyne/cm^2 , and c_s is the elastic wave velocity measured in units such as cm/s . Then Equation (A.18) can be rewritten as follows:

$$\Gamma_0 = \frac{K_c^2}{2\rho c_s^2} \quad (\text{A.19})$$

Substituting $V_0 = \dot{\varepsilon} D_0 / 2$, $\nu = 0$ and $\gamma = 0$ into Equations (A.11a), (A.12), and (A.13) yields:

$$D_{x^{m-1} \text{ avg}} = \frac{8c_{m-1}\Gamma_0}{c_m \rho D_0^2 \dot{\varepsilon}^2} \quad (\text{A.20})$$

Suppose that Equation (A.14) is replaced by the following:

$$V_j = \text{const.} \frac{\Gamma_0}{\rho \dot{\varepsilon} D_0 D_j} \quad (\text{A.21})$$

while Equation (A.15) is the same as before. Substituting $V_0 = \text{const.} \Gamma_0 / (\rho \dot{\varepsilon} D_0)$, $\nu = -1$ and $\gamma = 0$ into Equations (A.11b), (A.12), and (A.13) yields:

$$D'_{X^{m-1} avg} = \frac{\text{const. } c_m \Gamma_0}{c_{m-1} \rho D_0^2 \dot{\epsilon}^2} \quad (\text{A.22})$$

Notice that Equation (A.20) applies to positive size distributions while Equation (A.22) applies to negative size distributions.

Equations (A.20) and (A.22) can be converted to other average sizes using Equations (11) to (14). In general, this produces expressions for average fragment diameters in the following form:

$$\text{const.} \frac{\Gamma_0}{\rho D_0^2 \dot{\epsilon}^2} \quad (\text{A.23})$$

For example, for positive size distributions for liquids, substituting Equation (A.16) and (A.17) into Equation (A.23) gives:

$$\text{const.} \frac{\sigma}{\rho V_0^2} \quad (\text{A.24})$$

which approximately agrees with well-known results for atomization of flat and conical liquid sheets; see, e.g., Lefebvre (1992a, b) and Barreras et. al. (2006).

A.4 Case 2

Suppose that:

$$V_j = \frac{1}{2} \dot{\epsilon} D_j \quad (\text{A.25})$$

Notice that Equation (A.25) is the same as Equation (A.16), after replacing D_0 by D_j , In addition, based on constitutive equations for solids, Grady (1988) and Grady & Kipp (1993) suggest:

$$\Gamma_i = \frac{1}{6} \epsilon_c Y D_i \quad (\text{A.26})$$

where Y is a constant critical failure strength, such as the tensile yield strength, measured in units such as dynes/cm² and ϵ_c is a unitless “critical volumetric strain at void coalescence” assumed to be 0.15. Substituting $V_0 = \dot{\epsilon}/2$, $\nu = 1$, $\Gamma_0 = \epsilon_c Y / 6$, and $\gamma = 1$ into Equations (A.11a), (A.12), and (A.13) yields:

$$(D^2)_{D^m avg} = \frac{4c_{m-1} \epsilon_c Y}{3c_m \rho \dot{\epsilon}^2} \quad (\text{A.27})$$

Suppose Equation (A.25) is replaced by the following:

$$V_j = \text{const.} \frac{\Gamma_j}{\rho \dot{\epsilon} D_j^2} \quad (\text{A.28})$$

while Equation (A.26) is the same as before. Substituting Equation (A.26) into Equation (A.28) yields:

$$V_j = \text{const.} \frac{\epsilon_c Y}{\rho \dot{\epsilon} D_j} \quad (\text{A.29})$$

Substituting $V_0 = \text{const.} \epsilon_c Y / (\rho \dot{\epsilon})$, $\nu = -1$, $\Gamma_0 = \epsilon_c Y / 6$, and $\gamma = 1$ into Equations (A.11b), (A.12), and (A.13) yields:

$$(D^2)'_{D^m \text{ avg}} = \text{const.} \frac{c_m \epsilon_c Y}{c_{m-1} \rho \dot{\epsilon}^2} \quad (\text{A.30})$$

Notice that Equation (A.27) applies to positive size distributions while Equation (A.30) applies to negative size distributions.

Equations (A.27) and (A.30) can be converted to other average sizes using Equations (11) to (14). In general, this produces expressions for average fragment diameters in the following form:

$$\left(\frac{\text{const.} \epsilon_c Y}{\rho \dot{\epsilon}^2} \right)^{1/2} \quad (\text{A.31})$$

For example, for positive size distributions with $m = 3$, Equation (A.27) can be written as follows:

$$\bar{\mathcal{A}}_{M \text{ avg}} = \frac{4c_{m-1} \epsilon_c Y}{3c_m \rho \dot{\epsilon}^2} \quad (\text{A.32})$$

or:

$$D_{\text{avg}} = \left(\frac{C \epsilon_c Y}{\rho \dot{\epsilon}^2} \right)^{1/2} \quad (\text{A.33})$$

where:

$$C = \frac{4c_2}{3c_3 Q_{\bar{\mathcal{A}}}^2 S_{\bar{\mathcal{A}}}} \quad (\text{A.34})$$

For spherical fragments:

$$\frac{c_2}{c_3} = \frac{\pi}{\pi/6} = 6 \quad (\text{A.35})$$

Then:

$$C = \frac{8}{Q_{\mathcal{A}}^2 S_{\mathcal{A}}} \quad (\text{A.36})$$

If $Q_{\mathcal{A}}^2 S_{\mathcal{A}} \approx 1$, this agrees with expressions given by Mott (1947), Grady (1982), Grady (1988), and Grady & Kipp (1993) for explosively-driven metal shells.

A.5 Case 3

Suppose that:

$$V_j = \frac{1}{2} \dot{\epsilon} D_j \quad (\text{A.37})$$

$$\Gamma_i = \Gamma_0 = \text{const.} \quad (\text{A.38})$$

Notice that Equation (A.37) is the same as Equation (A.25) and Equation (A.38) is the same as Equation (A.15). Substituting $V_0 = \dot{\epsilon}/2$, $\nu = 1$, and $\gamma = 0$ into Equations (A.11a), (A.12), and (A.13) yields:

$$(D^3)_{D^{m-1} \text{ avg}} = \frac{8c_{m-1}\Gamma_0}{c_m \rho \dot{\epsilon}^2} \quad (\text{A.39})$$

Suppose Equation (A.37) is replaced by the following:

$$V_j = \text{const.} \frac{\Gamma_j}{\rho \dot{\epsilon} D_j^2} \quad (\text{A.40})$$

while Equation (A.38) is the same as before. Notice that Equation (A.40) is the same as Equation (A.28). Substituting $V_0 = \text{const.} \Gamma_0 / (\dot{\epsilon} \rho)$, $\nu = -2$, and $\gamma = 0$ into Equations (A.11b), (A.12), and (A.13) yields:

$$(D^3)'_{D^{m-1} \text{ avg}} = \text{const.} \frac{c_m \Gamma_0}{c_{m-1} \rho \dot{\epsilon}^2} \quad (\text{A.41})$$

Notice that Equation (A.39) applies to positive size distributions while Equation (A.41) applies to negative size distributions.

Equations (A.39) and (A.41) can be converted to other average sizes using Equations (11) to (14). In general, this produces expressions for average fragment diameters in the following form:

$$\left(\frac{\text{const} \Gamma_0}{\rho \dot{\epsilon}^2} \right)^{1/3} \quad (\text{A.42})$$

which agrees with the well-known expressions given by Mott & Linfoot (1943), Grady (1982), and Grady & Kipp (1993) for explosively-driven cylindrical metal shells.

For example, for positive size distributions with $m = 3$, Equation (A.39) can be written as follows:

$$M_{\bar{x} \text{ avg}} = \frac{8c_2 \Gamma_0}{\dot{\epsilon}^2} \quad (\text{A.43})$$

Because this example is so well-known, more details will be given for this example than for the others. By Equations (11) to (14), Equation (A.43) can be written as follows:

$$D_{\text{avg}} = \left(\frac{C\Gamma}{\rho \dot{\epsilon}^2} \right)^{1/3} \quad (\text{A.44})$$

$$D'_{\text{avg}} = \left(\frac{C'\Gamma}{\rho \dot{\epsilon}^2} \right)^{1/3} \quad (\text{A.45})$$

where:

$$C = \frac{8c_2}{c_3 Q_{\bar{x}}^3 S_M} \quad (\text{A.46})$$

$$C' = \frac{8c_2}{c_3 Q_{\bar{x}}^3 R^3 S_M} \quad (\text{A.47})$$

For Type II Weibull size distributions, Tables 3 and 4 give:

$$Q_{\bar{x}} = \frac{\Gamma\left(1 + \frac{3}{n}\right)}{\Gamma\left(1 + \frac{1}{n}\right) \Gamma\left(1 + \frac{2}{n}\right)}$$

$$R = \Gamma\left(1 + \frac{1}{n}\right) \Gamma\left(1 - \frac{1}{n}\right)$$

$$S_M = \frac{\Gamma\left(1 + \frac{3}{n}\right)}{\Gamma\left(1 + \frac{1}{n}\right)^3}$$

Then:

$$C = \frac{8c_2 \Gamma\left(1 + \frac{1}{n}\right)^6 \Gamma\left(1 + \frac{2}{n}\right)^3}{c_3 \Gamma\left(1 + \frac{3}{n}\right)^4} \quad (\text{A.48})$$

$$C' = \frac{8c_2 \Gamma\left(1 + \frac{1}{n}\right)^3 \Gamma\left(1 + \frac{2}{n}\right)^3}{c_3 \Gamma\left(1 - \frac{1}{n}\right)^3 \Gamma\left(1 + \frac{3}{n}\right)^4} \quad (\text{A.49})$$

Similarly, by Equations (11) to (14), Equation (A.43) can be written as follows:

$$D_{X \text{ avg}} = \left(\frac{C_X \Gamma}{\rho \dot{\epsilon}^2} \right)^{1/3} \quad (\text{A.50})$$

$$D'_{X \text{ avg}} = \left(\frac{C'_X \Gamma}{\rho \dot{\epsilon}^2} \right)^{1/3} \quad (\text{A.51})$$

Then:

$$C_X = \frac{8c_2 Q_X^3}{c_3 Q_{\dot{\epsilon}}^3 S_M} \quad (\text{A.52})$$

$$C'_X = \frac{8c_2 Q_X^3}{c_3 Q_{\dot{\epsilon}}^3 R_X^3 S_M} \quad (\text{A.53})$$

For Type II Weibull size distributions, Tables 3 and 4 give:

$$Q_{\mathcal{A}} = \frac{\Gamma\left(1 + \frac{3}{n}\right)}{\Gamma\left(1 + \frac{1}{n}\right)\Gamma\left(1 + \frac{2}{n}\right)}$$

$$Q_M = \frac{\Gamma\left(1 + \frac{4}{n}\right)}{\Gamma\left(1 + \frac{1}{n}\right)\Gamma\left(1 + \frac{3}{n}\right)}$$

$$R_{\mathcal{A}} = \frac{\Gamma\left(1 + \frac{3}{n}\right)\Gamma\left(1 + \frac{1}{n}\right)}{\Gamma\left(1 + \frac{2}{n}\right)^2}$$

$$R_M = \frac{\Gamma\left(1 + \frac{4}{n}\right)\Gamma\left(1 + \frac{2}{n}\right)}{\Gamma\left(1 + \frac{3}{n}\right)^2}$$

$$S_M = \frac{\Gamma\left(1 + \frac{i+3}{n}\right)\Gamma\left(1 + \frac{i}{n}\right)^2}{\Gamma\left(1 + \frac{i+1}{n}\right)^3}$$

Then:

$$C_{\mathcal{A}} = \frac{8c_2\Gamma\left(1 + \frac{3}{n}\right)^3}{c_3\Gamma\left(1 + \frac{2}{n}\right)^2\Gamma\left(1 + \frac{5}{n}\right)} \quad (\text{A.54})$$

$$C'_{\mathcal{A}} = \frac{8c_2\Gamma\left(1 + \frac{2}{n}\right)^4}{c_3\Gamma\left(1 + \frac{1}{n}\right)^3\Gamma\left(1 + \frac{5}{n}\right)} \quad (\text{A.55})$$

$$C_M = \frac{8c_2 \Gamma\left(1 + \frac{2}{n}\right)^3 \Gamma\left(1 + \frac{4}{n}\right)^6}{c_3 \Gamma\left(1 + \frac{3}{n}\right)^8 \Gamma\left(1 + \frac{6}{n}\right)} \quad (\text{A.56})$$

$$C'_M = \frac{8c_2 \Gamma \Gamma\left(1 + \frac{4}{n}\right)^3}{c_3 \Gamma\left(1 + \frac{3}{n}\right)^2 \Gamma\left(1 + \frac{6}{n}\right)} \quad (\text{A.57})$$

Notice that:

$$\frac{8c_2}{c_3} = 8 \quad (\text{A.58})$$

for rectangular fragments and:

$$\frac{8c_2}{c_3} = \frac{8\pi}{\pi/6} = 48 \quad (\text{A.59})$$

for spherical fragments. For spherical fragments, Figure A.1 shows how C , $C_{\mathcal{R}}$, and C_M vary with the Weibull exponent n , where small n corresponds to large fragment size spreads and large n corresponds to small fragment size spreads.

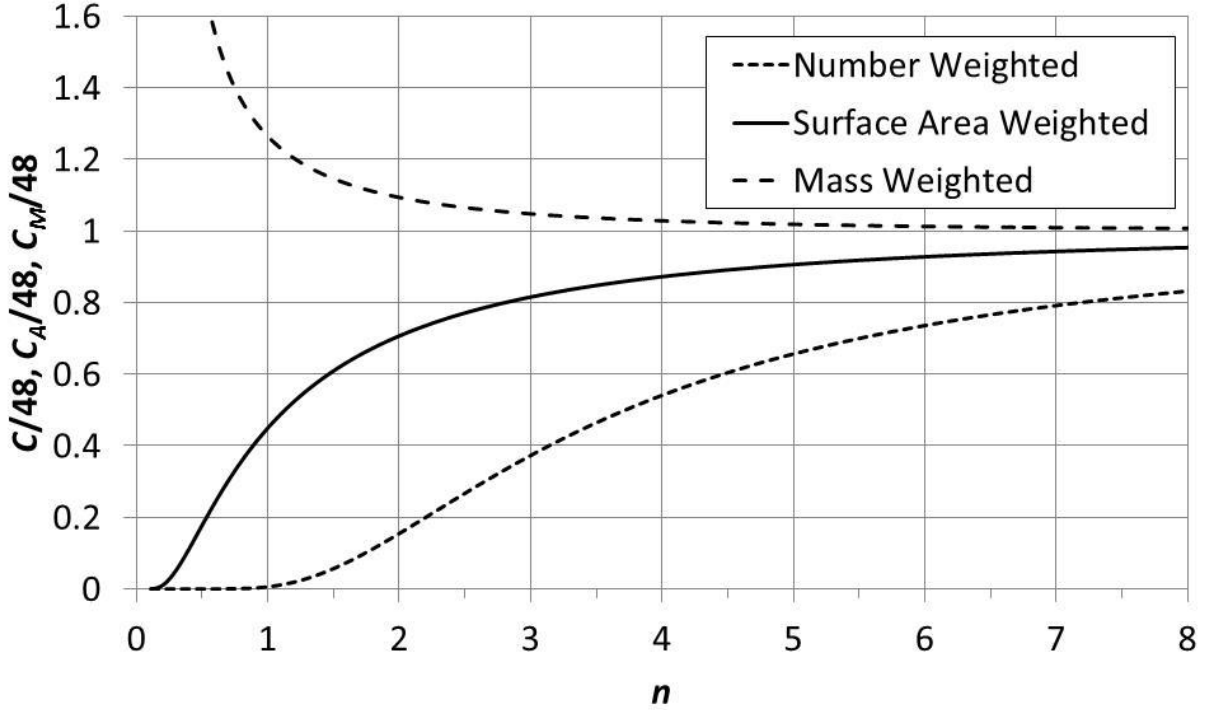


Figure A.1. Multiplicative constant vs. exponent n in a Type II Weibull size distribution for spherical fragments where “number weighted” refers to Equation (A.48), “surface area weighted” refers to Equation (A.54), and “mass weighted” refers to Equation (A.56).

As seen in Figure A.1, the number-weighted average fragment diameter changes dramatically with n . More specifically, C increases by a factor of over 150 when n increases from 1 to ∞ . This is mainly because, for large fragment size spreads, number-weighted averages are heavily skewed by a very large number of very small fragments. In fact, the very small fragments may contain a significant fraction of the overall surface energy, even though they contain only a trivial fraction of the overall mass, momentum, and kinetic energy.

As seen in Figure A.1, surface-area- and mass-weighted averages do not change dramatically with n . More specifically, $C_{\mathcal{A}}$ increases by a factor of about 2.2 and C_M decreases by a factor of about 0.8 when n increases from 1 to ∞ . This is mainly because, for large fragment size spreads, surface-area and mass-weighted averages are skewed – albeit not dramatically so – by a very small number of very large fragments.

Typical experiments obtain \bar{D}_{avg} and \bar{C} where the overbar refers to the effects of a minimum fragment size D_{min} . In cases where D_{min} is unusually small, number-weighting with a minimum fragment size may roughly correspond to surface-area weighting. In other words:

$$\bar{C} \approx C_{\mathcal{A}}$$

For example, for spherical fragments with Type II Weibull size distributions:

$$\bar{C} \approx C_{\mathcal{A}} = 21.6 \text{ for } n = 1 \quad (\text{A.60})$$

If D_{\min} is not unusually small, \bar{C} may roughly equal C_M or something larger.

Previous treatments typically assumed \bar{C} is constant. The fact that \bar{C} is not constant, but rather depends on the fragment size distribution through n , on the fragment shape through m and c_{m-1}/c_m , and on the minimum fragment size, helps to explain the wide range of values for \bar{C} found in the research literature. For example, Grady (1982) suggests $\bar{C} = 20$ while Grady & Kipp (1993) suggest $\bar{C} = 24, 48, \text{ or } 720$.

A.6 Case 4

Suppose that:

$$V_j = \frac{\dot{\epsilon} D_j^2}{2D_0} \quad (\text{A.61})$$

$$\Gamma_i = \frac{K_c^2 D_i}{2\rho c_s^2 D_0} \quad (\text{A.62})$$

Notice that Equation (A.61) is the same as Equations (A.25) times D_j / D_0 . Similarly, Equation (A.62) is the same as Equation (A.19) times D_i / D_0 . Substituting $V_0 = \dot{\epsilon} / (2D_0)$, $\nu = 2$, $\Gamma_0 = K_c^2 / (2\rho c_s^2 D_0)$, and $\gamma = 1$ into Equations (A.11a), (A.12), and (A.13) yields:

$$(D^4)_{D^m \text{ avg}} = \frac{4c_{m-1} K_c^2 D_0}{c_m \rho^2 c_s^2 \dot{\epsilon}^2} \quad (\text{A.63})$$

Suppose Equation (A.61) is replaced by the following:

$$V_j = \text{const.} \frac{\Gamma_j D_0}{\rho \dot{\epsilon} D_j^3} \quad (\text{A.64})$$

while Equation (A.62) is the same as before. Notice that Equation (A.64) is the same as Equation (A.28) times D_0 / D_j . Substituting Equation (A.62) into (A.64) yields:

$$V_j = \text{const.} \frac{K_c^2}{\rho^2 c_s^2 \dot{\epsilon} D_j^2} \quad (\text{A.65})$$

Substituting $V_0 = \text{const. } K_c^2 / (\rho^2 c_s^2 \dot{\epsilon})$, $\nu = -2$, $\Gamma_0 = K_c^2 / (2\rho c_s^2 D_0)$, and $\gamma = 1$ into Equations (A.11b), (A.12), and (A.13) yields:

$$(D^4)'_{D^m \text{ avg}} = \text{const.} \frac{c_m K_c^2 D_0}{c_{m-1} \rho^2 c_s^2 \dot{\epsilon}^2} \quad (\text{A.66})$$

Notice that Equation (A.63) applies to positive size distributions while Equation (A.66) applies to negative size distributions.

Equations (A.63) and (A.66) can be converted to other average sizes using Equations (11) to (14). In general, this produces expressions for average fragment diameters in the following form:

$$\left(\frac{\text{const.} K_c \sqrt{D_0}}{\rho c_s \dot{\epsilon}} \right)^{1/2} \quad (\text{A.67})$$

which approximately agrees with Equation (13.25) in Curran & Seaman (1996) for explosively-driven expanding cylindrical metal shells, where D_0 is the ‘‘characteristic size of the microcrack distribution ... [for] flaws (cracks) that have the potential of growing to coalescence to form fragments.’’

A.7 Case 5

Suppose that:

$$V_j = \frac{\dot{\epsilon} D_j^2}{2D_0} \quad (\text{A.68})$$

$$\Gamma_i = \Gamma_0 = \text{const.} \quad (\text{A.69})$$

Notice that Equation (A.68) is the same as Equation (A.61) while Equation (A.69) is the same as Equation (A.15). Substituting $V_0 = \dot{\epsilon} / (2D_0)$, $\nu = 2$, and $\gamma = 0$ into Equations (A.11), (A.12), and (A.13) yields:

$$(D^5)_{D^{m-1} \text{ avg}} = \frac{8c_{m-1} \Gamma_0 D_0^2}{c_m \rho \dot{\epsilon}^2} \quad (\text{A.70})$$

Suppose Equation (A.69) is replaced by the following:

$$V_j = \text{const.} \frac{\Gamma_0 D_0}{\rho \dot{\epsilon} D_j^3} \quad (\text{A.71})$$

while Equation (A.69) is the same as before. Notice that Equation (A.71) is the same as Equation (A.64). Substituting $V_0 = \text{const.} \Gamma_0 D_0 / (\rho \dot{\epsilon})$, $\nu = -3$, and $\gamma = 0$ into Equations (A.11), (A.12), and (A.13) yields:

$$(D^5)'_{D^{m-1} \text{ avg}} = \text{const.} \frac{c_m \Gamma_0 D_0^2}{c_{m-1} \rho \dot{\epsilon}^2} \quad (\text{A.72})$$

Notice that Equation (A.70) applies to positive size distributions while Equation (A.72) applies to negative size distributions.

Equations (A.70) and (A.72) can be converted to other average sizes using Equations (11) to (14). In general, this produces expressions for average fragment diameters in the following form:

$$\left(\frac{\text{const.} \Gamma_0 D_0^2}{\rho \dot{\epsilon}^2} \right)^{1/5} \quad (\text{A.73})$$

For example, by Equation (A.18), suppose that:

$$\Gamma_0 = \frac{1}{2} G_c \quad (\text{A.74})$$

In addition, suppose that:

$$D_0 = \frac{2G_c}{Y} \quad (\text{A.75})$$

Zhou et. al. (2005) call this the “critical opening distance of the nucleated crack.” Substituting Equations (A.74), (A.75), and $\rho = E / c^2$ into Equation (A.73) yields:

$$\left(\frac{\text{const.} c G_c^{3/2}}{E^{1/2} Y \dot{\epsilon}} \right)^{2/5} \quad (\text{A.76})$$

which agrees to some extent with Equation (12) in Zhou et. al. (2005) for dynamic fragmentation of a one-dimensional brittle bar; see also Drugan (2001). However, instead of a strain rate exponent of $-2/5 = -0.4$, Zhou et. al. (2005) obtained -0.4264 .

A.8 Case 6

Suppose that:

$$V_j = \frac{\dot{\epsilon} D_j^5}{2D_0^4} \quad (\text{A.77})$$

$$\Gamma_i = \frac{G_c D_i}{2D_0} \quad (\text{A.78})$$

Substituting $V_0 = \dot{\epsilon}/(2D_0^4)$, $\nu = 5$, $\Gamma_0 = G_c/(2D_0)$ and $\gamma = 1$ into Equations (A.11), (A.12), and (A.13) yields:

$$(D^{10})_{D^m \text{ avg}} = \frac{4c_{m-1} G_c D_0^8}{c_m \rho \dot{\epsilon}^2} \quad (\text{A.79})$$

In general, this produces expressions for average fragment diameters in the following form:

$$\left(\frac{\text{const.} G_c D_0^8}{\rho \dot{\epsilon}^2} \right)^{1/10} \quad (\text{A.80})$$

and expressions for average fragment masses in the following form:

$$\left(\frac{\text{const.} \rho^{7/3} G_c D_0^8}{\dot{\epsilon}^2} \right)^{3/10} \quad (\text{A.81})$$

which agrees to some extent with Equation (6.7) in Mott et. al. (1944) for explosively-driven expanding cylindrical metal shells. However, instead of a strain rate exponent of $-2 \times 3/10 = -0.6$, Mott et. al. (1944) obtained -0.623 .

A.9 Tensile Strain Rates

The examples given above require knowing a scalar tensile strain rate, which is assumed to be large, steady, and uniform. The best known cases involve thin rapidly-expanding rings and cylindrical shells of radius \mathcal{R} where:

$$\dot{\epsilon} = \frac{\dot{\mathcal{R}}}{\mathcal{R}} \quad (\text{A.82})$$

according to Hoggatt & Recht (1968); see also Warnes et. al. (1985) and Jones et. al. (2013). For thin-rapidly expanding spheres of radius \mathcal{R} :

$$\dot{\epsilon} = \frac{2\dot{\mathcal{R}}}{\mathcal{R}} \quad (\text{A.83})$$

according to Al-Hassani & Johnson (1969); see also Llorca & Juanicotena (1997) and Buy & Llorca (2002).

Notice that the previous two expressions apply only to *thin* fragmenting objects. At a radius r in a thick rapidly-expanding ring or cylindrical shell with an outer radius \mathcal{R} :

$$\dot{\varepsilon} = \frac{\dot{\mathcal{R}}\mathcal{R}}{r^2} \quad (\text{A.84})$$

where $\dot{\mathcal{R}}\mathcal{R} = \dot{r}r$ so that:

$$\dot{\varepsilon} = \frac{\dot{r}}{r} \quad (\text{A.85})$$

Similarly, at a radius r in a thick rapidly-expanding spherical shell with an outer radius \mathcal{R} :

$$\dot{\varepsilon} = 2 \frac{\dot{\mathcal{R}}\mathcal{R}^2}{r^3} \quad (\text{A.86})$$

where $\dot{\mathcal{R}}\mathcal{R}^2 = \dot{r}r^2$ so that:

$$\dot{\varepsilon} = \frac{2\dot{r}}{r} \quad (\text{A.87})$$

Finally, for uniformly-stretched one-dimensional objects such as rods, bars, strings, filaments, threads, ligaments, etc. of length L :

$$\dot{\varepsilon} = \frac{\dot{L}}{L} \quad (\text{A.88})$$

A.10 Extensions to Low Strain Rates

Many fragmentation events violate Equation (A.3). For example, Edwards & Deal (2011) found explosively-driven aluminum alloy cylindrical shells that produced as a few three fragments. For another example, in a literature survey, Zhou et. al. (2006c) found expanding ring experiments that produced as few as 18 fragments. The expressions given in Section A.2 can be extended to lower strain rates by eliminating Equation (A.3), i.e., by accounting for the surface area of the original fragmenting body.

First, consider thin fragmenting objects such as shells and sheets. Using conservation of mass, Lefebvre (1992a) argues that:

$$\mathcal{A} = \frac{2}{t} \sum_{j=1}^N c_m D_j^m \quad (\text{A.89})$$

where the shell or sheet thickness t is assumed to be small. The factor of two accounts for the two sides of the shell or sheet. In this case, Equation (A.10) becomes:

$$\sum_{j=1}^N D_j^{2\nu-\gamma+1} \frac{D_j^{\gamma+m-1}}{\sum_{i=1}^N D_i^{\gamma+m-1}} + \frac{4\Gamma}{t\rho V_0^2} \sum_{j=1}^N D_j^{-\gamma+1} \frac{D_j^{\gamma+m-1}}{\sum_{i=1}^N D_i^{\gamma+m-1}} = \frac{2c_{m-1}\Gamma_0}{c_m\rho V_0^2} \quad (\text{A.90})$$

Applying Equation (5), Equation (A.11) becomes:

$$X_{Y \text{ avg}} + \frac{4\Gamma}{t\rho V_0^2} Z_{Y \text{ avg}} = \frac{2c_{m-1}\Gamma_0}{c_m\rho V_0^2} \quad \text{for} \quad 2\nu - \gamma + 1 > 0, \quad -\gamma + 1 \geq 0, \quad \gamma + m - 1 \geq 0 \quad (\text{A.91a})$$

$$\frac{1}{X'_{Y \text{ avg}}} + \frac{4\Gamma}{t\rho V_0^2} \frac{1}{Z'_{Y \text{ avg}}} = \frac{2c_{m-1}\Gamma_0}{c_m\rho V_0^2} \quad \text{for} \quad 2\nu - \gamma + 1 < 0, \quad -\gamma + 1 \leq 0, \quad \gamma + m - 1 \geq 0 \quad (\text{A.91b})$$

where:

$$X = D^{|2\nu-\gamma+1|}; \quad Y = D^{\gamma+m-1}; \quad Z = D^{-|\gamma+1|}$$

Equation (A.91) has a simple solution if:

$$X = Z$$

or:

$$\nu = 0 \quad (\text{A.92})$$

In this case:

$$X_{Y \text{ avg}} = \frac{\frac{c_{m-1}}{2c_m}}{\frac{\Gamma}{t\Gamma_0} + \frac{\rho V_0^2}{4\Gamma_0}} \quad \text{for} \quad -\gamma + 1 \geq 0, \quad \gamma + m - 1 \geq 0 \quad (\text{A.93a})$$

$$X'_{Y \text{ avg}} = \frac{\frac{\Gamma}{t\Gamma_0} + \frac{\rho V_0^2}{4\Gamma_0}}{\frac{c_{m-1}}{2c_m}} \quad \text{for} \quad -\gamma + 1 \leq 0, \quad \gamma + m - 1 \geq 0 \quad (\text{A.93b})$$

If $V_0 = \dot{\epsilon}D_0/2$, then Equation (A.93a) is the same as Equation (A.20) for large enough strain rates. If $\gamma = 0$, $\Gamma = \Gamma_0 = \sigma$, $m = 3$, $c_m = \pi/6$, and $c_{m-1} = \pi$. Then Equation (A.93a) becomes:

$$D_{D^2 \text{ avg}} = \frac{3}{\frac{1}{t} + \frac{\rho V_0^2}{4\sigma}} \quad (\text{A.94})$$

which is similar to Lefebvre (1992a,b).

Alternatively, for uniformly-stretched one-dimensional objects such as expanding rods, bars, strings, filaments, threads, ligaments, etc. of initial length L_0 and fixed cross-sectional area \mathcal{A}_0

$$(D^{2\nu+1})_{\text{avg}} + \frac{4\Gamma_0 \mathcal{A}_0}{c_m \rho V_0^2 L_0} D_{\text{avg}} = \frac{4\Gamma_0 \mathcal{A}_0}{c_m \rho V_0^2} \quad \text{for } 2\nu+1 > 0 \quad (\text{A.95})$$

assuming $\gamma = 0$ and $m = 1$. The same expression applies to expanding rings if $L_0 = 2\pi R_{\infty 0}$.

Equation (A.95) assumes that:

$$N = \frac{L_0}{D_{\text{avg}}} \quad (\text{A.96})$$

For example, as in Section A.3, suppose that $\nu = 0$. Then Equation (A.95) becomes:

$$D_{\text{avg}} = \frac{1}{\frac{1}{L_0} + \frac{c_m \rho V_0^2}{4\Gamma_0 \mathcal{A}_0}} \quad (\text{A.97})$$

Note that Equation (A.99) is formally similar to Equations (A.93) and (A.94). As another example, as in Section A.5, suppose that $V_0 = \dot{\epsilon}/2$ and $\nu = 1$. Then Equation (A.95) becomes:

$$(D^3)_{\text{avg}} + \frac{16\Gamma_0 \mathcal{A}_0}{c_m \rho \dot{\epsilon}^2 L_0} D_{\text{avg}} = \frac{16\Gamma_0 \mathcal{A}_0}{c_m \rho \dot{\epsilon}^2} \quad (\text{A.99})$$

By the cubic equation:

$$D_{\text{avg}} = \left(\frac{8\Gamma_0 \mathcal{A}_0}{c_m \rho \dot{\epsilon}^2} \right)^{1/3} \left[\left(1 + \sqrt{\frac{64\Gamma_0 \mathcal{A}_0}{27c_m \rho \dot{\epsilon}^2 L_0^3} + 1} \right)^{1/3} + \left(1 - \sqrt{\frac{64\Gamma_0 \mathcal{A}_0}{27c_m \rho \dot{\epsilon}^2 L_0^3} + 1} \right)^{1/3} \right] \quad (\text{A.100})$$

For large strain rates, this is the same as Equation (A.39) with $m = 1$ and $c_{m-1} = c_0 = 2\mathcal{A}_0$.

In addition to the approach described here, Drugan (2001), Zhou et. al. (2004, 2005, 2006a,b,c), Levy & Molinari (2010) and Levy et. al. (2012) compare several other approaches for modeling low-strain-rate fragmentation with $m = 1$. For example, Levy & Molinari (2010) suggest an approximate solution, formally similar to Equations (A.95) and (A.97), found using empirical curve fits to models and test data. The comparisons given in these references help show how large the strain rate needs to be before Equation (A.11) applies.

A.11 Conclusions

This treatment assumes that a dominant scalar tensile strain rate $\dot{\epsilon}$ is steady and uniform. While this is a severe restriction, many problems can be subdivided into *local* regions where the tensile strain rate is *approximately* steady and uniform. For example, as seen in Section A.9, the strain rate is steady and uniform in each radial layer in a thick rapidly-expanding solid ring, cylinder, or sphere. More complex cases require applying expression such as Equation (A.11), (A.91), or (A.95) locally in first-principles structural, fluid dynamics, or hydrodynamics codes; see, e.g., Wilson et. al. (2001).

If the tensile strain rate $\dot{\epsilon}$ is large – in addition to being steady and uniform – then a series of examples shows that:

$$D_{ref} \sim \dot{\epsilon}^{-2/k} \tag{A.101}$$

where k is any positive integer and the subscript *ref* refers to the averages described in Section 3. In addition, the average fragment diameter depends on the material type (e.g., solid vs. liquid), the material properties (e.g. density, strength, elasticity), the fragment size distribution, the fragment shape, and the minimum fragment size, if any. The resulting expressions are well-validated for k equal to 1, 2, and 3 but are less well-validated for larger k . Despite the fact that the earliest work by Sir Nevill Mott and his co-workers found a variety of different values for k , the modern research literature has focused predominantly on $k = 3$.

The approaches described here are perhaps more popular in theory than in practice. This is partly because they may predict average fragments sizes near or even below the minimum fragment sizes imposed in typical experiments; this is especially true for the count mean diameter. Common semi-empirical alternatives include: the Gurney-Sarmousakis equation for cased munitions, e.g., Victor (1996) and Kennedy (1998); and Kuznetsov's equation for rock blasting, e.g., Cunningham (2005) and Ouchterlony (2016).

References for Appendix A

- F. Barreras, A. Lozano, J. Barroso, and E. Lincheta, Experimental Characterization of Industrial Twin-Fluid Atomizers, *Atomization and Sprays*, 16(2), 127-145, 2006
- F. Buy and F. Llorca, The Expanding Shell Test: Numerical Simulation of the Experiment, In M. D. Furnish, N. N. Thadhani, and Y. Horie, Editors, *Shock Compression of Condensed Matter – 2001*, American Institute of Physics, 2002
- C. V. B. Cunningham, The Kuz-Ram Fragmentation Model – 20 Years On, In R. Holmberg et. al., Editors, *Proceedings of the 3rd World Conference on Explosives and Blasting*, European Federation of Explosives Engineers, 2005
- D. R. Curran and L. Seaman, Simplified Models of Fracture and Fragmentation, In L. Davison, D. E. Grady, and M. Shahinpoor, Editors, *High-Pressure Shock Compression of Solids II: Dynamic Fracture and Fragmentation*, Springer-Verlag, 1996
- W. J. Drugan, Dynamic Fragmentation of Brittle Materials: Analytical Mechanics-Based Models, *Journal of the Mechanics and Physics of Solids*, 49(6), 1181–1208, 2001
- M. R. Edwards and C. Deal, Effect of Heat Treatment on Small Scale Fragmentation of Aluminium Alloy, *Materials Science and Technology*, 27(1), 332-338, 2011
- D. E. Grady, Application of Survival Statistics to the Impulsive Fragmentation of Ductile Rings, In M. A. Meyers and L. E. Murr, Editors, *Shock Waves and High-Strain-Rate Phenomena in Metals*, Plenum Press, 1981
- D. E. Grady, Local Inertial Effects in Dynamic Fragmentation, *Journal of Applied Physics*, 53(1), 322-325, 1982
- D. E. Grady, The Spall Strength of Condensed Matter, *Journal of Mechanics and Physics of Solids*, 36(3), 353–384, 1988
- D. E. Grady and M. E. Kipp, Dynamic Fracture and Fragmentation, In J. R. Asay and M. Shahinpoor, Editors, *High-Pressure Shock Compression of Solids*, Springer-Verlag, 1993 (see also D. E. Grady and M. E. Kipp, Fragmentation of Solids Under Dynamic Loading, in T. Wierzbicki and N. Jones, Editors, *Structural Failure*, Wiley, 1989)
- S. T. S. Al-Hassani and W. Johnson, The Dynamics of the Fragmentation Process for Spherical Shells Containing Explosives, *International Journal of Mechanical Sciences*, 11(10), 811-823, 1969
- C. R. Hoggatt and R. F. Recht, Fracture Behavior of Tubular Bombs, *Journal of Applied Physics*, 39(3), 1856-1862, 1968.

D. R. Jones, D. J. Chapman, and D. E. Eakins, A Gas Gun Based Technique for Studying the Role of Temperature in Dynamic Fracture and Fragmentation, *Journal of Applied Physics*, 114, 173508, 2013

J. E. Kennedy, The Gurney Model for Explosive Output for Driving Metal, in J. A. Zukas and W. P. Walters, editors, *Explosive Effects and Applications*, Springer-Verlag, 1998

K. Kirane, Y. Su, and Z. P. Bažant, Strain-Rate-Dependent Microplane Model for High-Rate Comminution of Concrete under Impact Based on Kinetic Energy Release Theory, *Proceedings of the Royal Society A: Mathematical, Physical and Engineering Sciences*, 471, 20150535, 2015

C. B. Laney, *Transformation and Self-Similarity Properties of Gamma and Weibull Fragment Size Distributions*, Defense Threat Reduction Agency Technical Report DTRA-TR-16-006, December 2015

A. H. Lefebvre, Energy Considerations in Twin-Fluid Atomization, *Journal of Engineering for Gas Turbines and Power*, 114(1), 89-96, 1992

A. H. Lefebvre, Twin-Fluid Atomization: Factors Influencing Mean Drop Size, *Atomization and Sprays*, 2(2), 101-119, 1992

S. Levy and J. F. Molinari, Dynamic Fragmentation of Ceramics, Signature of Defects and Scaling of Fragment Sizes, *Journal of the Mechanics and Physics of Solids*, 58(1), 12–26, 2010

Levy, S., J. F. Molinari, and R. Radovitzky, Dynamic Fragmentation of a Brittle Plate Under Biaxial Loading: Strength or Toughness Controlled?, *International Journal of Fracture*, 174(2), 203–215, 2012

F. Llorca and A. Juanicotena, Expanding Ring Test: Numerical Simulation - Application to the Analysis of Experimental Data, *Journal de Physique IV*, 7(C3), C3-235–C3-240, 1997

N. F. Mott and E. H. Linfoot, *A Theory of Fragmentation*, U.K. Ministry of Supply, A.C. 3348, January 1943; as reproduced in D. E. Grady, *Fragmentation of Rings and Shells: The Legacy of N. F. Mott*, Springer, 2006

N. F. Mott, J. H. Wilkinson, and T. H. Wise, *Fragmentation of Service Projectiles*, U.K. Ministry of Supply, A.C. 6338, May 1944; as reproduced in D. E. Grady, *Fragmentation of Rings and Shells: The Legacy of N. F. Mott*, Springer, 2006

N. F. Mott, Fragmentation of Shell Cases, *Proceedings of the Royal Society A: Mathematical, Physical and Engineering Sciences*, 189(1018), 300–308, 1947

F. Ouchterlony, The Case for the Median Fragment Size as a Better Fragment Size Descriptor than the Mean, *Rock Mechanics and Rock Engineering*, 49(1), 143-164, 2016

A. C. Victor, Warhead Performance Calculations for Threat Hazard Assessment, *Proceedings of the 27th DoD Explosives Safety Seminar*, DoD Explosives Safety Board, 1996

R. Warnes, R. Karpp, and P. Follansbee, The Freely Expanding Ring Test: A Test to Determine Material Strength at High Strain Rates, *Journal de Physique Colloques*, 46(C5), C5-583-C5-590, 1985

L.T. Wilson, D. R. Reedal, L. D. Kuhns, D. E. Grady, and M. E. Kipp, Using a Numerical Fragmentation Model to Understand the Fracture and Fragmentation of Naturally Fragmenting Munitions of Differing Materials and Geometries, In I. R. Crewther, Editor, *Proceedings of the 19th International Symposium on Ballistics*, IBS, 2001

P.-K. Wu, L.-K. Tseng, and G. M. Faeth, Primary Breakup in Gas/Liquid Mixing Layers for Turbulent Liquids, *Atomization and Sprays*, 2(3), 295-317, 1992

F. Zhou, J.-F. Molinari, and K. T. Ramesh, Strain Rate Effects on Fragment Size of Brittle Materials, In E. Lara-Curzio and M. J. Readey, Editors, *28th International Conference on Advanced Ceramics and Composites A: Ceramic Engineering and Science Proceedings*, 25(3), 605–611, 2004

F. Zhou, J.-F. Molinari, and K. T. Ramesh, A Cohesive Model Based Fragmentation Analysis: Effects of Strain Rate and Initial Defects Distribution, *International Journal of Solids and Structures*, 42(18), 5181-5207, 2005

F. Zhou, J.-F. Molinari, and K. T. Ramesh, Effects of Material Properties on the Fragmentation of Brittle Materials, *International Journal of Fracture*, 139(2), 169-196, 2006

F. Zhou, J.-F. Molinari, and K. T. Ramesh, Analysis of the Brittle Fragmentation of an Expanding Ring, *Computational Materials Science*, 37(1-2), 74-85, 2006

F. Zhou, J.-F. Molinari, and K. T. Ramesh, Characteristic Fragment Size Distributions in Dynamic Fragmentation, *Applied Physics Letters*, 88, 261918, 2006

**DISTRIBUTION LIST
DTRA-TR-16-52**

DEPARTMENT OF DEFENSE

DEFENSE THREAT REDUCTION
AGENCY
8725 JOHN J. KINGMAN ROAD
STOP 6201
FORT BELVOIR, VA 22060
ATTN: P. CLEMENT

DEFENSE TECHNICAL
INFORMATION CENTER
8725 JOHN J. KINGMAN ROAD,
SUITE 0944
FT. BELVOIR, VA 22060-6201
ATTN: DTIC/OCA

**DEPARTMENT OF DEFENSE
CONTRACTORS**

QUANTERION SOLUTIONS, INC.
1680 TEXAS STREET, SE
KIRTLAND AFB, NM 87117-5669
ATTN: DTRIAC